

Response to Anonymous Referee #1

General points

We would like to thank the reviewer for his/her thorough review and constructive comments. We have addressed all of them and provide below a detailed reply. Please note that the page and line numbers refer to the marked-up version of the revised manuscript.

Comment 1 (C1). The term mixing used throughout the paper is not well defined from the beginning. Does it refer to lateral (eddy-induced) or diapycnal mixing or both. Or does it correspond to the 3rd term of the rhs of equation 1? Please clarify. Also the lateral mixing term in equation 1 (2nd term rhs) is not well defined. Does it describe the subgrid-scale diffusivity? What is K_h in the model? Is it evaluated as part of the oxygen budget? Is it not important?

Response (R.): The reviewer is right. We have clarified what we refer to as mixing in the methods section (Section 2.3). Mixing corresponds in our study to the contribution of horizontal diffusion ($K_h \cdot \nabla^2 O_2$), vertical mixing ($\frac{\partial}{\partial z} \left(K_z \frac{\partial O_2}{\partial z} \right)$) and the mixing that is associated with the non-linear advection. The latter corresponds to $(u' \partial u' / \partial x) + (v' \partial v' / \partial y) + (w' \partial w' / \partial z)$, assuming the Reynolds decomposition for the velocity field, i.e. $\vec{u} + \vec{u}'$, where \vec{u}' accounts for the intraseasonal variability (periods lower than ~ 3 months).

In the model, the lateral mixing term in equation 1 refers to the subgrid-scale diffusivity. K_h corresponds to the eddy diffusivity coefficient, and it is a constant value in that version of ROMS (version 2.1), equal to $100 \text{ m}^2 \text{ s}^{-1}$. Note that the model also has a numerical diffusion associated with inherent spurious diapycnal mixing of the numerical scheme, so that K_h is empirically adjusted, and the term $K_h \cdot \nabla^2 O_2$ does not account for all the actual diffusion in the model.

As suggested by the reviewer, an explanation of the term mixing used in the analyses was added to the paper (Section 2.3).

C2. Fig. 12 seems to be a main result, but is very difficult to understand. It shows on the one hand the mean oxygen and energy flux resulting from the propagation of annual ETRW (Fig. 12a,b) and on the other hand the annual cycle of the DO eddy flux. It would be good to separate these 2 topics and discuss them separately. In this way you could add also phase information in a new panel to Fig. 12c, which would make the annual cycle of DO eddy flux better understandable.

R. (P55-56): Following the reviewers' recommendation, we now present two figures: one figure with the amplitude of the annual cycle of the climatological DO eddy flux, with the corresponding phase diagram (new Figure 15, see Figure A1) and the figure showing the results on the annual ETRW flux (new Figure 14).

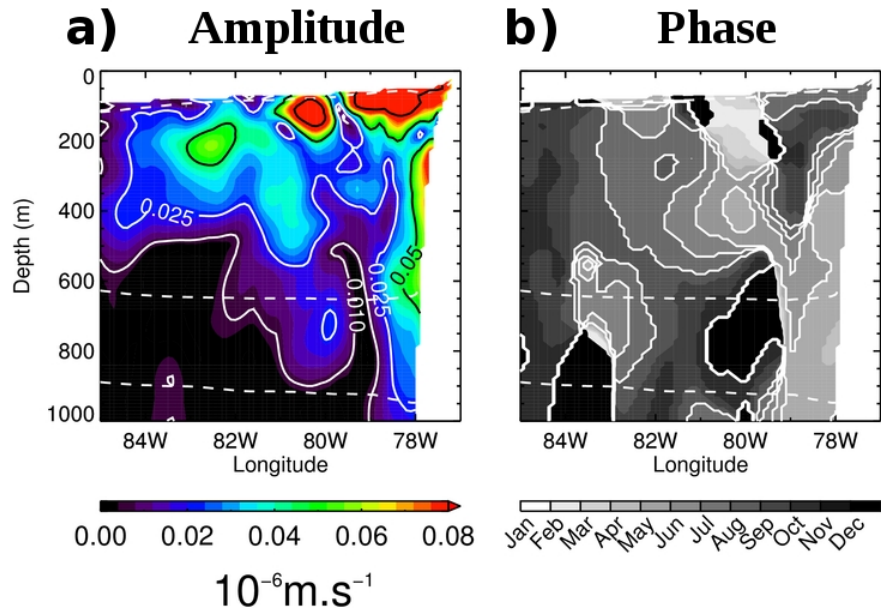


Figure A1. Zonal section of the annual harmonic of the module of the seasonal DO eddy flux vector $(\langle u' \cdot O_2' \rangle, \langle w' \cdot O_2' \rangle)$ at 12°S. (a) Amplitude of the harmonic and (b) phase of the annual maximum (in months). Dashed white contours indicate the 45 and 20 μM mean DO isopleths. DO was normalized by its RMS prior to carrying out analysis.

Specific points

C1. P2, L16: “... DO eddy flux dominates over the mean seasonal DO flux ...” It is not so clear what is meant: DO eddy flux includes a mean and a seasonal cycle; mean seasonal DO flux (is also not defined and difficult to understand) can also include a mean and a seasonal cycle. What “dominates” refer to?

R. (P2,L16): The reviewer is right. We meant that the mean DO eddy flux (i.e. $\langle \tilde{u} \cdot \tilde{O}_2 \rangle$) is larger over the mean seasonal DO flux $\langle \tilde{u} \cdot \tilde{O}_2 \rangle$, where the fields with tilde stand for the seasonal component (see also C13 in Specific points). We have also clarified the term “dominate” and changed the sentence to: “...an upper zone above 400m where mean DO eddy flux is larger on average than the mean seasonal DO flux”.

C2. P2, L19: what is “mean eddy flux” here?

R. (P2, L20): This was changed to “mean DO eddy flux”, and the sentence was modified accordingly.

C3. P2, L22: Implications of the results ...

R. (P2, L24): The sentence was corrected.

C4. P3, L5: presently

R. (P3, L6): The sentence was corrected.

C5. P3, L8: “climatic gases” sounds awkward and not correct: better “greenhouse gases”?

R. (P3, L8): This was corrected using “climatically-active gases”.

C6. P3, L9: “sequestration ocean role”, please reformulate

R. (P3, L10): The sentence was changed to “...ocean carbon sequestration...”

C7. P5, L6: reduce ... the offshore transport (of what?)

R. (P5, L9): We meant offshore transport of carbon. The sentence was changed to “... offshore carbon export...”

C8. P5, L7 also P5, L20: “eddy-induced” instead of “eddies-induced”

R. (P5, L10): The sentence was corrected.

C9. P5, L10-12: mesoscale activity can only be a ventilation process if the higher oxygen is found at the coast, which might be present during some time of the year. What are OMZ properties? Typically, I would assume that OMZ properties refer to minimum oxygen; the transport of it would not represent a ventilation of the offshore OMZ. Please clarify.

R. (P5, L14): We refer here to the exchange of tracers between the shelf and the open ocean induced by the mesoscale activity, and the OMZ properties refer to oxygen, organic carbon and/or nitrate. It was implicitly assumed that there exists a cross-shore gradient in water mass properties, so a transport can actually take place. The text has been clarified as follows: “In this sense, the mesoscale activity represents a ventilation pathway for the OMZ, through the offshore transport of oxygen-enriched waters”.

C10. P8, L4: “OMZ equilibrium is reached”: water mass ages are typically much older in OMZs compared to the length of the used simulation. Thus the equilibrium is probably not reached. However, the simulation can still be quite stable and drifting not much away from the initial conditions, which should be good for the used application of the model.

R. (P9, L2): The sentence was changed to: “Although, after the spin-up, the simulation has reached stable conditions and the OMZ volume does not drift, we focus in the present study only on the period 2000-2008”.

C11. P8, L20/21: something is missing like “obtained “ or similar.

R. (P9, L23): Added “computed”. The sentence was corrected to: “...with O₂sat computed following the methodology of Garcia and Gordon (1992)”.

C12. P9, L1 and L9: avoid the repetition

R. (P10, L4): The sentence corresponding to L1 was changed to: “...the simulation presents more details than the climatological product” in order to avoid the repetition.

C13. P10, L5: Here you have to define exactly the used terms: e.g., mean seasonal DO flux (also mentioned in the abstract), DO flux obtained from annual harmonics (Fig. 12), etc.; please be careful and use the defined terms throughout the manuscript. What is a mean flux and what is a seasonally varying flux?

R. (P11, L13): In order to clarify the definition of the different fluxes, we have added the mathematical formula each time we define a flux, and the adjective “mean” was also added when required in order to clarify. The text in the revised manuscript is now: “The DO flux associated with different timescales of variability is therefore estimated. This consists in computing the temporal average of the cross-products between DO and velocity anomalies. Anomalies can refer either to seasonal anomalies and in that case, this provides the mean seasonal DO flux ($\langle \tilde{u} \cdot \tilde{O}_2 \rangle$ where \sim refers to the seasonal anomalies), or to the intraseasonal anomalies (calculated here as the departure from the monthly mean) and in that case, this provides an estimate of the mean DO eddy flux ($\langle u' \cdot O_2' \rangle$, where the apostrophe refers to the intraseasonal anomalies). In this paper we are also interested in the seasonality of the DO eddy flux. This is estimated from the monthly-mean seasonal cycle of the mean DO eddy flux calculated over a 3-month running window, and is now referred to as $\overline{\langle u' \cdot O_2' \rangle}$ ”.

C14. P10, L5: I am not sure to what “latter” refers to.

R. (P11, L20): It refers to the estimation of DO flux associated with different scales of variability. The sentence was reformulated in order to avoid confusion: “The DO flux associated with different timescales of variability is therefore estimated. This consists in computing the temporal average of the cross-products between DO and velocity anomalies”.

C15. P10, L8: How is the departure from monthly mean calculated? Just subtracting from the time series monthly means during each month would result in step-like functions. Do you use a running mean or any other kind of interpolation?

R. (P11, L23): In order to derive intraseasonal anomalies, we first compute the monthly mean data. We then interpolate the monthly mean data on the original time grid (3-day mean) using a cubic spline, and use this as a baseline: the anomalies are obtained from the difference between the original total field (direct model output) and the interpolated monthly mean. This methodology has been used in previous studies (Lin et al., 2000; Dewitte et al., 2011) to study intraseasonal variability in surface winds and SST. This method is similar to a high-pass filter with a transfer function, estimated by computing intraseasonal anomalies of a daily Gaussian white noise, characterized by a -1 , -3 , and -10 dB attenuation (79%, 50%, 10% of the input power persists) at 59, 68, and 96 days⁻¹ frequency, respectively. This would be also equivalent to a Lanczos filter with a cut-off period of 90 days.

References:

Dewitte, B., Illig, S., Renault, L., Goubanova, K., Takahashi, K., Gushchina, D., Mosquera, K., and Purca, S.: Modes of covariability between sea surface temperature and wind stress intraseasonal anomalies along the coast of Peru from satellite observations (2000–2008), *J. Geophys. Res.*, 116, C04028, doi:10.1029/2010JC006495, 2011.

Lin, J. W. B., Neelin, J. D., and Zeng, N.: Maintenance of tropical intraseasonal variability: Impact of evaporation–wind feedback and midlatitude storms, *J. Atmos. Sci.*, 57, 2793–2823, doi:10.1175/1520-0469, 2000.

C16. P10, L13: How is K_z and K_h defined in the model.

R. (P12, L5): In this version of ROMS (version 2.1), K_h is fixed to 100 m² s⁻¹.

K_z is calculated by the vertical mixing scheme which is based on the KPP scheme (Large et al., 1994).

References:

Large, W. G., McWilliams, J. C., and Doney, S. C.: Oceanic vertical mixing: A review and a model with a nonlocal boundary layer parameterization, *Rev. Geophys.*, 32, 363–403, doi:10.1029/94RG01872, 1994.

C17. P10, L16: How large is K_h ? Is the horizontal diffusion further used in the oxygen budget, e.g. Fig 11b? What is mixing in Fig. 11b (on P5, L7 and L20 you use the term mixing for eddy-induced mixing)? What represents the residual in Fig. 11B?

R. (P12, L6): In this version of ROMS (version 2.1), K_h is fixed to 100 m² s⁻¹.

In figure 11b, the term mixing refers just to the contribution of both vertical and horizontal mixing terms from Eq. 1. We have changed the notation in Figure 10g and 11b (Fig. 12g and 13b in the revised version of the manuscript) and now use the notation: $H_{mix}+V_{mix}$, where H_{mix} and V_{mix} refer to

horizontal diffusion and vertical diffusivity respectively.

The residual in Figure 13b corresponds to the difference between the rate of DO change and the sum of all the terms on the rhs of Eq. 1 for the normalized PC timeseries. Our purpose is to verify that the DO budget is nearly closed when considering the first EOF modes of each term. Although the residual is not zero, it remains weak (two orders of magnitude smaller than the PCs of the DO budget terms), allowing for the interpretation of the different terms using their first EOF modes.

Modifications were introduced to the caption of Figure 11 (Figure 13 in the revised version of the manuscript) in order to clarify: “The residual corresponds to the difference between the rate of DO change and the sum of all the terms of the rhs of Eq. 1 in terms of the normalized PC timeseries. The weak residual indicates that the seasonal DO budget can be interpreted from the EOF decomposition.”

Note that we have also clarified the caption of Figure 10 (Figure 12 in the revised version of the manuscript): “The EOF mode patterns were multiplied by the RMS of the PC timeseries. Multiplying the EOF pattern by the PC timeseries plotted in Figure 13 yields the contribution of the first EOF mode to the original field, in dimensionalized units (i.e. $\mu\text{M s}^{-1}$ for the tendency terms)”.

C18. P11, L3-6: Please clarify here, why do you need baroclinic mode decomposition to derive WKB ray paths. According to Ramos et al. (2008), in the long wave approximation the WKB ray path depend on the local vertical wave number. Such vertical wavenumber could be derived from the vertical distribution of the annual harmonic amplitude and phase. Please explain, why do you use instead phase speed values from different baroclinic modes and how this is in agreement with the WKB assumptions?

R. (P13, L3-8): The slope of ray paths in the (x, z) plane is $\frac{dx}{dz} = 2 \frac{\omega f^2}{\beta c N}$ (see Appendix in Ramos et al. (2008)) where c is the “observed” phase speed of the Extra-tropical Rossby wave which consists in a superposition of different baroclinic modes, so the speed can range from values c_1 to c_n , where c_n is the theoretical phase speed of a n^{th} baroclinic mode, obtained from the vertical mode decomposition of the local density profile. We have clarified the text, mentioning that the vertical mode decomposition is only aimed at providing a range of values for c, consistent with the model stratification.

References:

Ramos, M., Dewitte, B., Pizarro, O., and Garric, G.: Vertical propagation of extratropical Rossby waves during the 1997 – 1998 El Niño off the west coast of South America in a medium-resolution OGCM simulation, J. Geophys. Res., 113, C08041, doi:10.1029/2007JC004681, 2008.

C19. P11, L15: With the given normalization it is difficult to understand the amplitude of the annual harmonic. It would help to also see the harmonic amplitude without normalization.

R. (P13, L25): The objective of the DO normalization is to highlight the regions where the DO concentration is weak. We expect to have a weak annual cycle where the DO is very low (see Figure

A2). By doing the normalization, the phase pattern is unaltered but the spatial variation of the annual cycle amplitude is emphasized.

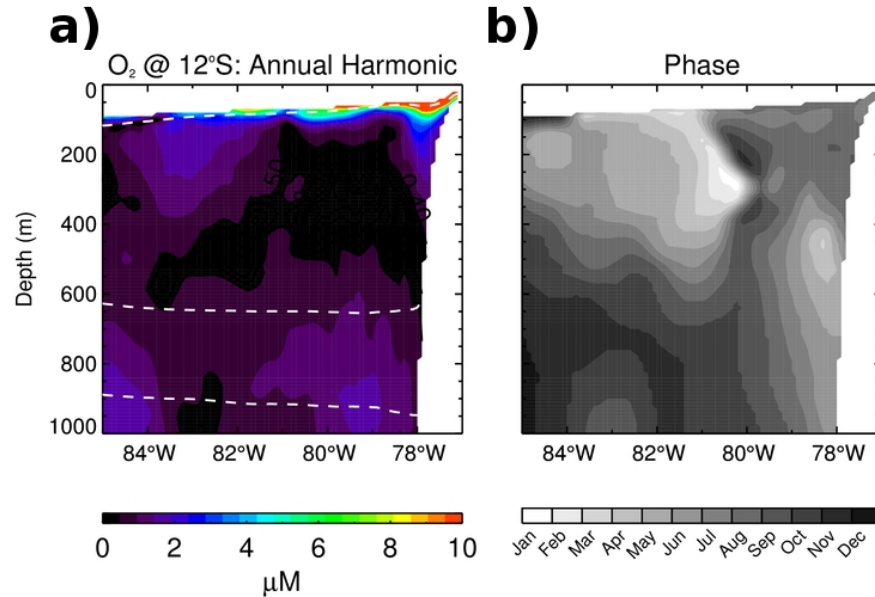


Figure A2. (a) Amplitude and (b) phase (in months) of the DO annual harmonic over a zonal section at 12°S (without normalization). Dashed lines in (a) correspond to the 20 et 45 μM mean DO isopleths.

C20. P12, L4: at this stage it is not clear what is meant with advection and mixing. What is about eddy fluxes, and horizontal diffusion?

R. (P14, L14): At this stage of the paper, we first diagnose the DO budget using the Eq. (1). Therefore, advection refers to the first rhs term in that equation, and mixing refers to the sum of the lateral and vertical mixing terms from the same equation (2nd and 3rd rhs terms in Eq. (1)). We are now referring to the Equation 1 for this sentence, that was added to the paper: “Advection corresponds to the first term on rhs of Eq. (1), whereas mixing refers to the sum of the lateral and vertical mixing terms (2nd and 3rd rhs terms in Eq. (1))”.

We have added arrows on to top of the parameters in Eq. 1 in order to clarify:

$$\frac{\partial O_2}{\partial t} = -\vec{u} \cdot (\vec{\nabla} O_2) + K_h \nabla^2 O_2 + \frac{\partial}{\partial z} \left(K_z \frac{\partial O_2}{\partial z} \right) + SMS(O_2)$$

C21. P13, L19: What does (deoxygenated) mean in brackets next to oxygen?

R. (P15, L28): A word was missing in this sentence. It was replaced by: “...the DO exchange between the coastal domain and the OMZ takes place through the offshore transport of DO poor waters by

eddies (Czeschel et al., 2011)...”.

C22. P14, L6: What is mixing here?

R. (P16, L23): Mixing refers here to “total” mixing that is: horizontal diffusion + vertical mixing + mixing associated with non-linear advection (see C1 in General Comments). Later on in the paper, unless stated otherwise, the term mixing alone (i.e. without specifying horizontal and/or vertical) will always refer to that. This has been clarified in the revised version of the manuscript (Section 2.3).

C23. P14, L27-30: What is the constant input of low oxygen waters? This should be mean advection. Please clarify or reformulate.

R (P17, L17-18): The reviewer is right. *Constant input* refers to the mean advection by the PUC. The sentence was changed to: “...balanced out by the mean advection of low DO waters carried by the PUC...”

C24. P16, L11: Mean seasonal flux: My understanding is that Fig 12a shows a contribution of annual oscillations to the mean oxygen budget as it is averaged over time. This is very different from the remaining part of the section “Mean seasonal flux”. Fig12c shows the annual oscillation of the DO eddy flux. Please clarify why these two terms are discussed together?

R (P19, L1): Following the reviewer’s recommendation we have clarified the text. By averaging the cross-product of the annual harmonics of velocity and DO, we obtain the contribution of the annual harmonic to the seasonal DO flux (i.e. $\langle u^{1\text{yr}} \cdot O_2^{1\text{yr}} \rangle$), which we compare to the annual harmonic of the DO eddy flux in order to highlight the different amplitude patterns. Our objective is here to identify the regions of influence of the different timescales of variability (annual versus intraseasonal) in terms of DO flux. For clarity we now present two figures: the Figure 14 for the mean annual flux (for DO and momentum) and the Figure 15 for the amplitude and phase of the annual DO eddy flux (cf. C2 in General Points). The text of the paper was modified accordingly.

C25. P16, L13: Is the seasonal DO flux maximum below 400 m? It is difficult to see as in Fig 12a as DO is normalized by the variance of its climatology. How does it compare to the contribution of the DO eddy flux to the mean budget?

R (P19, L5): Below 400m, the seasonal DO flux reaches values around 10% to 40% of those found around the depth of the oxycline, as illustrated in Figure A3a (which is similar to Fig. 14a of the revised version of the manuscript, but without normalization). At this location, the contribution of the annual DO flux is around 10 times larger than the contribution of the mean zonal eddy DO flux (Fig. A3b).

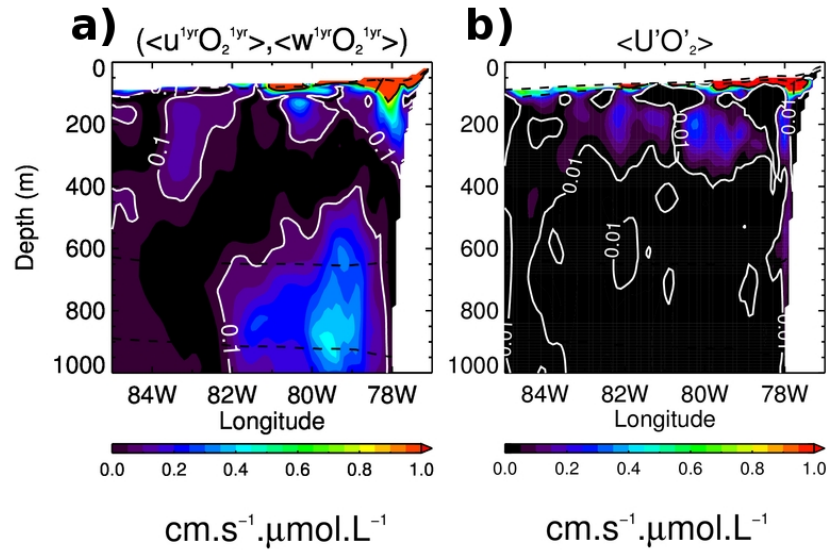


Figure A3. (a) Norm of the annual DO flux vector (i.e. $\sqrt{\langle u^{1yr} \cdot O_2^{1yr} \rangle^2 + \langle w^{1yr} \cdot O_2^{1yr} \rangle^2}$) for a cross shore section at 12°S. The superscript “1yr” refers to the contribution of the annual harmonic. (b) Mean zonal DO eddy flux along the same section. Dashed black contours indicate the 45 and 20 μM oxygen isopleths. Units are in $\text{cm s}^{-1} \mu\text{M}$.

C26. P16, L17: “annual energy flux vector”. Please be consistent throughout the manuscript with the use of annual” and “seasonal”. Here (Fig. 12b) annual is used, while for Fig. 12a seasonal is used. Annual is typical used for annual harmonics, while seasonal might be used for the mean seasonal cycle.

R (P19, L8): “Seasonal” was changed for “annual” when addressing the Figure 14a (Figure 12a in the first version of the manuscript). We checked for consistency throughout the paper and have done the necessary changes to the text.

C27. P17, L3: “thus” seems awkward at the beginning of a new section.

R (P19, L25): The sentence was changed to: “As previously described, the annual amplitude of the climatological DO eddy flux is the largest in the upper 400 m near the coast”

C28. P17, L4,5: Offshore transport of DO also depends on the DO gradient, which can be directed onshore or offshore (see e.g. Fig. 2c) and might vary on seasonal time scales.

R (P19, L28-30): The reviewer is right. The offshore transport will depend on the DO gradient direction. We have changed the sentence: “Since EKE is large along the coast of Peru, exchange of DO induced by eddies could be expected at all latitudes, with a direction that depends on the sign of the DO gradient at the coast”.

C29. P19, L17: latitudinal variability: variability of what? I am not sure what is meant: variability of meridional velocity?

R (P22, L16): This was a mistake. The correct sentence is: “At both boundaries, the zonal wavelength of the seasonal eddy flux variability along the boundary is estimated to be of the order of $\sim 10^2$ km, a scale that falls within the range of observed eddies diameter (Chaigneau and Pizarro, 2005), which indicates that locally there can be an injection or removal of DO across the boundary on average over a season”.

C30. P19, L18,19: I don't see the connection: Why indicate the existence of eddies that they can remove DO from the OMZ, which represents a up gradient flux? Can the DO eddy flux become negative or only anomalous weak?

R (P22, 19): The Figure 19 (Figure 16 in the first version of the manuscript) indicates that locally the DO eddy flux can be either positive or negative depending on the season, so that there can be a local injection or removal of DO across the boundary. The sentence has been clarified (see C29).

C31. P19, L24: “DO exhibits ... amplitude” seems not to be correct. I would suggest: ... regions with enhanced amplitude or specific propagation characteristics, suggesting ...

R (P28, L28): The sentence was changed following the suggestion of the reviewer: “The annual harmonic of DO reveals three main regions with enhanced amplitude or specific propagation characteristics, suggesting distinct dynamical regimes”.

C32. P20, L8: upper 300 m.

R (P29, L12): The sentence was changed to: “This appears to operate effectively in the upper 300 m”.

C33. P21, L6: suggestion: ...Anticyclone, and the peak in the seasonal DO eddy flux coincides with the reported ...

R (P27, L9-10): The sentence was changed following the suggestion of the reviewer: “and the peak in the seasonal DO eddy flux coincides with the reported intensity peak of the seasonal cycle of the Anticyclone”.

C34. P21, L9: Similar processes were discussed in Qiu et al. (2013, JPO).

R (P27, L12-16): We thank the reviewer for mentioning this interesting paper. We have added this reference to the text of the revised manuscript: “Dewitte et al. (2008) also report that intraseasonal (internal) variability in currents can originate from the interactions between the annual extra tropical

Rossby wave and the mean circulation in a medium resolution oceanic regional model over this region, a process also observed and documented from a high-resolution model over the North Pacific (Qiu et al., 2013).”

C35. P21, L20: please specify the range of frequency that you have in mind

R (P27, L25-26): We refer to the annual to interannual range. The sentence was changed to: “at frequencies ranging from annual (Dewitte et al., 2008) to interannual (Ramos et al., 2008)”.

C36. P31, Figure 1 and following figures: if used term „depth“ in contour labels or at the axes it should be always positive

R (P42): We thank the reviewer for pointing out that mistake. All the figures were modified accordingly.

C37. P32, L32: mean zonal speed

R (P43, L3): The sentence was corrected.

C38. P34, L5: what is total? Please define.

R (45, L4): We refer to the total Particulate Organic Carbon (POC) flux at the depth of 100m. We obtain this quantity by integrating the POC flux over the horizontal area in the Figure 5 (Figure 4 in the first version of the manuscript). This definition was added to the figure caption in order to clarify.

C39. P36, phase figure could be in color to better see the different regions/phase propagation

R (P48): The phase diagram was shaded in gray scale in order to highlight the phase variations.

C40. P36, L4-5: “ray paths for a baroclinic mode” seems not correct, as a single baroclinic mode cannot produce a ray path.

R (P48, L24-27): We agree with the reviewer. We have modified the manuscript and have clarified that we use the value of phase speed associated with different baroclinic modes to draw the WKB ray paths, in order to estimate the range of trajectories that WKB ray paths can take at a given frequency.

The caption of Figure 8 (Figure 6 in the first version of the manuscript) was changed to: “The slanted vertical lines indicate the theoretical WKB ray paths at a frequency of $\omega=2\pi\cdot 1\text{year}^{-1}$, for different value of phase speed. The theoretical trajectories were computed using the phase speed of the first (full), second (dashed) and third (dotted) baroclinic modes of a long Rossby wave.”

C41. P36, L6: oxygen not capital

R (P48, L29): Corrected.

C42. P39, caption: Solid white lines (c) denote

R (P51, L3): This was corrected.

C43. P40: Is horizontal diffusion from equation 1 included in one of these terms or is it neglected?

R (P52): Caption and title of Figure 12g (Figure 10g in the first version of the manuscript) was clarified. In particular “Mix” was replaced by Hmix+Vmix, in order to clarify that we are referring to horizontal and vertical diffusivity, respectively (i.e. the second and third terms on the rhs of Eq. 1).

C44. P41, L5,6: It is not clear, how to reconstruct the original fields from the EOF pattern, the principle components and RMS. Which terms are dimensional, which are non-dimensional, how is the RMS calculated, has the RMS units?

R (P53, L11-12): We have clarified this point (see also C17 in Specific Points): Figure 12 (Figure 10 in the first manuscript version) corresponds to the dimensionalized EOF mode patterns. These mode patterns were dimensionalized with (i.e. multiplied by) the RMS of the PC timeseries that are presented in normalized form in Figure 13 (Figure 11 in the first version of the manuscript). So multiplying the patterns by the associated timeseries of Figure 13 provides the reconstructed field (in dimensionalized units). The RMS values are therefore in dimensionalized unit.

The caption of Figure 13 (Figure 11 in the first manuscript version) was clarified as follows: “(a, b) Non dimensional principal components (PC) associated with the EOF patterns in Figure 12. Multiplying the principal component by the associated EOF pattern (from Fig. 12) yields a first EOF-mode reconstruction of the original field. RMS values of the principal components are indicated in parenthesis (corresponding units as in Fig. 12).”

C45. P41, L6: definition (region, width of the band along the coast, etc.) of alongshore winds, coastal sea level, Chl- a and MLD are required.

R (P54, L2-8): The recommended modifications were introduced to the figure caption: “...coastal alongshore wind (AS wind) and coastal alongshore wind Running Variance (variance over a 30 day running window) at 12°S, sea level at the coast at 12°S, surface chlorophyll-a from CR BIO (Chla) and from SeaWiFS (Chla SW) averaged over a coastal band of 2° width at 12°S, and Mixed Layer Depth at the coast (MLD) at 12°S”.

C46. P42, Fig. 12: This figure is very difficult to understand and addresses different topics (so far I can understand). From the given formulas, I would assume that Figs. 12a and b represent mean fluxes. Fig. 12a represents a contribution to the mean oxygen budget (however, the importance of such a term relative to other terms of the budget is unknown). Fig. 12C represents the annual cycle of the DO eddy flux corresponding to an annually oscillating on- and offshore DO flux (is this correct?). Why are these terms together in one figure? Other points regarding this Figure: a) units are not given, taken into account the normalization, it should be m/s. Is this correct? b) why is the unit m^2/s , how is it calculated? Arrows indicate vector direction and strength. For Fig. 12c a phase information would be helpful.

R (P55, Fig. 14): First in order to clarify, we have divided this figure in two separate figures: The new Figure 14 presents the norm of the annual DO and momentum flux vector, and the new Figure 15 presents the amplitude and phase of annual harmonic of the module of the seasonal DO eddy flux (see also C2 in General Points and C24 in Specific points).

The three terms in Figure 12 of the first manuscript version were initially discussed together in order to contrast the influence of the different timescales of variability on the DO flux (see C24 in Specific points).

The reviewer is correct: with the given normalization the units for the DO flux (Fig. 14a) are indeed m s^{-1} . The units were added to the figure.

The units in Figure 14b (Figure 12b in the first manuscript version) correspond to the product of the velocity and pressure, with pressure expressed in m, rather than the usual N m^{-2} , which yields m^2s^{-1} .

As suggested by the reviewer, a new figure that represents the annual amplitude and phase of the climatological DO eddy flux was included in the paper (cf. C2 in General Points).

C47. P42, L11: What is DO: O_2' or O_2^{1yr} . It is not clear, how the normalization is performed. I would suggest to be consistent throughout the manuscript in using either DO, O_2 , oxygen concentration etc.

R (P55): O_2' represents the intraseasonal DO anomaly, whereas O_2^{1yr} is the DO annual harmonic. O_2 was replaced by DO throughout the paper in order to be consistent. However, the symbol for oxygen is used in the figure titles. The figure caption was changed in order to clarify how the DO normalization was made. The text for the caption now includes the sentence (Fig. 14): “The DO signal was normalized by its Root Mean Square value before computing the annual harmonic, in order to

emphasize the flux patterns where DO concentration is very low”.

C48. P43, L6: delete “average profile”?

R (57, L5): Modified as suggested.

C49. P44, L5: direction and strength

R (P58, L5): Modified as suggested.

C50. P44, L5: include “mean oxygen values”

R (P58, L6): The sentence was modified to include this change.

C51. P45, L5: denote mean oxygen

R (P59, L3): Sentence corrected.

C52. P46, figure caption: very difficult to understand. Please clarify and better specify what is shown. Be consistent “dominant EOF” and “first EOF”. L6: “running variance of currents (dominant EOF mode)”: I am not sure what is meant. L7: “... section (blue line in Fig. 14)”. L13: “Dispersion” is very unusual term and I would suggest to find a better description of it. Are the spatial pattern normalized before calculating RMS and standard deviation.

R (P60-61): Following the reviewer’s suggestion, we have improved the notation. “dominant EOF” was replaced by “first EOF”. The running variance of the currents is now explained. It refers to the RMS of current intraseasonal anomalies over a 1-month running window, with the intraseasonal anomalies estimated as the departure from the monthly mean (like for the DO). We then compute the seasonal cycle of this field, and perform an EOF analysis in order to extract the spatial pattern, and the associated timeseries (plotted in Fig. 19b as the red line and in 19d as the full/dashed blue lines).

What we meant by dispersion is the error associated with a slightly different location of the northern and southern boundaries (cf. Figure 17 for the mean position of the boundaries). We selected sections parallel to the original section that are at a distance comprised between +/-120km (every ~20 Km), providing an ensemble of 12 EOF results. This ensemble is used to estimate the error defined as the standard deviation among 12 PC timeseries (for (b) and (d)) and EOF patterns (for (e)).

We have clarified the figure caption as follows (Fig. 19): “(a) First EOF mode of the seasonal cycle of the DO eddy flux normal to the section depicted in Fig. 17 by the dashed red line (Northern boundary).

(b) Principal component (PC) timeseries associated with the first EOF mode (black line). The red line in (b) corresponds to the PC timeseries associated with the first EOF mode of the seasonal cycle of the 30-day running variance of intraseasonal currents normal to the section. (c) First EOF mode of the seasonal cycle of the DO eddy flux normal to the oblique section depicted in Fig. 17 by the dashed blue line (Southern boundary). (d) PC timeseries associated with the first EOF mode (black line). The blue curves (full and dashed lines) in (d) corresponds to the PC timeseries associated with the first and second EOF modes of the seasonal cycle of the 30-day running variance of the intraseasonal currents normal to the section (computed as in (b)). Percentage of explained variance and RMS value are indicated in parentheses in the panels (b) and (d) (in $\text{cm s}^{-1} \mu\text{M}$ and cm s^{-1} , for DO eddy flux and currents respectively). White contours in (a) and (c) denote mean DO concentration values, in μM . (e) RMS of the spatial patterns (a) and (c), computed along the horizontal direction. Note the scale leap at 300 m. Red/blue shading in (b), (d) and (e) represents an estimate of the error associated with slight changes in the location of the boundaries, that is when the EOF is performed over a section that is located at a distance from the original section (cf. Figure 17) compromised between $\pm 120\text{km}$ (see text). The error corresponds to the standard deviation among 12 PC timeseries (for (b) and (d)) and EOF patterns (for (e)).”

C53. P47, Fig. 17: Why is the oxygen flux from the coastal boundary into the OMZ not back and forth as the eddy fluxes at the northern-southern boundaries? Fig. 12c would suggest this. L7: The position ... at which depth? Please also explain the green line, where it is calculated. Again, this schematic seems to mix mean and seasonally varying fluxes. Is this the aim?

R (P62): The reviewer is right. The DO flux at the coast should be represented by back and forth arrows. This has been corrected. (see Fig. A4).

The green line corresponds to the position of the $45\mu\text{M}$ mean DO isopleth, calculated at 25°S .

Although some mean features of the OMZ (the mean position of the $45 \mu\text{M}$ isopleth at 25°S , and the mean DO concentration at 100 m depth) are represented in the Figure 17 (new Figure 20), the aim of this figure is to synthesize the processes that intervene in the seasonal variability of the OMZ. The mean DO field was included only as a reference for the OMZ mean shape and position.

We added to the figure the modifications suggested by the reviewer concerning the representation of the DO flux from the coast, as well as the “Depth” axis label (Fig. A4). The figure caption was also improved. This figure corresponds to Figure 20 in the revised version of the manuscript.

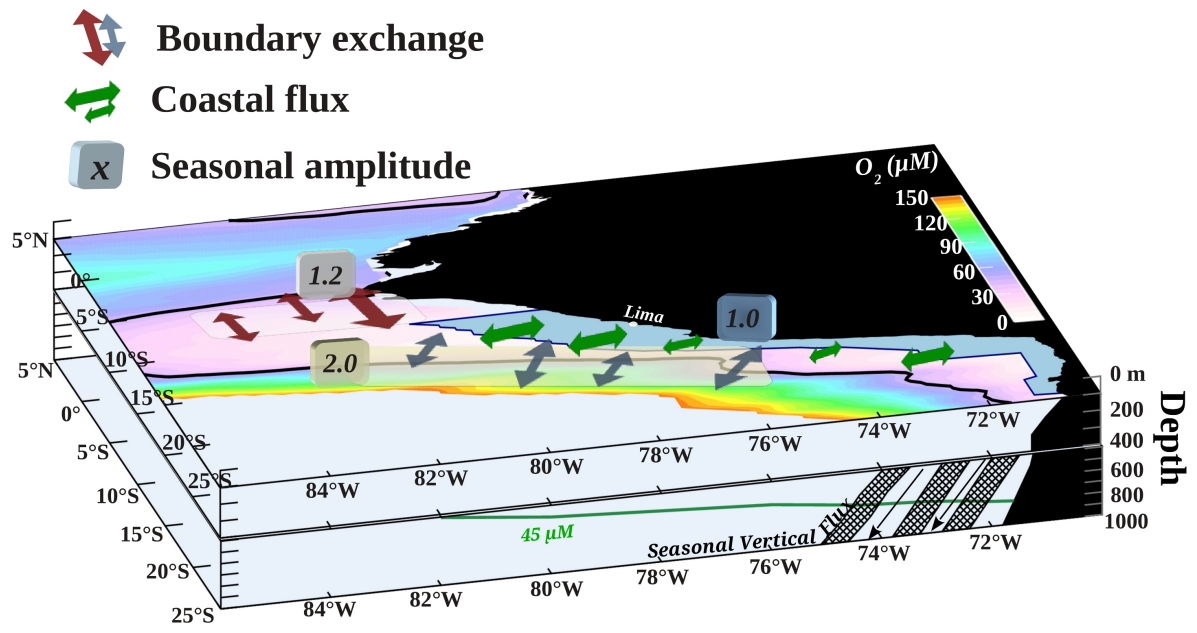


Figure A4. Schematic of the main processes driving the seasonal variability in the SEP OMZ: The DO eddy flux through the northern-southern boundaries and the DO flux that takes place at the coastal boundary of the OMZ. The coastal band limits are defined by the light blue shading adjacent to the coast. A scale of the seasonal amplitude of the eddy driven DO flux at each OMZ boundary is indicated (units in $\text{cm s}^{-1} \mu\text{M}$). The mean DO concentration (color shading) and the position of the 45 μM isopleth (thick black contour) at 100 m depth are also represented. The vertical/offshore DO flux induced by the propagation of the annual ETRW across the 45 μM isopleth at 25°S is represented in the bottom panel.

Response to Anonymous Referee #2

We would like to thank the anonymous reviewer for his/her detailed review and helpful comments. As suggested by the reviewer, we have modified the current organization of the paper, improving the model validation (including an EKE comparison between the simulation and the available data and a Taylor diagram; Section 2.2) and separating the discussion from the conclusions. Please note that the page and line numbers refer to the marked-up version of the revised manuscript.

1. Response to major comments

Comment 1 (C1): The additional section regarding the validation of the mesoscale activity within the model seems critical to identifying this mechanism. Specifically, the validation referenced in Gutknecht et al. 2013 seems to focus on validating the mean conditions, and Figure 6 of that work indicates some clear subsurface biases that need to be taken into account for these mechanisms. How do comparisons to the AVISO data set look? What about temperature? Can you rule out advection and confirm that the bias is in the biogeochemical model? The bias needs to be put in context –if the authors can describe the bias and then put their results in context that would provide much more information to the reader. The validation provided here is not only qualitative, but it also focuses on the average conditions. Some indication as to how well the model does at representing the variability and fluxes is necessary. Fluxes can include the SMS terms – like production. It is common now for Taylor or target diagrams to be used to visualize the metrics of skill, this work would benefit from one that may also include some physical terms and goes beyond the climatology.

Response (R.): We agree with the reviewer that it is important to validate the simulation as much as we can, not only in terms of mean state but also in terms of seasonal variability. This model configuration has been validated from satellite and in situ observations in a previous study for the physical component (Dewitte et al., 2012). In particular the model exhibits a rather realistic mean SST (see figure A1) and mean thermocline along the coast (validated from the IMARPE cruise data, see figure 9 in Dewitte et al. (2012)) and the model mean EKE is comparable to the available observations (Fig. A2), although in general more intense, consistently with other model simulations in the region (see for example Fig. 5 in Colas et al. (2012)). The mean circulation near the coast is also in agreement with former modeling studies (See figure 3f of Dewitte et al. (2012); Montes et al., 2010). While Dewitte et al. (2012) focused on the validation of the circulation at interannual and decadal timescales, we provide in this paper material for assessing the realism of the seasonal variability, which consists in the Figure 5b (Figure 7b in the revised manuscript version) showing the comparison between CARS and model DO in terms of the seasonality of the volume distribution. In addition to providing further material for assessing the simulation, and following the reviewer's recommendation, we have also added a Taylor diagram to the revised version of the paper (Fig. A3), which complements the validation of the mean state and seasonal cycle inside the OMZ (Fig. 6). We obtain similar results to Montes et al. (2014) in terms of DO, temperature and salinity (see figure 1 in Montes et al., (2014)).

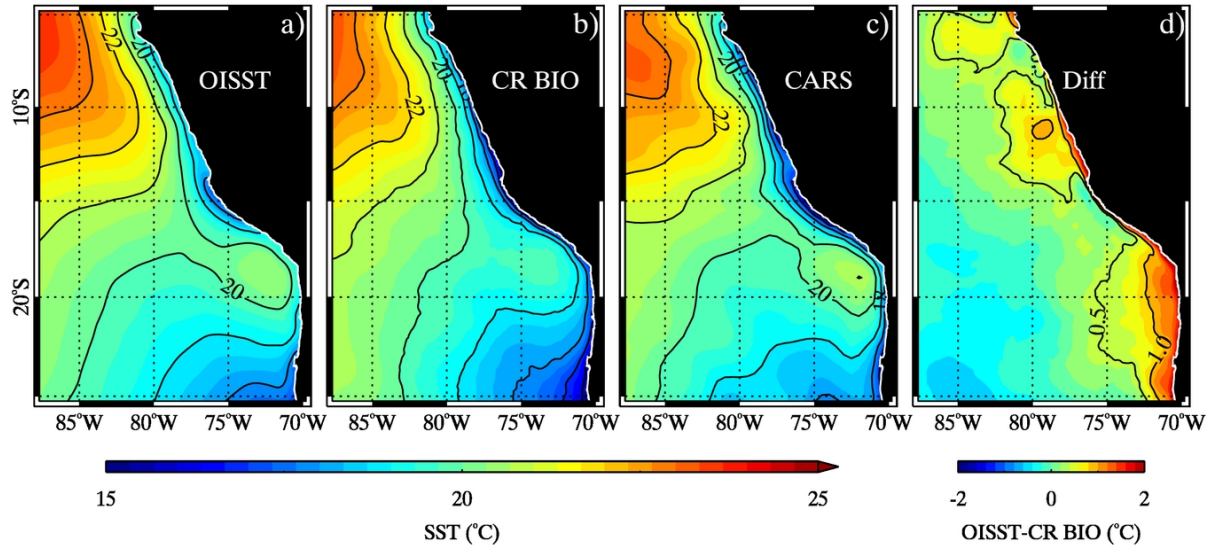


Figure A1. Mean sea surface temperature (SST) between 2000 and 2008 for (a) OISST product ($0.25^\circ \times 0.25^\circ$), (b) the simulation ($1^\circ/12$) and (c) CARS dataset ($0.5^\circ \times 0.5^\circ$). (d) Difference between the OISST product and the simulation.

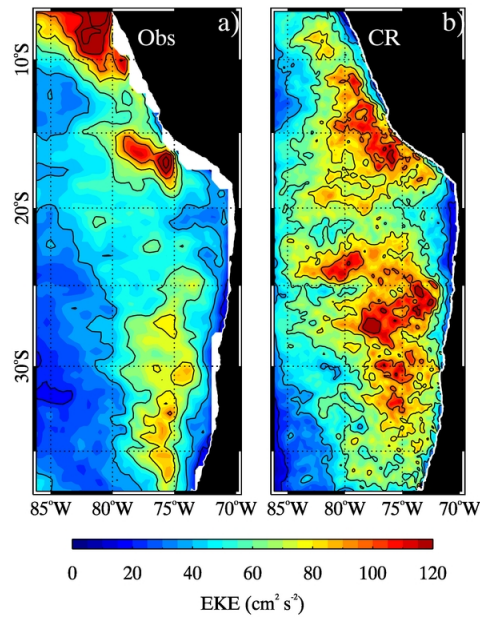


Figure A2. Mean Eddy Kinetic Energy (EKE) between 1993 and 2008 (satellite altimetry era), for (a) TOPEX/Poseidon Jason 1-2 merged product ($0.25^\circ \times 0.25^\circ$), and (b) Simulation ($1^\circ/12$). EKE was derived from the interannual anomalies of the geostrophic velocity field.

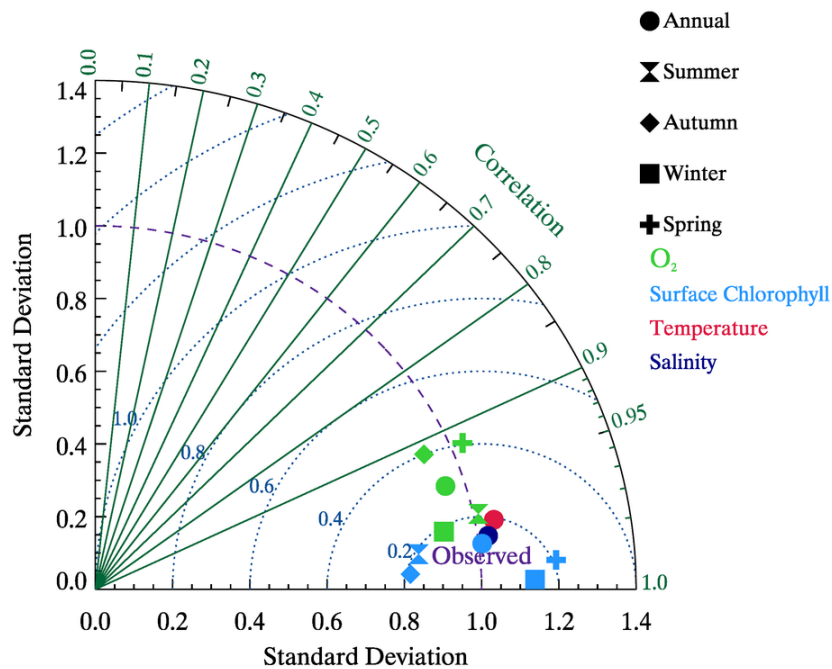


Figure A3. Taylor diagram of the seasonal mean (hourglass, diamond, square and cross) and annual mean (circle) pattern of DO and Surface Chlorophyll (25°S-5°N, 88°W-70°W). Only annual mean pattern comparisons are shown for temperature and salinity (same spatial domain). DO, temperature and salinity were vertically averaged between 100 and 600m depth (focus on the OMZ core). Only the surface chlorophyll values within 250 km next to the coast were considered. The comparisons are made between the simulation and CARS (for DO, temperature and salinity) and SeaWiFS (for surface chlorophyll). Ordinate and abscissa axes represent the standard deviation normalized by the observations standard deviation. Blue dotted radial lines indicate the RMS difference between the observations and the simulation.

References:

Colas, F., McWillimas, J. C., Capet, X., and Kurian, J.: Heat balance and eddies in the Peru-Chile current system. *Clim. Dyn.*, 39:509-529, doi:10.1007/s00382-011-1170-6, 2012.

Dewitte, B., Vazquez-Cuervo, J., Goubanova, K., Illig, S., Takahashi, K., Cambon, G., Purca, S., Correa, D., Gutierrez, D., Sifeddine, A., and Ortlieb, L.: Change in El Nino flavours over 1958–2008: Implications for the long-term trend of the upwelling off Peru, *Deep Sea Res., Part II*, 77–80, 143–156, doi:10.1016/j.dsr2.2012.04.011, 2012.

Montes, I., Colas, F., Capet, X., and Schneider, W.: On the pathways of the equatorial subsurface currents in the Eastern Equatorial Pacific and their contributions to the Peru-Chile Undercurrent, *J. Geophys. Res.*, 115, C09003, doi:10.1029/2009JC005710, 2010.

Montes, I., Dewitte, B., Gutknecht, E., Paulmier, A., Dadou, I., Oschlies, A., and Garçon, V.: High-

resolution modeling of the Eastern Tropical Pacific oxygen minimum zone: Sensitivity to the tropical oceanic circulation, *J. Geophys. Res. Oceans*, 119, doi:10.1002/2014JC009858, 2014.

C2: Also, the model climatology is an average over 10 years, while the data climatology is over 50 years. It seems a better apples to apples comparison could be made.

R.: The reviewer is correct, the duration of the experiment could impact the results obtained in the paper. In fact over the 50 years period of the climatological data set, the OMZ exhibits a decadal variability in the model which is difficult to validate from data (due to the scarcity of the data or the availability of data sets). The model is better constrained over the period 2000-2008, since the wind forcing uses the seasonal cycle from QuickSCAT data that spans 2000-2008 (cf. Goubanova et al. (2011) for details of the method for deriving the wind forcing), therefore we consider that it is more appropriate to concentrate over this period to calculate the seasonal cycle. Note that previous comparable modeling studies for this region (Penven et al., 2005; Montes et al., 2010; 2014; Echevin et al., 2011; Colas et al., 2012) have also used a wind forcing from QuickSCAT, which has provided a benchmark for assessing our simulation. We have expanded the text in the revised manuscript in order to better justify the focus on the 2000-2008 period.

References:

Echevin, V., Colas, F., Chaigneau, A., and Penven, P.: Sensitivity of the Northern Humboldt Current System nearshore modeled circulation to initial and boundary conditions, *J. Geophys. Res.*, 116, C07002, doi:10.1029/2010JC006684, 2011.

Goubanova, K., Echevin, V., Dewitte, B., Codron, F., Takahashi, K., Terray, P., and Vrac, M.: Statistical downscaling of sea-surface wind over the Peru–Chile upwelling region: diagnosing the impact of climate change from the IPSL-CM4 model. *Clim. Dyn.* DOI 10.1007/s00382-010-0824-0, 2011.

Penven, P., Echevin, V., Pasapera, J., Colas, F., and Tam, J.: Average circulation, seasonal cycle, and mesoscale dynamics of the Peru Current System: a modeling approach. *J. Geophys. Res.*, 110, C10021, 2005.

C3: The budget analysis is a powerful tool and has a lot of information within it. The authors appropriately use this tool to try and tease out the relative contribution of biological processes to the physical processes. It seems necessary to show the budget balances in the regions that this tool is used to discern the relative processes. A table of the budget terms would be one suggested way to achieve this goal. What does the climatological base budget look like? How big are the anomalies and residuals focused on in this work?

R. (P40): Following the reviewer’s recommendation we provide in the revised manuscript a table (Table A1) that summarizes the seasonal anomalies in the DO budget inside the OMZ (comparing the Austral winter and summer values).

Table A1. Austral summer (DJF mean) and winter (JJA mean) seasonal anomalies of the DO budget, averaged over the core of the Peru Under Current at 12°S (as depicted by the red contour in Figure 12). The values for the seasonal cycle and the reconstructed first EOF mode (Figures 12 and 13) are presented along with the difference Climatology-EOF. All values are in $10^{-6}\mu\text{M s}^{-1}$. Mixing here consists in the summe-up contribution of horizontal diffusion and $(K_h \nabla^2 O_2)$ and vertical diffusivity ($K_v \frac{\partial^2 O_2}{\partial z^2}$).

$$\frac{\partial}{\partial z} \left(K_z \frac{\partial O_2}{\partial z} \right)).$$

	Climatology		EOF		Difference	
	Summer	Winter	Summer	Winter	Summer	Winter
dO₂/dt	1.10	-2.74	1.30	-2.67	-0.2	-0.07
Adv	0.61	-9.38	0.85	-9.30	-0.24	-0.08
Mixing	-0.42	7.99	-0.35	7.99	-0.07	0.0
Biogeochemical Flux	0.91	-1.35	1.00	-1.35	-0.09	0.0

C4: The methods section ends with a paragraph that seems more like discussion – describing vertical model decomposition. This doesn't seem to be very well woven into the rest of the paper and comes off as a bit of a distraction or outlier.

R. (P13, L5): The reviewer is right. In fact the modal decomposition is only used for providing a range of values for the phase speed of the Extra-tropical Rossby wave consistent with the model stratification. The phase speed values are further used to draw possible trajectories of the WKB ray paths (Figures 8 and 14). Following the reviewer's suggestion, we have simplified this paragraph and complemented the text in the results section, when we described the related figures.

C5: Given the paper's premise that the high resolution study provides further information than a coarse simulation would, some comparison seems warranted showcasing that result.

R.: Since the focus of the study is on the eddy flux driving the seasonality of the OMZ boundaries, the use of a high-resolution model is a requirement considering that low-resolution models will not realistically simulate the eddy activity (in general too low in IPCC-class models). Here we could not compare the model outputs used as boundary conditions of our regional model (i.e. SODA) and the actual regional model simulation in terms of DO concentration and seasonal DO eddy flux, since SODA does not provide DO concentration and we have been using DO from CARS as boundary condition of the regional model. In fact we provide in the paper a qualitative comparison between global models and our simulation, based on the OMZ geographical overlapping index defined by Cabré et al. (2015), which indicates that our model simulation is rather realistic compared to global models. This has to be attributed not only to the model's ability to realistically resolve the mean upwelling thanks to its resolution, but it has to do also with the realism of the simulated turbulent flow. This is certainly something that would be worth quantifying through dedicated model experiments. However it is beyond the scope of the present paper.

References:

Cabré, A., Marinov, I., Bernardello, R., and Bianchi, D.: Oxygen minimum zones in the tropical Pacific across CMIP5 models: mean state differences and climate change trends, *Biogeosciences*, 12, 6525-6587, doi:10.5194/bg-12-6525-2015, 2015.

C6: Some of the framing in the abstract about greenhouse gases is isolated there. While it is interesting, the authors never return to that idea in the discussion. Either return to it or remove those ideas.

R. (P28, L19): We agree with the reviewer on the importance of this point, in terms of the impact of the OMZ and its variability. Rather than removing it, we elaborated on this idea in the discussion, in terms of the implications that the seasonal ventilation of the OMZ could have on the nitrogen and carbon cycle that take place in the hypoxic region of the OMZ. We added the following paragraph to the discussion section: “Lastly, the seasonal changes in the OMZ evidenced in this work are associated with a seasonal change of the oxycline depth (and an oxycline intensity change; not shown), which can be considered a proxy for the production of greenhouse gases (CO₂ and N₂O) inside the OMZ (e.g. Paulmier et al., 2011; Kock et al., 2016). Our results suggest that the impact of the OMZ on the atmosphere through the production of climatically-active gases, such as CO₂ and N₂O, would be seasonally damped during austral winter, due to a deepening of the oxycline and a weakening of its intensity”.

References:

Kock, A., Arévalo-Martínez, D. L., Löscher, C. R., and Bange, H. W.: Extreme N₂O accumulation in the coastal oxygen minimum zone off Peru, *Biogeosciences*, 13, 827-840, doi:10.5194/bg-13-827-2016, 2016.

Paulmier, A., Ruiz-Pino, D., and Garçon, V.: CO₂ maximum in the oxygen minimum zone (OMZ), *Biogeosciences*, 8, 239–252, doi:10.5194/bg-8-239-2011, 2011.

2. Response to minor technical comments

C1: Lines 10-12 on Page 9 of the introduction points blame at the resolution of the CARS data set – the authors could add this resolution to some of their figures in order to better make this point, but without proper validation of the model, it is hard to blame the observations.

R. (P10, L14-15): The resolution was added to the figures in order to improve comparisons (cf. C3 in the Figure comments section).

C2: Line 4 on Page 3 – in introduction – understand should be understanding.

R. (P3, L5): This was corrected.

C3: Lines 10-11 on Page 3 in intro – The sentence beginning with Furthermore refers to a process called “habitat compression”. The phrase may be more clear than the current explanation.

R. (P3, L13-15): Following the reviewer's suggestion, we replaced the original sentence: “Furthermore, the OMZs contribute to the habitat compression of marine organisms, in a zone that sustains 10% of the world fish catch (Prince and Goodyear, 2006; Chavez et al., 2008)”.

References:

Chavez, F. P., Bertrand, A., Guevara-Carrasco, R., Soler, P., and Csirke, J.: The northern Humboldt Current System: Brief history, present status and a view towards the future, *Prog. Oceanogr.*, 79, pp. 95–105, 2008.

Prince, E. D., and Goodyear, C. P.: Hypoxia-based habitat compression of tropical pelagic fishes. *Fish. Oceanogr.* 15:6, 451-464, doi:10.1111/j.1365-2419.2005.00393.x, 2006.

C4: Line 12 page 16 – Relatively should be Relative.

R. (P19, L4): Corrected.

3. Response to figure comments

C1: The main comment in all the figures from the model fields is about the white space – what does it indicate?

R.: The white space represents a region where no data is available. In order to avoid confusion, we added this information in each figure caption where this is present.

C2: Figure 1 seems to indicate the model does not achieve the same onshore/offshore gradients in oxygen around 10 deg S. This seems critical to some of the points in the paper about transport mechanisms and goes unaddressed in the text.

R.: The reviewer is right. This could be a model bias. Note however that this is still in the range of what is expected from the use of different ocean boundary conditions. In particular, Montes et al. (2014) compared two simulations with OBCs having a slightly different mean circulation near the equator, and found differences between the simulations that are comparable to the one between CARS and our simulation. In addition it should be pointed out again that CARS data set is built from data covering a different period than our simulation, which could also explain the differences. It is difficult here to demonstrate if the difference between model and data originate from model bias, decadal variability or sampling issue in the data set. This has been mentioned in the text of the revised manuscript (P9, L15-17).

C3: Figures 1-3 would benefit from additional dots on the figures to identify where the samples the made up the climatology from the observations were made. The reader could discern from that addition the errors in interpolation to errors in the model.

R.: As suggested by the reviewer, the spatial resolution was included on the margins of the mentioned figures (as dots), in order to avoid difficulties in the interpretation. Figures 1-3 correspond to Figures 2-4 in the revised version of the manuscript.

C4: Figure 4 would benefit from isobaths contours so the shelf region was highlighted.

R.: The figure (Fig. 5 in the revised version of the manuscript) was modified as suggested by the reviewer.

C5: Figure 5 seems to indicate the model is biased high – that the model underestimates the hypoxic volume. Is that because of advection, temperature, or the bio model? Or could it be the different time periods compared between the model and obs?

R.: As pointed out by the reviewer, the simulation underestimates the hypoxic volume by ~6% compared to CARS, although very similar discrepancies between model and data have been obtained by previous modeling studies (e.g. Montes et al., 2014). As suggested by the reviewer, this could be due to several factors, including the OBCs used in our experiment, as well as the different time periods used to compute the DO climatology. Also, the model does not consider the benthic exchanges (no

sediment model) that would tend to consume oxygen near the coast at the bottom of the water column, and could also explain such deficiency. Following the reviewer recommendation, we further expanded on this point in order to contextualize our results (P25, L21).

C6: Figure 6 – this figure and discussion are out of context and need to be reorganized at a more appropriate time in the results. These numbers need to be put in context with the other important fluxes as you do in the budget. So this needs to follow the budget.

R. (P13, L20-25): The purpose of Figure 6 (Figure 8 in the revised version of the manuscript) is to illustrate the spatial heterogeneity of the seasonal DO signal across the OMZ (Fig. 8a and 8b), and to document the propagating characteristics at different depths (Fig. 8c and 8d). It aims at introducing the idea that the upper OMZ seasonal cycle is eddy driven while the lower OMZ seasonal cycle is influenced by the propagation of the annual ETRW (Section 4.2). We believe that it would be confusing if we present it after the budget. Still, we have clarified the text at the beginning of Section 3, so as to put the figure and discussion in context. The text was modified as follows:

“3 Characteristics of the DO annual cycle

While the annual signal is a conspicuous feature inside the region (Fig. 6), it could manifest differently across the OMZ. As a first step towards investigating processes driving the rate of DO change, it appears important to document the vertical structure variability of the DO annual cycle within the OMZ. The amplitude and phase of the annual harmonic of the model DO climatology is presented along a zonal section off central Peru (12°S, Fig. 8ab), where the OMZ core is extensive (Fig. 2”).

C7: Figure 8 a and b panels do not appear to be on the same scale. Refer to Equation 2 from the text in the caption.

R.: They are indeed not in the same scale because the variability of the physical flux tends to be much larger than the variability of the biogeochemical flux. The equation 2 is not used for this figure (Fig. 10 in the revised version of the manuscript), it is just the variability (RMS), which can be viewed here as a measure of the amplitude of the seasonal cycle.

C8: Figure 10 is confusing but important. Clarity to the reader would be achieved through a longer caption explaining the different colorbars in a-c and d-g, as well as the percentages – which don’t add up. Why is the undercurrent identified? Is it referred to in the text? Are these all model results? What transect is this in the domain? Does the choice of the transect change the results? The text refers to this figure describes seasonality, but this figure just says climatology – is it a seasonal climatology? In that case, what time of year is shown?

R. (P52): Following the reviewer’s recommendation, we have detailed and improved the caption. The figure was also modified (Figure 12 of the revised manuscript version). This figure displays the results of an EOF analysis performed on different climatological fields for a zonal section at 12°S. Each percentage indicates the variance explained by the first EOF mode, for each field, in order to ascertain that the mode that is presented accounts for a significant share of the variance, and that we are not describing some peculiarities of the climatological fields. Therefore, the percentages are not meant to be summed-up. The temporal variability of these EOF mode patterns is provided in Figure 13 of the revised version of the manuscript.

The signal represented corresponds to the seasonal cycle, or seasonal climatology (see also the reply to C3 in major comments)

In our interpretation of the results, the seasonal intensification (destabilization) of the coastal

alongshore current plays a decisive role in the seasonal DO changes at the shelf, which is to a large extent associated with transport within the Peru Chile Undercurrent (Montes et al., 2010), that is why it is included in the panels of Figure 12 and mentioned several times in the text.

We choose to illustrate the seasonality of the OMZ with a section at 12°S given that it is located at the core of the OMZ. The results are insensitive to the choice of the latitude at which the EOF analysis is performed, for a given latitude between 7°S and 14°S, which corresponds to the latitude range where the PUC is well defined (See for instance the results for 9°S (Fig. A4)).

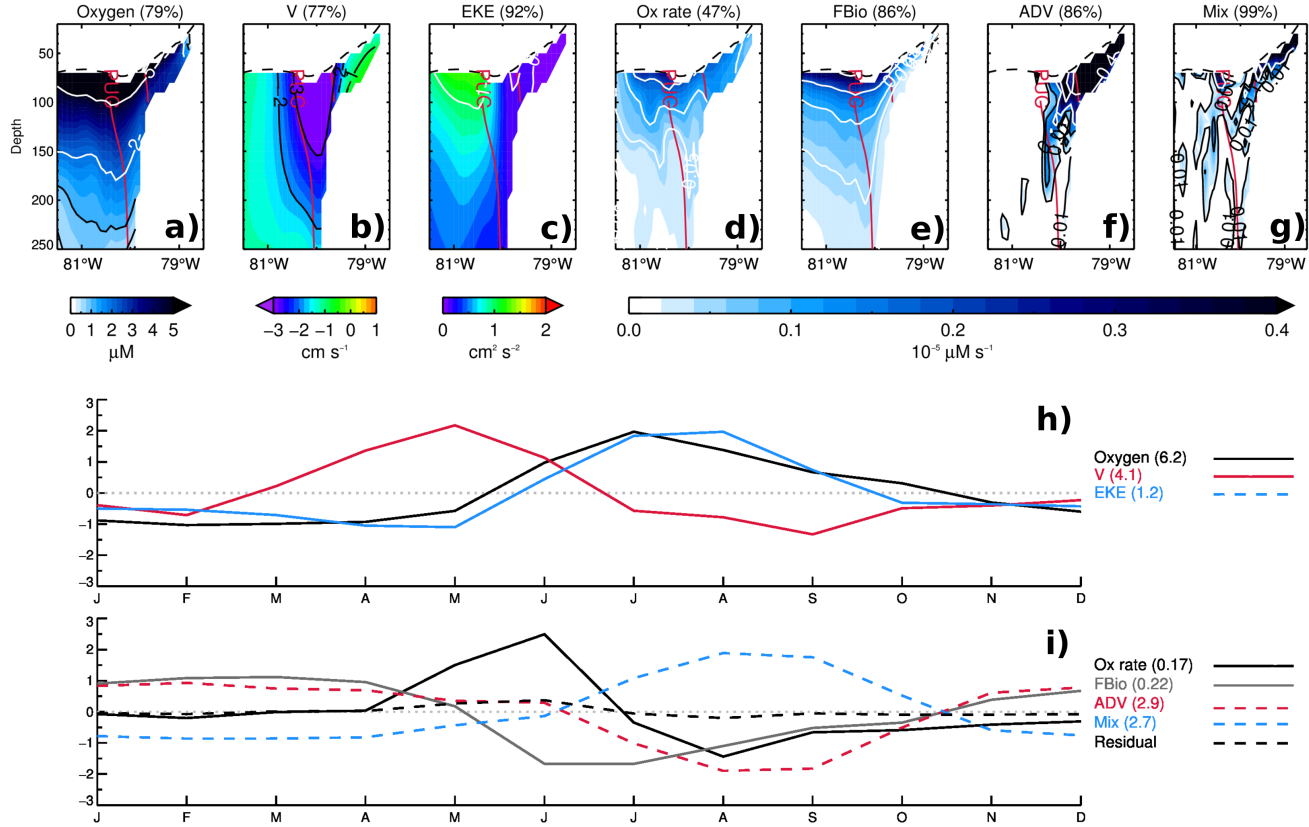


Figure A4. First EOF mode pattern of (a) DO, (b) Alongshore currents component, (c) Eddy Kinetic Energy, (d) oxygen rate, (e) biogeochemical flux, (f) advective terms (sum of horizontal and vertical components) and (g) mixing terms (sum of horizontal and vertical components). Percentage of explained variance by each EOF mode pattern is indicated in parentheses on top of each panel. The red contour denotes the mean position of the Peru Under Current core, defined here as along-shore southward current exceeding 4 cm s^{-1} . The black dashed contour denotes the mean DO 45 μM isopleth. (h, i) Non dimensional principal components (PC) associated with the EOF patterns. RMS values are indicated between parentheses. The residual corresponds to the difference between the rate of DO change and the sum of all the terms of the rhs of Eq. 1 in terms of the normalized PC timeseries. The weak residual indicates that the seasonal DO budget can be interpreted from the EOF decomposition. The EOF decomposition was performed over the climatological (mean seasonal cycle) fields. Multiplying the EOF pattern by the corresponding PC timeseries yields the contribution of the first EOF mode to the original field, in dimensionalized units. Land and the region outside the 45 μM mean DO isopleth are masked in white (a-g).

C9: Figure 11 requires more explanation as to how it was made. No explanation of residuals etc is provided in the text. How should the reader interpret the residual? Is it meant to just be physical?

R. (P53-54): Following the reviewer's recommendation we have detailed the caption of Figure 11 (Fig. 13 in the revised manuscript version; see also C8). The residual is computed from the difference between the principal component of the rate of DO change and the summed-up contribution of the principal components corresponding to the physical and biogeochemical DO fluxes in terms of the normalized PC timeseries. This calculation is performed in order to verify that the DO budget based on the EOF decomposition is almost closed, which allows for its interpretation.

The residual should be interpreted as the "error" in approximating the terms of the DO budget by their first EOF component. This approximation has the advantage of synthesizing the DO budget, yielding (1) a spatial pattern that allows identifying where the seasonal variations are more important and (2) the phase of the seasonal maximum.

As suggested by the reviewer, the caption of the Figure 11 (now Fig. 13) was improved in order to clarify what the residual means: "The residual corresponds to the difference between the rate of DO change and the sum of all the terms of the rhs of Eq. 1 in terms of the normalized PC timeseries. The weak residual indicates that the seasonal DO budget can be interpreted from the EOF decomposition.".

1 **Seasonal Variability of the Oxygen Minimum Zone off Peru in a**
2 **high-resolution regional coupled model**

3
4 **O. Vergara¹, B. Dewitte¹, I. Montes², V. Garçon¹, M. Ramos^{3,4,5}, A. Paulmier¹, and O.**
5 **Pizarro^{6,7}**

6
7 [1]{Laboratoire d'Études en Géophysique et Océanographie Spatiales, CNRS/CNES/UPS, UMR5566,
8 Toulouse, France}

9 [2]{Instituto Geofísico del Perú (IGP), Lima, Perú}

10 [3]{Departamento de Biología, Facultad de Ciencias del Mar, Universidad Católica del Norte,
11 Coquimbo, Chile}

12 [4]{Millennium Nucleus for Ecology and Sustainable Management of Oceanic Islands (ESMOI),
13 Coquimbo, Chile}

14 [5]{Centro de Estudios Avanzado en Zonas Áridas (CEAZA), Coquimbo, Chile}

15 [6]{Department of Geophysics, University of Concepcion, Chile}

16 [7]{Millennium Institute of Oceanography, Chile}

17

18 Correspondence to: O. Vergara (oscar.vergara@legos.obs-mip.fr)

1 Abstract

2 In addition to being one of the most productive upwelling systems, the oceanic region off Peru is
3 embedded in one of the most extensive Oxygen Minimum Zones (OMZs) of the world ocean. The
4 dynamics of the OMZ off Peru remain uncertain, partly due to the scarcity of data and to the ubiquitous
5 role of mesoscale activity on the circulation and biogeochemistry. Here we use a high-resolution
6 coupled physical/biogeochemical model simulation to investigate the seasonal variability of the OMZ
7 off Peru. The focus is on characterizing the seasonal cycle in Dissolved O₂ (DO) eddy flux at the OMZ
8 boundaries, including the coastal domain, viewed here as the eastern boundary of the OMZ,
9 considering that the mean DO eddy flux in these zones has a significant contribution to the total DO
10 flux. Along the coast, despite the increased seasonal low DO water upwelling, the DO peaks
11 homogeneously over the water column and within the Peru Undercurrent (PUC) in austral winter,
12 which results from mixing associated with the increase in both the intraseasonal wind variability and
13 baroclinic instability of the PUC. The coastal ocean acts therefore as a source of DO in Austral winter
14 for the OMZ core, through eddy-induced offshore transport that is also shown to peak in Austral winter.
15 In the open ocean, the OMZ can be divided vertically into two zones: an upper zone above 400m where
16 ~~DO eddy flux dominates over the mean seasonal DO flux~~ the mean DO eddy flux is larger on average
17 than the mean seasonal DO flux, and varies seasonally, and a lower part where the mean seasonal DO
18 flux exhibits vertical-zonal propagating features that share similar characteristics than those of the
19 energy flux associated with the annual extra-tropical Rossby waves. At the OMZ meridional boundaries
20 where the mean DO eddy flux is large, the DO eddy flux has also a marked seasonal cycle that peaks in
21 austral winter (spring) at the northern (southern) boundary. In the model, the amplitude of the seasonal
22 cycle is 70% larger at the southern boundary than at the northern boundary. Our results suggest the
23 existence of distinct seasonal regimes for the ventilation of the OMZ by eddies at its boundaries.
24 ~~Results-implications~~Implications for understanding the OMZ variability at longer timescales are
25 discussed.

1 **1 Introduction**

2 In addition to hosting one of the most productive upwelling systems, the South Eastern Pacific (SEP) is
3 home to one of the most extensive Oxygen Minimum Zones (OMZs) of the world ocean (Fuenzalida et
4 al., 2009; Paulmier and Ruiz-Pino, 2009). These oxygen deficient regions are key to
5 ~~understand~~understanding the role of the ocean in the greenhouse gases budget and in climate, and in the
6 ~~present~~presently unbalanced nitrogen cycle (Gruber, 2008). The OMZs represent a net nitrogen loss to
7 the atmosphere in the form of N₂O (particularly the SEP OMZ: Farías et al., 2007; Arévalo-Martínez et
8 al., 2015), in addition with other toxic or ~~climatic gases~~ climatically-active gases, such as H₂S and CH₄,
9 respectively, in extremely low dissolved oxygen (DO) concentrations (Libes, 1992; Law et al., 2013).
10 They might even limit the ~~CO₂-sequestration ocean role~~ ocean carbon sequestration and act as CO₂
11 sources for the atmosphere (Paulmier et al., 2008; 2011). ~~Furthermore, the OMZs represent a~~
12 ~~respiratory barrier for marine organisms, and restrain their niche habitat in a zone which sustains 10%~~
13 ~~of the world fish catch (Chavez et al., 2008)~~ Furthermore, the OMZs contribute to the habitat
14 compression of marine organisms, in a zone that sustains 10% of the world fish catch (Prince and
15 Goodyear, 2006; Chavez et al., 2008). Therefore, understanding the dynamics behind the OMZ
16 becomes not just a matter of scientific interest, but also a major societal concern.

17 In general, these low oxygen regions are considered to result from the interaction of biogeochemical
18 and physical processes (Karstensen et al., 2008). The SEP presents high biological productivity,
19 inducing a significant DO consumption mainly through the remineralization associated with a complex
20 nutrient cycle supported by the intense upwelling. In addition, the SEP encompasses a so-called
21 'shadow zone', a near stagnant/sluggish circulation region next to the eastern basin boundary, not
22 ventilated by the basin scale wind driven circulation (Luyten et al., 1983). Assuming a steady state,
23 lateral oxygen fluxes from subtropical water masses and diapycnal mixing are expected to balance the
24 oxygen consumption (Brandt et al., 2015). However, the diversity of environmental forcings in the SEP,
25 and the variety of timescales at which they operate (Pizarro et al., 2002; Dewitte et al., 2011; 2012) has
26 eluded a proper understanding of the processes controlling the OMZ structure and variability. On the
27 one hand, the scarcity of data and rare surveys have only permitted to document the DO temporal
28 variability at a few locations (e.g. Morales et al., 1999; Cornejo et al., 2006; Gutiérrez et al., 2008;
29 Llanillo et al., 2013). On the other hand, the highly complex interaction between physical and
30 biogeochemical mechanisms makes modeling and prediction of OMZ location, intensity and its

1 temporal variability a challenging task (Karstensen et al., 2008; Cabré et al., 2015). Low resolution
2 CMIP class coupled models still have severe biases of physical and biogeochemical origins,
3 particularly in Eastern Boundary Current systems (Richter, 2015), which has eluded the interpretation
4 of long term trends in OMZ (Stramma et al., 2008; 2012; Cabré et al., 2015). Regional coupled
5 biogeochemical modeling nonetheless has provided a complementary approach to gain insight in the
6 dynamics of OMZ and its relationship with climate (Resplandy et al., 2012; Gutknecht et al., 2013a).
7 One recent modeling effort in understanding the dynamics behind the OMZ in the Eastern Tropical
8 Pacific comes from Montes et al. (2014). This study provided a first regional simulation of the OMZ in
9 the SEP, and summarized the elements involved in maintaining the OMZ found off the coast of Peru as
10 resulting from a delicate balance between (i) the equatorial current system dynamics: the relatively
11 oxygen-rich waters carried by the Equatorial Undercurrent (EUC), the relatively oxygen poor and
12 nutrient rich waters carried by the primary and secondary Tsuchiya Jets (primary and secondary
13 Southern Subsurface Countercurrents, pSSCC and sSSCC, respectively), and (ii) the high surface
14 productivity rates induced by the coastal upwelling, which in turn triggers an intense oxygen
15 consumption in the subsurface. Their model experiments also showed that different Eddy Kinetic
16 Energy (EKE) levels, induced by different representations of the mean vertical structure of the coastal
17 current, may contribute to expand or erode the upper boundary of the OMZ.

18 The study by Montes et al. (2014) established a benchmark in terms of numerical modeling of the OMZ
19 in the SEP, focusing on its permanent regime and connection with the equatorial current dynamics. In
20 the present study, we also take advantage of the regional modeling approach in order to investigate the
21 mechanisms associated with the seasonal cycle of DO within the OMZ. The motivation for focusing on
22 seasonal variability is three-folds: 1) A better knowledge of the processes acting on the OMZ at
23 seasonal timescale is viewed as a prerequisite for interpreting longer timescales of variability (ENSO,
24 decadal); 2) the scarcity of quality long term subsurface biogeochemical data in the SEP is a limitation
25 for tackling the investigation of OMZ variability at low frequency; 3) To the authors' knowledge, this
26 issue has not been addressed in the literature for the Eastern Tropical Pacific, although it has been a
27 concern for other tropical oceans (Resplandy et al., 2012; Gutknecht et al., 2013a; Duteil et al., 2014).
28 Here, besides investigating to which extent the seasonal OMZ variability can relate to the variability of
29 the environmental forcing in the SEP (local wind, equatorial Kelvin and extra-tropical Rossby waves),
30 our interest is on examining the DO budget (i.e. the balance between oxygen sources and sinks) and

1 relating it to the physical DO flux. In particular, since the Peruvian region is the location of a relatively
2 intense eddy activity (Chaigneau et al., 2009), the question of whether or not eddy activity is involved
3 in the seasonal variability of the OMZ arises, and calls for assessing its contribution to the DO flux.
4 There is growing evidence that mesoscale activity has a key role on the biogeochemical cycles and the
5 OMZ structure in EBUS (Duteil and Oschlies, 2011, Nagai et al., 2015). Most studies addressing the
6 role of mesoscale processes in the OMZs have focused on the ventilation from the coastal domain,
7 where the primary production bloom provides nutrients and DO anomalies that are in turn transported
8 offshore (Stramma et al., 2013; Czeschel et al., 2015; Thomsen et al., 2016). Gruber et al. (2011)
9 showed that mesoscale activity is prone to reduce the biological production and offshore [carbon](#) export
10 in upwelling systems by both rectifying on the mean circulation (i.e. [eddies](#)-induced mixing tends
11 to flatten the isotherms nearshore and reduce the upwelling) and changing its nutrient transport
12 capacity. This process has been to some extent supported by observations in the Peruvian OMZ
13 (Stramma et al., 2013). In this sense, the mesoscale activity represents a ventilation pathway for the
14 OMZ, through the offshore transport of [OMZ-properties oxygen-enriched waters](#). The ventilation of the
15 OMZ could also take place at its meridional boundaries where strong mean DO gradients are found
16 along with eddy activity. Recently, Bettencourt et al. (2015) proposed that mesoscale eddies shape the
17 Peruvian OMZ by controlling the diffusion of DO into the OMZ at the meridional boundaries.
18 Although it is likely that both processes are important for understanding the OMZ structure, it has not
19 been clarified to which extent the variability of the OMZ could be understood in terms of the changes
20 in the DO eddy flux into the OMZ through these different pathways. The mesoscale activity also
21 exhibits a significant meridional variability off Peru (Chaigneau et al., 2009), which questions if the
22 offshore ventilation process can operate effectively for modulating the whole OMZ. Another related
23 open question is at which timescales the ventilation process through eddies-induced mixing can operate
24 effectively. In this paper we will tackle these issues from a regional modeling approach, focusing on the
25 seasonal timescale.

26 The paper is organized as follows. After the Introduction (Section 1), we detail the observations and
27 model configuration used in the study, as well as the methodology employed in the treatment of the
28 information (Section 2). We also evaluate the realism of the simulation against the available
29 observations in reproducing the main characteristics of the OMZ. The subsequent section (Section 3)
30 characterizes the DO annual cycle inside the OMZ. Section 4 opens with the analysis of the seasonal

variability of the coastal OMZ, and the contribution of the DO budget terms associated with it. This analysis is followed by the results on DO flux directed offshore and completed by the analysis of DO flux across the OMZ meridional boundaries. ~~The final section (Section 5) presents a summary and a discussion of the main results, followed by perspectives for future work. Section 5 presents a discussion of the main results and Section 6 presents a summary and the concluding remarks.~~

2 Data description and Methods

2.1 Data

Dissolved Oxygen concentration from CARS

The CSIRO Atlas of Regional Seas (CARS) is a climatological product derived from a quality-controlled archive of historical subsurface ocean measurements, most of which was collected during the past 50 years (Additional information might be found in the website of the project: <http://www.marine.csiro.au/~dunn/cars2009/>). For the present study, we use the CARS2009 version of the CARS product (Ridgway et al., 2002), which has an horizontal resolution of $0.5^{\circ} \times 0.5^{\circ}$ and 79 vertical levels, with a 10m resolution near the surface layer. We use CARS to assess the model skills in simulating the OMZ mean state and variability. One advantage of this product is its refined interpolation treatment near steep topography, in comparison to other products such as the World Ocean Atlas (Dunn and Ridgway, 2002). Also, it includes the annual and semiannual oxygen cycles, although the semiannual cycle is available only for the first 375 m over the region of interest due to the scarcity of data.

Chlorophyll-a concentration from SeaWiFS

SeaWiFS 8 day composites at $0.5^{\circ} \times 0.5^{\circ}$ resolution chlorophyll product (version 4), between January 2000 and December 2008, is used to compute the surface chlorophyll seasonal cycle (McClain et al., 1998; O'Reilly et al., 2000).

Sea Surface Temperature (SST)

The NOAA Optimum Interpolation SST (OISST V2) product, is contrasted against the simulation SST. This product is an analysis constructed by combining observations from different platforms (satellites, ships, buoys) on a regular global grid. More information about the methodology used to construct this data set may be found in Reynolds et al. (2007), and the product website (<https://www.ncdc.noaa.gov/oisst>). The version used in this study corresponds to daily SST maps with

1 | [a spatial resolution of 0.25°x0.25°, spanning the period 2000-2008.](#)

2 | **Sea Level Height (SLH)**

3 | [TOPEX/JASON1 merged SLH data set, distributed by the Sea Level Research Group, University of](#)
4 | [Colorado \(<http://sealevel.colorado.edu/>\) is used to derive the geostrophic velocity field and the mean](#)
5 | [EKE field. This data set corresponds to a globally-gridded 0.25°x0.25° weekly product. The](#)
6 | [information used corresponds to the period 1993-2008. Further details on this product may be found in](#)
7 | [Nerem et al. \(2010\).](#)

8 | **2.2 Model simulation**

9 | We use a high resolution simulation of the South Eastern Pacific, based on the hydrodynamic model
10 | Regional Ocean Modeling System (ROMS) circulation model (see Shchepetkin and McWilliams,
11 | 2005; 2009 for a complete description of the model) coupled with a nitrogen-based biogeochemical
12 | model developed for the Eastern Boundary Upwelling Systems (BioEBUS, Gutknecht et al., 2013ab),
13 | hereby referred as CR BIO.

14 | The model is used at an eddy-resolving resolution ($1/12^\circ$ at the equator) for a region extending from
15 | 12°N to 40°S and from the coast to 95°W -nevertheless this study only focuses on the domain spanning
16 | the latitudes of Peru and Ecuador (Fig. 1)- with lateral open boundaries at its northern, southern and
17 | western frontiers. The physical model resolves the hydrostatic primitive equations with a free-surface
18 | explicit scheme, and a stretched terrain-following sigma coordinates on 37 vertical levels. The
19 | configuration is similar to Dewitte et al. (2012), that is the open boundary conditions are provided by
20 | 3-daily mean oceanic outputs from SODA (Version 2.1.6) for temperature, salinity, horizontal velocity
21 | and sea level for the period 1958-2008, while wind stress and speed forcing at the air/sea interface
22 | come from the NCEP/NCAR reanalysis. The atmospheric fields have been statistically downscaled
23 | following the method by Goubanova et al. (2011) in order to correct for the unrealistic wind stress curl
24 | near the coast of the NCEP Reanalysis (see Cambon et al. (2013) for a validation of the method for
25 | oceanic applications). Atmospheric fluxes were derived from the bulk formula using the temperature
26 | from COADS $1^\circ\times 1^\circ$ monthly climatology (daSilva et al., 1994). Relative humidity and short wave and
27 | long wave radiations are also from COADS. Bottom topography is from the GEBCO 30 arc-second
28 | grid data set, interpolated to the model grid and smoothed as in Penven et al. (2005) in order to
29 | minimize the pressure gradient errors and modified at the boundaries to match the SODA bottom
30 | topography. [This model configuration has been validated from satellite and in situ observations in](#)

1 [Dewitte et al. \(2012\)](#) with a focus on mean state interannual variability. In general the model is skillful
2 [in simulating the mean SST field \(Fig. 1ac\) as well as other main aspects of the mean circulation \(e.g.](#)
3 [Peru Chile Undercurrent, EKE, see Figure 3 in Dewitte et al. \(2012\)\)](#), although with a slight cold bias
4 [\(\$\sim 1^{\circ}\text{C}\$ \), that could be partly attributed to the use of climatological heat flux forcing \(Fig. 1d\). The cold](#)
5 [bias observed here could be also due to a systematic warm bias in the AVHRR Pathfinder data,](#)
6 [observed in the nearshore regions where high SST gradients exist, specifically in the Humboldt region](#)
7 [\(cf. Dufois et al., 2012\). This product is extensively used in the construction of the OISST dataset](#)
8 [\(Reynolds et al., 2007\).](#)

9 [The mesoscale activity diagnosed from the mean EKE, has a comparable pattern than altimetry,](#)
10 [although with a larger amplitude \(Fig. 1ef\). Similar levels of mesoscale activity have been obtained by](#)
11 [previous modeling studies in the Peruvian region \(e.g. Echevin et al., 2011; Colas et al., 2012\).](#)

12 The ocean model within this configuration is coupled to the BioEBUS model following similar
13 methodology than Montes et al. (2014). BioEBUS uses two compartments of phytoplankton and
14 zooplankton, small (flagellates and ciliates, respectively) and large (diatoms and copepods,
15 respectively), detritus, dissolved organic nitrogen and the inorganic nitrogen forms nitrate, nitrite and
16 ammonium, as well as nitrous oxide (see Gutknecht et al., 2013ab, for a description of the model). The
17 open-boundary conditions for the biogeochemical model are provided by the climatological CARS data
18 set (nitrate and oxygen concentrations) and by SeaWiFS archive (chlorophyll-a concentration).
19 Additional biogeochemical tracers are computed following Gutknecht et al. (2013ab). Initial
20 phytoplankton concentration is defined as a function of vertically extrapolated satellite Chl-a following
21 Morel and Berthon (1989). An offshore decreasing cross shore profile, following in situ observations, is
22 applied for zooplankton, and a vertical constant (exponential) profile is used for detritus (nitrite,
23 ammonium and dissolved organic nitrogen), respectively. In order to get a realistic solution for the
24 region, the model parameters were tuned to simultaneously fit modeled oxygen and nitrate fields to
25 observations (see Table A1 of Montes et al. (2014) for parameter values). These changes were
26 motivated by the need to adjust the microbiological rates to values observed in the SEP. Within this
27 parameter configuration, BioEBUS has been shown to be skillful for simulating the OMZ off Peru
28 (Montes et al., 2014). In particular the pattern correlations between the model and observations for both
29 the annual mean and the seasonal cycle inside the OMZ present comparable scores (>0.85 , cf. Montes
30 et al. (2014)) as well as low standard deviations (i.e. in the order of the observed values). [The model](#)

1 [was run over the period 1958-2008 with a 10-year spin-up obtained by repeating the year 1958.](#)
2 [Although, after the spin-up, the simulation has reached stable conditions and the OMZ volume does not](#)
3 [drift, we focus in the present study only on the period 2000-2008.](#)

4 [The reason for focusing on the last ten years of our simulation is also motivated by the fact that the](#)
5 [atmospheric momentum forcing is close to the satellite QuickSCAT winds by construction \(see](#)
6 [Goubanova et al. \(2011\) for details\) so that this period of the simulation is the one when the model is](#)
7 [the most constrained by observations. Most previous modeling studies for this region \(Penven, et al.](#)
8 [2005; Montes et al., 2010, 2014; Echevin et al., 2011; Colas et al., 2012\) have also used a wind forcing](#)
9 [from the QuickSCAT scatterometer, which provides a benchmark for assessing our simulation.](#)

10 A monthly mean climatology is calculated for all variables over this period from the 3-day mean
11 outputs of the model, which can be compared to the CARS data.

12 Consistently with Montes et al. (2014), the coupled simulation is skillful in simulating the mean
13 characteristics of the OMZ off the Peruvian coast (Figures [42](#) and [23](#)). In particular the thickness and
14 location of the model OMZ core limits are realistic, and in good agreement with previous studies (Fig.
15 [42](#); e.g. Paulmier et al., 2006; Cornejo and Farías, 2012; Montes et al. 2014). [Note that the simulation](#)
16 [reproduces a thinner OMZ around 10°S in comparison to CARS, which agrees with the results](#)
17 [obtained by Montes et al. \(2014\). \(see Fig. 2 in that study\).](#) Close to the western boundary of our model
18 domain, the simulated OMZ also exhibits a realistic vertical structure (Fig. [23](#)) with comparable
19 concentration in DO than observations in the vicinity of the Equatorial Undercurrent (~100 m;
20 Equator). Furthermore, the simulation is consistent in reproducing the oxygen consuming processes, as
21 supported by the Apparent Oxygen Utilization (AOU; Fig. [34](#)), also in good agreement with previous
22 studies (cf. Figure 8 in Cabré et al. (2015)). AOU was computed as the difference between the DO
23 concentration and the saturated oxygen ($O_2\text{sat}$) concentration ($\text{AOU} = O_2\text{sat} - O_2$) with $O_2\text{sat}$ [computed](#)
24 following the methodology of García and Gordon (1992). The realistic representation of the oxygen
25 consuming processes is reflected by the Particulate Organic Carbon flux as well (Fig. [45a](#)), whose
26 values at 100m fall within the observed range for the region ($30\text{-}60 \text{ gC m}^{-2} \text{ yr}^{-1}$ in the shelf area; Dunne
27 et al., 2005; Henson et al., 2012). In addition, the low transfer efficiency of carbon (10-15% or lower
28 over and next to the shelf; Henson et al., 2012), from the euphotic zone to greater depths (Fig. [45b](#)),
29 implies that the remineralization processes take place at realistic depths, and therefore allow for a
30 correct vertical representation of the OMZ (cf. Fig. S2 in Cabré et al. (2015) for comparison).

1 The core of the OMZ, defined with a suboxic concentration ($[DO] < 20 \mu M$; μM will be used to refer to
2 $\mu mol L^{-1}$ in all the text and Figures), occupies nearly 23% of the domain volume (Fig. 56a), with the
3 less oxygenated layers comprised between $5^{\circ}S$ and $15^{\circ}S$, and 100 m and 600 m depth (Fig. 23). As
4 expected, the simulation presents ~~a finer spatial variability~~ more details than the climatological product
5 (Fig. 23). Moreover, we computed a geographical OMZ overlapping metric following Cabré et al.
6 (2015), which quantifies the spatial agreement of the OMZ volume distribution between the simulation
7 and CARS, varying between 0 (no agreement) and 1 (perfect collocation). We obtained a value of 0.79,
8 which is ~58% above the best CMIP5 models used in Cabré et al. (2015).

9 Despite the overall good agreement between the model and observations, the modeled oxygen content
10 is however underestimated as compared to CARS in certain regions of the domain, particularly
11 southwards of $20^{\circ}S$ (Fig. a23a) and close to the coast (Fig. 2d3d). In particular, the volume of the
12 suboxic DO concentration range is 6% lower in the simulation (Fig. 6a), which is comparable to the
13 differences obtained by Montes et al. (2014) in a similar analysis of the OMZ.

14 -The modeled DO distribution is also characterized by finer spatial scales of variability inside the OMZ
15 compared to observations (Figures 2e3c and 2d3d). In particular, the model oxycline is shallower and
16 with a more intense DO gradient than the observations, which has been also observed in a simulation of
17 the Arabian Sea OMZ (Resplandy et al., 2012), suggesting that the CARS data set may not have a
18 sufficient vertical resolution to realistically resolve the oxycline at some locations. Also, it must be kept
19 in mind that CARS is built using all the available data from the second half of the twentieth century
20 (1940-2009), whereas we focus on the period 2000-2008 for the simulation, which is known to be a
21 colder period than the previous decades in the eastern tropical Pacific (Henley et al., 2015). Other
22 limitation for the comparison between model and data includes the errors associated with the scarcity
23 of data in some regions (Bianchi et al., 2012). Nonetheless, the simulation is in good agreement with
24 CARS in terms of mean characteristics of the OMZ, as well as the mean oxygen concentration and its
25 distribution (Figures 34, 5a6a).

26 In order to evaluate the realism of the seasonal cycle, we estimate the seasonal variability of the
27 volume of water within the suboxic DO concentration range $0-20 \mu M$ in both the model and data (Fig.
28 5b6b). The results indicate that, despite a weaker amplitude (by 15% on average), the seasonal cycle of
29 the OMZ core is relatively well simulated by the model. For hypoxic DO volume in the range $40-50$
30 μM , the agreement is as good as inside the OMZ core, with a Pearson correlation value of 0.9 and a

1 volume RMS difference of 16%, between the simulation and the observations.
2 In order to summarize the model validation, we present a Taylor diagram showing the statistics of the
3 comparison between the model and observations for a depth range encompassing the OMZ (Fig. 7).
4 This analysis indicates that within the present model configuration, we reach a comparable skill than
5 the model configuration of Montes et al., (2014) (their Figure 1). The good agreement of the seasonal
6 cycle between CARS and the simulation, in addition to the consistency of our results with those of
7 Montes et al. (2014), provides confidence in using the model outputs for investigating the processes
8 associated with the seasonal variability of the OMZ.

9 **2.3 Methods**

10 In this work, our approach is twofold: First, the biogeochemical processes for DO are investigated
11 explicitly through the on-line oxygen budget (1). Although this methodology can provide a direct
12 estimate of the seasonal variability in advection and mixing, it does not allow for a direct estimate of
13 the eddy contribution to DO change that can also vary seasonally. The DO flux associated with
14 different timescales of variability is therefore estimated. ~~The latter consists in calculating the temporal~~
15 ~~average of the cross-products between DO and velocity anomalies. Anomalies can refer either to~~
16 ~~seasonal anomalies and in that case, this provides the seasonal DO flux, or to the intraseasonal~~
17 ~~anomalies (calculated here as the departure from the monthly mean) and in that case, this provides an~~
18 ~~estimate of the DO eddy flux. We also estimated the seasonal activity of the DO eddy flux, which~~
19 ~~consists in calculating the DO eddy flux over a 3-month running window and then a monthly~~
20 ~~climatology of this quantity. This consists in computing the temporal average of the cross-products~~
21 ~~between DO and velocity anomalies. Anomalies can refer either to seasonal anomalies and in that case,~~
22 ~~this provides the mean seasonal DO flux ($\langle \tilde{u} \cdot \tilde{O}_2 \rangle$ where \sim refers to the seasonal anomalies), or to the~~
23 ~~intraseasonal anomalies (calculated here as the departure from the monthly mean) and in that case, this~~
24 ~~provides an estimate of the mean DO eddy flux ($\langle u' \cdot O_2' \rangle$), where the apostrophe refers to the~~
25 ~~intraseasonal anomalies). In this paper we are also interested in the seasonality of the DO eddy flux.~~
26 ~~This is estimated from the monthly-mean seasonal cycle of the mean DO eddy flux calculated over a 3-~~
27 ~~month running window, and is now referred to as $\overline{\langle u' \cdot O_2' \rangle}$. The climatological EKE activity is~~
28 estimated similarly.

29 The DO budget consists in the following Equation:

$$\frac{\partial O_2}{\partial t} = -\vec{u} \cdot (\vec{\nabla} O_2) + K_h \nabla^2 O_2 + \frac{\partial}{\partial z} \left(K_z \frac{\partial O_2}{\partial z} \right) + SMS(O_2) \quad (1)$$

The first three terms on the right hand side represent the physical processes involved in the changes in oxygen concentration. The first term stands for the advection of oxygen, with \vec{u} the velocity vector (note that the model determines the vertical velocity component from the continuity equation). The second term corresponds to the ~~horizontal diffusion~~ horizontal subgrid-scale diffusivity (with K_h the eddy diffusion coefficient equal to $100 \text{ m}^2\text{s}^{-1}$ in this version of the model), and the third term corresponds to the vertical mixing (with turbulent diffusion coefficient K_z calculated based on the KPP mixing scheme (Large et al., 1994). Note that the model has also numerical diffusion associated with inherent spurious diapycnal mixing of the numerical scheme, so that K_h is empirically adjusted

The fourth term represents the “Sources-Minus-Sinks” contribution to the oxygen changes, directly due to biogeochemical activity. Biogeochemical processes correspond to the sum of oxygen sources and sinks, namely the photosynthetic production, and the aerobic processes (oxic decomposition, excretion and nitrification). In this study, for simplicity, those will be considered as a summed-up contribution to the DO rate of change, whereas physical processes will be divided into advection and mixing terms. Each term of this oxygen budget is determined on line at each time integration. While horizontal diffusion and vertical diffusivity are explicit sources of mixing, they are not the only terms contributing to mixing. Later on in the paper, unless stated otherwise, the term mixing will refer to the integrated effect of all processes contributing mixing directly or indirectly. Besides the horizontal diffusion ($K_h \cdot \nabla^2 O_2$) and vertical mixing ($\frac{\partial}{\partial z} (K_z \frac{\partial O_2}{\partial z})$), mixing can be also induced by non-linear advection.

The latter corresponds to $(u' \partial u' / \partial x) + (v' \partial v' / \partial y) + (w' \partial w' / \partial z)$, assuming the Reynolds decomposition for the velocity field, i.e. $\vec{u} + \vec{u}'$, where \vec{u}' accounts for the intraseasonal variability (periods lower than ~3 months).

In the SEP, the subthermocline seasonal variability can be interpreted as resulting from the propagation of Extra-Tropical Rossby Waves (ETRW). ETRW radiate from the coast and propagate vertically, inducing a vertical energy flux, whose trajectory follows the theoretical Wentzel-Kramers-Brillouin (WKB) ray paths (Dewitte et al., 2008; Ramos et al., 2008). The energy flux results from the phase relationship between vertical velocity associated with the vertical displacement of the isotherms, and the pressure fluctuations associated with them. In the regions sufficiently below the thermocline for

DO consumption to become weak (that is DO can be considered a passive tracer), it is expected that changes in DO relate to the anomalous velocity field, and that the DO flux shares comparable characteristics than the Eliassen-Palm flux (EP flux; Eliassen and Palm, 1960). The trajectories of the WKB ray paths are a function of latitude, local stratification and the phase speed of the Rossby wave (see Ramos, et al., (2008)). The latter consists in the superposition of a certain number of baroclinic modes, in order to propagate vertically, so the phase speed can range from values between c_1 to c_n , where c_n is the theoretical phase speed of a n^{th} baroclinic mode, obtained from the vertical mode decomposition of the local density profile.

~~In order to derive the trajectories of the WKB ray paths, a vertical mode decomposition of the mean model stratification at each grid point of the simulation was performed, which provides the phase speed values of each baroclinic mode. According to the theory, in the case of vertical/westward propagation, the highest amplitudes should be found along the WKB trajectories, and the phase lines should orientate approximately parallel to the WKB ray paths. For details on the WKB theory applied to the extra-tropical latitudes, the reader is invited to refer to Ramos et al. (2008).~~

3 Characteristics of the DO annual cycle

~~As previously stated, the annual signal is a conspicuous feature inside the region (Fig. 5), although it manifests differently across the OMZ. As an illustration, the amplitude and phase of the annual harmonic of the model DO climatology is presented along a section off central Peru (12°S, Fig. 6ab), where the OMZ core is extensive (Fig. 1). While the annual signal is a conspicuous feature inside the region (Fig. 6b), it could manifest differently across the OMZ. As a first step towards investigating processes driving the rate of DO change, it appears important to document the vertical structure variability of the DO annual cycle within the OMZ. The amplitude and phase of the annual harmonic of the model DO climatology is presented along a zonal section off central Peru (12°S, Fig. 8ab), where the OMZ core is extensive (Fig. 2).~~ The DO climatology has been normalized by its RMS (Root Mean Square), in order to emphasize the regions where the amplitude in DO changes (and mean DO) is weak. The amplitude reveals a complex pattern with three regions of large relative variability: 1) near the coast (i.e. fringe of ~150 km) between the oxycline and 400 m; 2) offshore between 82°W and 84°W in the upper 400 m and 3) below 500 m. The phase lines over these three regions suggest distinct propagating characteristics: whereas in the coastal region there is no propagation, in the offshore and

1 deep region, there is indication of a westward propagation. In the region below 500 m, the phase lines
 2 tend also to be parallel and slope downward, suggestive of westward-downward propagation (estimated
 3 phase speed of $\sim 2.5 \text{ cm s}^{-1}$). These propagating characteristics can be evidenced in the Hovmöllers of
 4 the recomposed annual cycle at the depth of 150 m (Fig. 6e8c) and 700 m (Fig. 6e8d). While at 150 m
 5 the annual signal does not clearly propagate and only shows two domains of high amplitude, separated
 6 by low amplitude values (Fig. 6e8c), there is a clear westward propagation of the DO anomalies at 700
 7 m, with the phase speed increasing westward. At 400 m, the propagation is only observed west of
 8 81°W (Fig. 6b8b). In addition to the large vertical structure variability of the annual cycle, the OMZ
 9 annual cycle is also characterized by a large horizontal variability in particular at its northern and
 10 southern boundaries. This is illustrated from Figure 79, that displays the amplitude of the annual cycle
 11 of the DO climatology at 400 m, and evidences amplitude peaks at the OMZ meridional boundaries
 12 (between the 20 and $45 \mu\text{M}$ isopleths).

13 The annual variability pattern evidenced above results from a delicate balance between the physical
 14 processes (namely advection and mixing, cf. Eq. (1)) and the biogeochemical processes (consumption
 15 versus production). As a first step towards investigating each term of the DO budget, it is interesting to
 16 evaluate the relative contribution of the physical and biogeochemical fluxes to the DO variability at
 17 seasonal scale. The RMS of the climatological fluxes along a section at 12°S indicates that the
 18 maximum amplitude of the seasonal fluxes takes place near the oxycline and along the coast over the
 19 whole water column (Figure 810). The relative importance of the physical processes against the
 20 biogeochemical processes varies across the OMZ. At the coast and near the oxycline, the annual
 21 variability of the biogeochemical processes reaches values almost half those of the variability in
 22 physical processes (Fig. 8e10c), as a consequence of the proximity to both the well lit and highly
 23 productive part of the water column, and the high remineralization activity that occurs near the
 24 oxycline. Towards offshore and at depth, the relative importance of the variability of the
 25 biogeochemical processes reduces gradually. Near $\sim 300 \text{ m}$ the variability of the biogeochemical
 26 processes is nearly $1/5$ of the physical processes variability. Below $\sim 300 \text{ m}$, and towards the lower part
 27 of the OMZ core and below, the physical processes variability is one order of magnitude larger.
 28 Consequently, the distribution of DO in the lower part of the OMZ is rather a function of
 29 advection/diffusion than a consequence of the biogeochemical processes, although DO consumption
 30 even at very low levels has the potential to generate local gradients and therefore induce advection. The

1 spatial heterogeneity in the seasonal DO changes induced by the biogeochemistry and dynamics as
 2 described above, appears as an ubiquitous feature in the OMZ. To illustrate this, we estimate the
 3 proportion of explained variance of the seasonal DO rate of change by the physical fluxes as:

$$4 \quad R_{phys.}^2 = (1 - RMS(Biogeochemical\ Fluxes) / RMS(Total\ Fluxes)) \cdot 100 . \quad (2)$$

5 Figure [9a11ab](#) presents the results of $R_{phys.}^2$ at 100 and 450 m depth, which evidences that the relative
 6 importance of the physical fluxes versus the biogeochemical fluxes in the seasonal DO variability
 7 increases with depth, and is enhanced at the OMZ boundaries. On the other hand, the biogeochemical
 8 fluxes explain more than 50% of the variance in seasonal DO change rate in a narrow (~ 200 km width)
 9 coastal fringe that extends more offshore to the north of the domain (around 8°S; Fig. [9a11a](#)) and
 10 vertically down to 300 m (Fig. [9e11c](#)).

11 Based on the above analysis, it is clear that the coastal region (first 200-300 km from the coast) below
 12 the oxycline corresponds to a territory where the seasonal variability of biogeochemical and physical
 13 fluxes have a comparable magnitude, whereas outside this region, notably in the lower part of the OMZ
 14 core, the physical fluxes variability dominates over the biogeochemical fluxes variability at seasonal
 15 timescale. Hereafter we examine the possibility of two distinct regimes of OMZ dynamics at seasonal
 16 timescale: one associated with the upper OMZ (including coastal domain and meridional boundaries),
 17 and the other one associated with the deep OMZ. In the following we investigate the processes
 18 responsible for the DO flux.

19

20 **4 Seasonality of the OMZ ventilation**

21 It has been shown for the SEP that the DO content near the coast is set to a large extent from the
 22 transport of oxygen deficient waters from the equatorial current system, particularly the oxygen
 23 depleted sSSCC (Montes et al., 2014). Therefore, the seasonal variability of DO is likely to result in
 24 part from the seasonal variability of the different branches of the EUC in the far eastern Pacific. Local
 25 wind stress forcing (and its intraseasonal activity) has also a marked seasonal cycle off Peru (Dewitte et
 26 al., 2011) which may impact both the upwelling dynamics -through Ekman pumping/transport- and
 27 mixing. Some studies also argue that ~~the ventilation of the OMZ takes place through the offshore~~
 28 ~~transport of oxygen (deoxygenated) by eddies from the coastal domain~~ the DO exchange between the
 29 coastal domain and the OMZ takes place through the offshore transport of DO poor waters by eddies.

(Czeschel et al., 2011), implying that the variability of such processes is set up by coastal processes that determine the nature of the DO source. As a first step, we investigate the mechanisms responsible for the seasonal variability in DO along the coast, which can be considered as the eastern boundary of the OMZ. This is aimed at providing material for the interpretation of the offshore DO flux variability.

4.1 The coastal domain as the eastern boundary of the OMZ: variability and mechanisms

We analyze the seasonal variability along the coast, at a section at 12°S. Similar results are obtained for latitudes between 7°S and 14°S (not shown), which corresponds to the latitude range where the PUC is well defined. The results are also presented in terms of the first EOF mode, in order to ease the interpretation of the variability, reduced as a spatial pattern modulated by a seasonal timeseries. It was verified in particular that the consideration of the first EOF mode of each term leads to an almost perfect closure of the DO budget (see below, Table 1). Figure 4012 displays the ~~dominant first~~ EOF mode of various climatological fields in a section at 12°S near the coast and from the oxycline (45 μ M isoline) to the depth of 300 m. Figure 4413 shows the principal components associated with ~~dominant these the first~~ EOF mode patterns. The seasonal DO cycle is dominated by an annual component, with a peak centered in August (Fig. 44a13a), and the largest variability at the coast below the oxycline that extends offshore and downward, resulting in an elongated tongue below 100 m near ~78°W (Fig. 40a12a). During the first quarter of the year, oxygen anomalies remain relatively stable (oxygen rate nearly zero, Fig. 44b13b), and negative, due to a high production of organic matter in Austral summer (cf. Fig. 1c of Gutiérrez et al., 2011) that stimulates a subsurface oxygen consumption associated with the degradation of this organic matter. DO anomalies start to increase during the second quarter, become positive in June and reach their maximum in August (Fig. 44a13a). The peak anomaly in Austral winter could be understood in terms of the increased mixing (see Fig. 44a13a showing EKE peaking in July) associated with the increase in baroclinic instability due to the seasonal intensification of the PUC from June. Note that the pattern of the ~~dominant first~~ EOF of the alongshore current coincides with the mean position of the PUC (see Fig. 40b12b), so that seasonal variations of the PUC can be interpreted in terms of the variations in the vertical shear of the coastal current system. Other processes that may explain the peak DO anomaly in Austral winter includes the reduced productivity and downwelling that peaks in June (Fig. 44e13c), associated with seasonal equatorial downwelling Kelvin wave.

1 The following investigates the tendency terms of the DO budget, in order to quantitatively interpret the
 2 DO seasonal cycle near the coast. Given that the analysis is performed inside the 45 μM isopleth, the
 3 biogeochemical flux term is largely dominated by the “Sinks” terms (aerobic processes; one order of
 4 magnitude larger than “Sources”), driven by organic matter remineralization and zooplankton
 5 respiratory metabolic terms (not shown). For clarity, the seasonal DO budget is presented synthetically,
 6 from the ~~dominant first~~ EOF mode of the climatological advection, mixing ([horizontal and vertical](#)
 7 [diffusion](#)) and biogeochemical fluxes terms. Although this does not warranty a perfect closure, it eases
 8 the interpretation. Note that the residual resulting from the difference between the first EOF mode of
 9 the rate of DO changes and [the summed-up contribution](#) of all the other terms in Figure [44b13b](#) is
 10 rather weak, validating to some extent our approach ([see also Table 1](#)). First of all, we find that the
 11 largest amplitude of the mode patterns is found near the coast and inside the mean PUC core (Figs.
 12 ~~40d12d~~ to ~~40g12g~~). During the first part of the year (January to May), positive advection anomalies are
 13 compensated by mixing ([horizontal and vertical diffusion](#)), and maintain the rate of DO change
 14 relatively low (Fig. [44b13b](#); [Table 1](#)). Biogeochemical fluxes anomalies are positive during that period,
 15 associated with a positive anomaly of primary production in the well lit surface layers, implied by the
 16 high chlorophyll-a values (Fig. [44e13c](#)). A positive oxygen anomaly is sustained by the advection terms
 17 and the biogeochemical terms, and is balanced out by the ~~constant input of low oxygen mean advection~~
 18 [of low DO](#) waters carried by the PUC (Montes et al. 2010; 2014), generating the relatively stable
 19 oxygen values (oxygen rate nearly zero).
 20 From May, the rate of DO changes increases concomitantly with EKE (Fig. [44ab13ab](#)), followed one
 21 month later by mixing ([horizontal and vertical diffusion](#)), whereas advection and biogeochemical
 22 fluxes decrease. By June-July, the intensification in alongshore winds (Fig. [44e13c](#)) starts to propel the
 23 coastal upwelling, which has two compensating effects: on one hand it triggers photosynthesis in the lit
 24 surface layers (DO rate turns to positive values) and on the other, it uplifts low oxygen waters from the
 25 OMZ. The intraseasonal wind activity also starts to increase at that time (cf. Fig. [44e13c](#); see also
 26 Dewitte et al., 2011) which favors mixing, and so the downward intrusion of positive DO anomalies
 27 (note the deepening of the mixed layer in Fig. [44e13c](#)). The overall effect is an increase in DO which
 28 leads to a peak anomaly in August. At that time, the DO rate drops sharply due to the strong subsurface
 29 DO consumption ([Table 1](#)) associated with aerobic remineralization of organic matter produced earlier
 30 in the season (DO rate moves sharply to negative values) and the high mixing that brings DO depleted

waters from the subsurface into the deepened mixed layer. Note that this is consistent with the decrease in surface chlorophyll-a (Fig. 4e13c) and the interpretation proposed by Echevin et al. (2008) to explain the Austral summer minimum in surface chlorophyll-a observed off Central Peru.

This change to oxygen poor conditions combines with the natural decrease in oxygen production towards the end of the upwelling season and coincides with a restratification of the water column, which restricts the oxygenated waters near the surface (Echevin et al., 2008). This altogether contributes to maintain a negative DO rate inside the coastal OMZ, despite the increase in anomalous DO flux from the advective terms and (later on) biogeochemical processes towards the end of the year. As a result, oxygen returns to low values towards the end of the year.

4.2 Offshore flux

While the coastal OMZ variability is heavily constrained by the environmental forcings –coastal upwelling, coastal current system and local wind– due to the shallow oxycline there, the offshore OMZ, as embedded in the shadow zone of the thermohaline circulation, is somewhat insensitive to direct local forcing and rather experiences remote influence in the form of westward propagating mesoscale eddies (Chaigneau et al., 2009) and ETRW (Ramos et al., 2008; Dewitte et al., 2008). The influence of westward propagating mesoscale eddies on the OMZ translates as the transfer of coastal water properties towards the open ocean (DO included), while these properties are altered during transport due to physical-biogeochemical interactions (Stramma et al., 2014; Karstensen et al., 2015). Towards the end of their lifetime, hydrographic and biogeochemical anomalies carried by eddies are redistributed in the ocean (Brandt et al., 2015), linking the coast and the open ocean. Although most eddies genesis takes place near the coast (Chaigneau et al., 2009) and seasonal ETRW have a coastally forced component (Dewitte et al., 2008), we expect different characteristics of the seasonal variability in DO between the coast and the open ocean, given that oxygen demand will change from one region to the other. We also distinguish the mean DO flux associated with the annual component of the circulation that represents the transport in DO associated with seasonal change in the large scale circulation, and the annual variability of the eddy DO flux that corresponds to the annual changes in the transport due to eddies. These two quantities are diagnosed at 12°S (Figs. 42ae 14 and 15). The DO has been normalized by its climatological variability in order to emphasize variability patterns where DO is low.

Mean seasonal flux

1 We ~~now first~~ document the mean DO flux associated with the annual component of the circulation. ~~To~~
2 ~~this extent, we estimate the contribution of the annual harmonic to the seasonal DO flux as~~ It consists
3 in the mean of the cross-product of the annual harmonics of the climatological velocity and DO (Fig.
4 14a). ~~Relatively~~ The results indicate that the amplitude of the ~~seasonal~~annual DO flux is maximum near
5 the coast and below ~ 400 m and it tends to be orientated westward-downward, following
6 approximately the trajectories of theoretical WKB paths for the annual period Rossby wave. Note that
7 this is consistent with the westward propagating pattern of DO below 400 m evidenced earlier (Fig.
8 68). As a consistency check, we also estimated the annual energy flux vector in the (x,z) plan
9 associated with a long extra tropical Rossby wave, that is $(\langle p^{1\text{yr}} \cdot u^{1\text{yr}} \rangle, \langle p^{1\text{yr}} \cdot w^{1\text{yr}} \rangle)$ where the superscript
10 denotes the annual harmonics and the bracket the temporal average (Fig. 12b14b). The flux vector
11 indicates vertical propagation of energy at the annual period and the pattern of maximum flux
12 coincides approximately with the region of maximum amplitude of the mean seasonal DO flux. This
13 suggests that the annual ETRW is influential on the DO flux below ~ 400 m. This is interpreted as
14 resulting from the advection of DO by the ETRW since biogeochemical fluxes have much less
15 influence on the DO rate of change below 400 m (Fig. 8e10c) and the amplitude of the annual cycle of
16 climatological DO eddy flux has a much reduced amplitude below that depth (Fig. 12e15a) suggesting
17 a reduced contribution of ~~mixing horizontal and vertical diffusion~~ to the DO budget. Note that the DO
18 (Fig. 12e15a) was normalized prior to compute the ~~oxygen DO~~ eddy flux in order to render both the
19 analysis akin, and therefore contrast the flux associated with the annual ETRW against the annual DO
20 eddy flux. It was verified that the vertical structure variability of the annual DO flux described above
21 for the section of 12°S is comparable at other latitudes within the OMZ. In particular the annual DO
22 flux tends to remain homogeneous along trajectories mimicking the energy paths of the ETRW at
23 annual period which slope becomes steeper to the South (not shown).

24 Seasonal eddy flux

25 ~~The annual amplitude of the climatological DO eddy flux is thus the largest in the upper 400 m~~ As
26 previously described, the annual amplitude of the climatological DO eddy flux is the largest in the
27 upper 400 m near the coast at 12°S consistently with the high EKE in this region. Since EKE is large
28 along the coast of Peru, ~~an offshore transport of DO by eddies is~~ exchange of DO induced by eddies
29 could be expected at all latitudes, with a direction that depends on the sign of the DO gradient at the
30 coast. Figure 1316 presents the annual harmonic of the climatological DO eddy flux along the coast

1 and averaged in a coastal fringe distant 1° from the coast and 2° width. The maximum amplitude –
2 reaching $\sim 1 \text{ cm s}^{-1} \mu\text{M}$ – is concentrated in the upper oxycline (Fig. [13a16a](#)) with a peak during Austral
3 winter. The peak season is also confirmed by the EOF analysis of the climatological DO eddy flux (not
4 shown). Despite the relative large meridional variability in the amplitude, the mean vertical structure of
5 the DO eddy flux consists in an approximate exponentially decaying profile with depth, with a decay
6 scale of $\sim 90 \text{ m}$ (Fig. [13b16b](#)), so that at 300 m the seasonal DO eddy flux is only 19% of that at 100 m
7 on average along the coast. Figure [13a16a](#) also reveals that the annual DO eddy flux is larger towards
8 the northern rim of the domain and extends deeper than towards the south. The high values are
9 increasingly confined close to the surface towards the southern part of the domain, in comparison to the
10 northern part, although the vertical attenuation displays a similar scale.

11 **4.3 Meridional boundaries**

12 Here, our objective is to document the seasonality of the DO eddy flux, ~~considering the marked~~
13 ~~seasonal cycle in EKE and oxygen eddy flux in this region~~. As a first step, we estimate the distribution
14 of mean DO eddy flux, in order to identify the regions where its magnitude is large and thus where it is
15 likely to vary seasonally with a significant amplitude.

16 **Mean seasonal flux**

17 The horizontal distribution of mean ~~oxygen DO~~ eddy flux displays the highest values at the boundaries
18 of the OMZ core (Fig. [1417](#)), and adjacent to the $45 \mu\text{M}$ isopleth. Towards the inner OMZ, the mean
19 ~~oxygen DO~~ eddy flux values decrease notoriously, with a factor of nearly 10 between the interior and
20 exterior of the $10 \mu\text{M}$ contour. In agreement with the observations reported in the previous section, the
21 mean ~~oxygen DO~~ eddy flux decreases sharply with depth (approximately one order of magnitude
22 between 100 m and 700 m), with the highest values concentrated near the oxycline as expected from
23 the increasing oxygen concentration in this part of the OMZ. In this sense, the pattern of ~~oxygen DO~~
24 eddy flux around the depth of the oxycline encloses a region of high variability (not shown).

25 To gain further insight with respect to the vertical structure of the ~~oxygen DO~~ eddy flux and at the
26 same time, diagnose the role of the mesoscale activity at the boundaries of the OMZ, we compute the
27 mean ~~oxygen DO~~ eddy flux across the two sections that correspond to the northern and southern limits
28 of the OMZ (depicted in Fig. [1418](#)). These limits are defined based on Figure 17, and are located in
29 the, which fairly agree with the OMZ northern and southern limits (Fig. 15) and correspond to the
30 provinces of high amplitude of the mean DO eddy flux, previously defined (Fig. 13).

The ~~oxygen DO~~ eddy flux across each of the north and south boundaries was computed by averaging the product of the fluctuating velocity component normal to the boundary in the horizontal directions and the fluctuating DO concentration component, thereby obtaining horizontal eddy fluxes. As observed in Figure ~~4417~~, the highest values for both north and south boundary sections are also comprised between the oxycline and the lower OMZ core limit (Fig. 18), being almost one order of magnitude smaller at greater depths (Fig. ~~45e18c~~). These high values, located between ~100-300 m, are followed by a sharp decrease (average decrease of $1.5 \text{ cm s}^{-1} \mu\text{M}$ in 100 m). At the range of depths between 100 m and 300 m, the DO eddy flux displays higher values at the southern boundary (nearly twice as large) when compared with the northern boundary. ~~This ratio tends to vanish when analyzing the lower part of the OMZ. At both boundaries, there is a gap of nearly one order of magnitude in the difference between the lower and upper parts of the OMZ. This relationship is less clear when analyzing the lower part of the OMZ. At both meridional boundaries, the mean DO eddy flux in the upper part of the OMZ is nearly one order of magnitude larger than in the lower part.~~

Seasonal eddy flux

We now document the seasonal variability of the ~~oxygenDO~~ eddy flux across the OMZ boundaries analyzed above (Fig. ~~4518~~). An EOF analysis of the mean seasonal cycle of the ~~oxygenDO~~ eddy flux is performed at the boundary sections previously defined. The Figure ~~4619~~ presents the ~~dominant first~~ EOF mode patterns along with the associated timeseries. In order to estimate the uncertainty associated with the location of the OMZ boundaries, we repeated this analysis for 12 nearby sections parallel to the boundaries and spaced by ~20Km. This leads to an estimated ~~dispersionerror~~ (standard deviation across the different sections) of the ~~oxygenDO~~ eddy flux. The ~~dispersionerror~~ is represented as a colored shading in the Figures ~~46bde19bde~~. At both locations, the first EOF accounts for a well defined seasonal cycle. At the northern boundary (Fig. ~~46a19a~~), the seasonal cycle of the DO eddy flux peaks in Austral Winter, in phase with the DO changes along the coast (Fig. ~~4316~~). Note that the seasonal cycle is in phase with the one of the intraseasonal activity of the horizontal current normal to the section, which was estimated the same way than the climatological eddy flux (see red line in Fig. ~~46b19b~~), supporting the idea that the climatological DO eddy flux results from anomalous advection. The amplitude of the mode pattern is maximum at the oxycline with DO between 20 and 45 μM , and presents a sharp decrease below the OMZ core depth (Fig. ~~46a19a~~). This sharp decrease is evidenced by the mean vertical profile of the DO eddy flux seasonal variability estimated as the RMS across the

section of the EOF mode pattern (Fig. 46e19e). The vertical structure of the DO eddy flux variability indicates that there is a difference of nearly one order of magnitude between 100 and 300 m depth. From that depth on, the DO eddy flux variability decreases linearly. In contrast with the northern boundary, the seasonal variability at the southern boundary peaks during Austral Spring (Fig. 46d19d), in phase with the intraseasonal activity of the horizontal currents normal to the section. The amplitude of the seasonal cycle is the largest around the depth of the oxycline, and remains high down to the vicinity of the OMZ core upper limit (Fig. 46e19c). Below the depth of the OMZ core, the amplitude of the EOF mode decreases sharply (~one order of magnitude in 100m; Fig. 46e19c). This is evidenced by the profile of the DO eddy flux seasonal variability, estimated in the same manner as for the northern boundary (Fig. 46e19e). This profile shares some characteristics with its counterpart at the northern boundary, meaning, a sharp decrease between the oxycline and the OMZ core depths, suffering a reduction of nearly 90% (Fig. 46e19e). On the other hand, the variability along the southern boundary is ~70% larger than along the northern boundary. ~~At both boundaries, the zonal wavelength of the latitudinal variability is estimated to be of the order of $\sim 10^2$ km, a scale that falls within the range of observed eddies diameter (Chaigneau and Pizarro, 2005), which indicates that locally, eddies can either inject or remove DO from the OMZ on average over a season. At both boundaries, the zonal wavelength of the seasonal DO eddy flux variability along the boundary is estimated to be of the order of $\sim 10^2$ km, a scale that falls within the range of observed eddies diameter (Chaigneau and Pizarro, 2005), which indicates that locally there can be an injection or removal of DO across the boundary on average over a season.~~ The mean ~~oxygen~~DO eddy flux across the boundaries is nevertheless positive.

5 Discussion and concluding remarks

~~A high-resolution coupled physical/biogeochemical model experiment is used to document the seasonal variability of the OMZ off Peru. The annual harmonic of DO reveals three main regions where DO exhibits specific propagating characteristics and amplitude, suggesting distinct dynamical regimes: 1) The coastal domain; 2) the offshore ocean below 400 m and 3) at the southern and northern boundaries. In the coastal portion of the OMZ, the seasonal variability is related to the local wind forcing, and therefore follows to a large extent the paradigm of upwelling triggered productivity, followed by~~

1 remineralization. It is shown in particular that the DO peaks in Austral winter which is associated with
2 mixing induced by both the increase in baroclinic instability and intraseasonal wind activity. This is
3 counter intuitive with regards to the seasonality of the alongshore upwelling favorable winds also
4 peaking in Austral winter, which would favor the intrusion of deoxygenated waters from the open
5 ocean OMZ to the shelf. Instead, the coastal domain can be viewed as a source of DO in Austral winter
6 for the OMZ through offshore transport. The latter is induced by eddies that are triggered by the
7 instabilities of the PUC. In the model, the offshore DO eddy flux has a marked seasonal cycle that is in
8 phase with the seasonal cycle of the DO along the coast, implying that the coastal domain, viewed here
9 as the eastern boundary of the OMZ, is a source of seasonal variability of the OMZ. This appears to
10 operate effectively in the first 300 m. Below that depth, the DO eddy flux is much reduced due to both
11 a much weaker eddy activity, and very low DO concentration. On the other hand, a mean seasonal DO
12 flux is observed and exhibits propagating features reminiscent of the vertical propagation of energy
13 associated with the annual extra tropical Rossby wave.

15 In the upper 300 m, the OMZ seasonal variability is also associated with the DO eddy flux at the OMZ
16 meridional boundaries where it is the most intense. We find that, at the northern boundary, the seasonal
17 cycle in DO eddy flux peaks in Austral winter, while it peaks a season later at the southern boundary.
18 Additionally, the amplitude of the seasonal cycle in DO eddy flux is larger at the southern boundary
19 than at the northern boundary. The schematics of Figure 17 summarize the main processes documented
20 in this paper to explain the seasonality of the OMZ volume.

21 While previous studies have mostly focused on the role of the mean DO eddy flux in shaping the OMZ
22 boundaries (Resplandy et al., 2012; Brandt et al., 2015; Bettencourt et al., 2015), we have documented
23 here the seasonal variability in the DO eddy flux at the OMZ boundaries, including the “eastern
24 boundary” formed by the coastal system. We infer that the seasonality of the DO eddy flux is
25 controlled by distinct physical processes depending on the boundary: At the “eastern boundary”, there
26 is a constructive coupling between eddies resulting from the instability of the PUC peaking in Austral
27 winter, and the enhanced DO along the coast resulting from enhanced mixing at the same season. At
28 the northern boundary of the OMZ, the DO eddy flux is also related to the strong EKE around 5°S that
29 peaks in Austral winter. Whether or not the strong EKE found there results from the instability of the
30 coastal current system or of the EUC and the South Equatorial Current (SEC), would need to be

1 explored. Despite the fact that the OMZ northern boundary is embedded in the equatorial wave guide,
2 since the intraseasonal Kelvin wave activity tends to peak in Austral summer (Illig et al., 2014) it can
3 be ruled out that the seasonal cycle in DO eddy flux is strongly linked to the intraseasonal long-
4 equatorial waves.

5 Regarding the southern boundary, it is interesting to note that the DO eddy flux peaks in Austral spring,
6 three months later than at the northern boundary. A possible mechanism driving the local variability
7 observed at the southern section is the generation of local baroclinic instability and vorticity input from
8 wind stress curl as observed for the California system (Kelly et al., 1998). The southern section lies
9 within the northeast rim of the Southeast Pacific Anticyclone, and the seasonal cycle phase peak agrees
10 with the reported intensity peak of the seasonal cycle of the Anticyclone, towards the end of the year
11 (Rahn et al., 2015; Acapichun and Garcés-Vargas, 2015). In this sense, the mesoscale activity in this
12 region could be directly modulated by the winds. Dewitte et al. (2008) also report that intraseasonal
13 (internal) variability in currents can originate from the interactions between the annual extra-tropical
14 Rossby wave and the mean circulation in a medium-resolution oceanic regional model over this region.
15 The actual source of the eddy activity in this region would also deserve further investigation.

16 Our study also reveals that the most prominent propagating features in DO inside the OMZ at annual
17 frequency is below ~300 m, where the seasonal DO flux follows approximately the theoretical WKB
18 ray paths of the annual ETRW. From that depth, we also show that the seasonal variability in physical
19 fluxes becomes one order of magnitude larger than the one of the biogeochemical fluxes (Fig. 8c). This
20 supports the observation that DO tends to behave as a passive tracer so that vertical displacements of
21 the DO isopleths mimic those of the isotherms, inducing a seasonal DO flux that resembles the energy
22 flux path of the ETRW. This mechanism adds a dimension to the understanding of the OMZ variability,
23 considering that the vertical propagation of ETRW can take place at a wide range of frequencies
24 (Ramos et al., 2008).

25 We now discuss implications of our results with regards to current concerns around OMZ variability at
26 long timescales. A recent study has suggested a trend in the OMZ towards expansion and
27 intensification (Stramma et al., 2008) whose forcing mechanism remains unclear (Stramma et al.,
28 2010). Observations in the Pacific Ocean also suggest that the OMZ characteristics vary decadal
29 (Stramma et al., 2008; 2010). Since decadal variability can manifest as a low frequency modulation of
30 the seasonal cycle, our study may provide guidance for investigating OMZ variability at long

timescales. In particular we find that the amplitude of the seasonal cycle is nearly twice as large at the southern boundary than at the northern boundary and “coastal boundary”, which suggests a larger sensitivity of the OMZ variability at the southern boundary to the modulation of eddy activity by climate forcing. This view would preferentially link the OMZ low frequency fluctuations to mid-latitudes changes in the circulation. We note however that the relative contribution of the mean DO flux and the DO eddy flux exhibits significant interannual fluctuations at the boundaries (not shown), which suggests that eddy induced DO flux may not be the only key player for understanding long term trend in the OMZ. It is interesting to note that so far, it has been difficult to reconcile the observed trend in the OMZ with the trend simulated by the current generation of coupled models (Stramma et al., 2012), which has been attributed to biases in the mean circulation and inadequate remineralization representation (Cocco et al., 2013; Cabré et al., 2015). Our results support the view that such discrepancy may partly originate from the inability of the low resolution models to account for the DO eddy flux and its modulation. Regional modeling experiments also showed that eddy activity can be modulated at ENSO and decadal timescales (Combes et al., 2015; Dewitte et al., 2012). This issue would certainly require further investigation, and could benefit from the experimentation with our coupled model platform. This is planned for future work.

5 Discussion

We now discuss some limitations and implications of our results. While the model realistically simulates the main characteristics of the OMZ (position, intensity, average volume and seasonal variations), it still presents biases that could be influential on our results. In particular, and since the coastal domain is viewed here as a boundary of the OMZ, it is important to have a realistic mean DO concentration there. Compared to CARS, the simulated suboxic volume is however underestimated by ~6%, and 85% of this error can be attributed to the coastal domain (fringe of 3° from the coast). This bias could be due to several factors. Montes et al. (2014) observed variations of the suboxic volume in the order of 5%, when contrasting two simulations that used different oceanic open boundary conditions, which indicates a sensibility of the simulated OMZ to the physical parameters and the representation of the Equatorial Current system. This bias could also be partly due to coastal sediments processes (DO demanding processes) that are not represented in our simulation. Using a similar configuration to the one used in the present study on the Namibian OMZ, Gutknecht et al. (2013a)

1 observed that the differences between the simulated OMZ volume and CARS increased towards the
2 shelf, which could be related to the exclusion of the DO demand from the sediments in the model. On
3 the other hand, in a study on the impact of sediment biogeochemistry upon the water column
4 biogeochemical cycles in the northern end of the California Current system, Bianucci et al. (2012)
5 argued that the sediment denitrification is balanced by a nitrification in the water column, obtaining
6 similar bottom DO concentrations between their experiments even when disregarding the DO sediment
7 demand. Nevertheless, the interaction between the sediments processes and the water column in terms
8 of DO consumption in the mid latitude upwelling systems is still unclear. Regarding this point, the
9 inclusion of a sediment module in the current model setting is planned for future work.

10 Besides other likely sources of biases related to an imperfect model setting (e.g. use of relatively low
11 resolution atmospheric forcings near the coast, absence of air-sea coupling at mesoscale, absence of
12 coupling with benthic oxygen demand or consideration of N₂ fixation), another inherent limitation of
13 our study is related with the difficulty to validate some aspects of the eddy field, in particular its
14 vertical structure. This might be overcome in the future as the Argo coverage increases (cf.
15 TPOS2020).

16 With the limitations of our regional modeling approach in mind, it is worthwhile discussing some
17 implications of our results. While previous studies have mostly focused on the role of the mean DO
18 eddy flux in shaping the OMZ boundaries (Resplandy et al., 2012; Brandt et al., 2015; Bettencourt et
19 al., 2015), we have documented here the seasonal variability in the DO eddy flux at the OMZ
20 boundaries, including the “eastern boundary” formed by the coastal system. We infer that the
21 seasonality of the DO eddy flux is controlled by different physical processes depending on the
22 boundary. At the “eastern boundary”, there is a constructive coupling between eddies resulting from the
23 instability of the PUC peaking in Austral winter, and the enhanced DO along the coast resulting from
24 an increased horizontal and vertical diffusion at the same season.

25 At the northern boundary of the OMZ, the DO eddy flux is also related to the strong EKE around 5°S
26 that peaks in Austral winter. Despite the fact that the OMZ northern boundary is embedded in the
27 equatorial wave guide, since the intraseasonal Kelvin wave activity tends to peak in Austral summer
28 (Illig et al., 2014) it can be ruled out that the seasonal cycle in DO eddy flux is strongly linked to the
29 intraseasonal long equatorial waves. The results of Echevin et al. (2011) also suggest that the enhanced
30 mesoscale activity observed near the northern OMZ boundary during winter would not be related to the

1 equatorial Kelvin wave activity, but rather to local variations of the local current system (intrinsic or
2 induced by the local wind stress). Whether or not the strong EKE found there results from the
3 instability of the coastal current system or of the EUC and the South Equatorial Current (SEC), would
4 need to be explored.

5 Regarding the southern boundary, it is interesting to note that the DO eddy flux peaks in Austral spring,
6 three months later than at the northern boundary. A possible mechanism driving the local variability
7 observed at the southern section is the generation of local baroclinic instability and vorticity input from
8 wind stress curl as observed for the California system (Kelly et al, 1998). The southern section lies
9 within the northeast rim of the Southeast Pacific Anticyclone, and the peak in the seasonal DO eddy
10 flux coincides with the reported intensity peak of the seasonal cycle of the Anticyclone, towards the
11 end of the year (Rahn et al., 2015; Ancapichún and Garcés-Vargas, 2015). In this sense, the mesoscale
12 activity in this region could be directly modulated by the winds. Dewitte et al. (2008) also report that
13 intraseasonal (internal) variability in currents can originate from the interactions between the annual
14 extra tropical Rossby wave and the mean circulation in a medium resolution oceanic regional model
15 over this region, a process also observed and documented from a high-resolution model over the North
16 Pacific (Qiu et al., 2013). The actual source of the eddy activity in this region would also deserve
17 further investigation.

18 Our study also reveals that the most prominent propagating features in DO inside the OMZ at annual
19 frequency is below ~300 m, where the seasonal DO flux follows approximately the theoretical WKB
20 ray paths of the annual ETRW. From that depth, the seasonal variability in physical fluxes becomes one
21 order of magnitude larger than the one of the biogeochemical fluxes (Fig. 10c). This supports the
22 observation that DO tends to behave as a passive tracer so that vertical displacements of the DO
23 isopleths mimic those of the isotherms, inducing a seasonal DO flux that resembles the energy flux
24 path of the ETRW. This mechanism adds a dimension to the understanding of the OMZ variability,
25 considering that the vertical propagation of ETRW can take place at frequencies ranging from annual
26 (Dewitte et al., 2008) to interannual (Ramos et al., 2008).

27 We now discuss some implications of our results with regards to current concerns around OMZ
28 variability at long timescales. A recent study has suggested a trend in the OMZ towards expansion and
29 intensification (Stramma et al., 2008) whose forcing mechanism remains unclear (Stramma et al.,
30 2010). Observations in the Pacific Ocean also suggest that the OMZ characteristics vary decadal

(Stramma et al., 2008; 2010). Since decadal variability can manifest as a low frequency modulation of the seasonal cycle, our study may provide guidance for investigating OMZ variability at long timescales. In particular we find that the amplitude of the seasonal cycle is nearly twice as large at the southern boundary than at the northern boundary and “coastal boundary”, which suggests a larger sensitivity of the OMZ variability at the southern boundary to the modulation of eddy activity by climate forcing. This view would preferentially link the OMZ low frequency fluctuations to mid latitudes changes in the circulation. We note however that the relative contribution of the mean DO flux and the DO eddy flux exhibits significant interannual fluctuations at the boundaries (not shown), which suggests that eddy induced DO flux may not be the only key player for understanding long term trend in the OMZ. It is interesting to note that so far, it has been difficult to reconcile the observed trend in the OMZ with the trend simulated by the current generation of coupled models (Stramma et al., 2012), which has been attributed to biases in the mean circulation and inadequate remineralization representation (Cocco et al., 2013; Cabré et al., 2015). Our results support the view that such discrepancy may partly originate from the inability of the low resolution models to account for the DO eddy flux and its modulation. Regional modeling experiments also showed that eddy activity can be modulated at ENSO and decadal timescales (Combes et al., 2015; Dewitte et al., 2012). This issue would certainly require further investigation, and could benefit from the experimentation with our coupled model platform. This is planned for future work.

Lastly, the seasonal changes in the OMZ evidenced in this work are associated with a seasonal change of the oxycline depth (and an oxycline intensity change; not shown), which can be considered a proxy for the production of greenhouse gases (CO_2 and N_2O) inside the OMZ (e.g. Paulmier et al., 2011; Kock et al., 2016). Our results suggest that the impact of the OMZ on the atmosphere through the production of climatically-active gases, such as CO_2 and N_2O , would be seasonally damped during austral winter, due to a deepening of the oxycline and a weakening of its intensity.

6 Summary and conclusions

A high resolution coupled physical/biogeochemical model experiment is used to document the seasonal variability of the OMZ off Peru. The annual harmonic of DO reveals three main regions with enhanced amplitude or specific propagation characteristics, suggesting distinct dynamical regimes: 1) The coastal domain; 2) the offshore ocean below 400 m and 3) at the southern and northern boundaries. In the

1 [coastal portion of the OMZ, the seasonal variability is related to the local wind forcing, and therefore](#)
2 [follows to a large extent the paradigm of upwelling triggered productivity, followed by](#)
3 [remineralization. It is shown in particular that the DO peaks in Austral winter which is associated with](#)
4 [horizontal and vertical diffusion induced by both the increase in baroclinic instability and intraseasonal](#)
5 [wind activity. This is counter intuitive with regards to the seasonality of the alongshore upwelling.](#)
6 [favorable winds also peaking in Austral winter, which would tend to favor the intrusion of](#)
7 [deoxygenated waters from the open ocean OMZ to the shelf. Instead, the coastal domain can be viewed](#)
8 [as a source of DO in Austral winter for the OMZ through offshore transport. The latter is induced by](#)
9 [eddies that are triggered by the instabilities of the PUC. In the model, the offshore DO eddy flux has a](#)
10 [marked seasonal cycle that is in phase with the seasonal cycle of the DO along the coast, implying that](#)
11 [the coastal domain, viewed here as the eastern boundary of the OMZ, is a source of seasonal variability](#)
12 [for the OMZ. This appears to operate effectively in the upper 300 m. Below that depth, the DO eddy](#)
13 [flux is much reduced due to both a much weaker eddy activity, and very low DO concentration. On the](#)
14 [other hand, a mean seasonal DO flux is observed and exhibits propagating features reminiscent of the](#)
15 [vertical propagation of energy associated with the annual extra tropical Rossby wave.](#)
16 [In the upper 300 m, the OMZ seasonal variability is also associated with the DO eddy flux at the OMZ](#)
17 [meridional boundaries where it is the most intense. We find that the seasonal cycle in DO eddy flux](#)
18 [peaks in Austral winter at the northern boundary, while it peaks a season later at the southern boundary.](#)
19 [Additionally, the amplitude of the seasonal cycle in DO eddy flux is larger at the southern boundary](#)
20 [than at the northern boundary. The schematic of Figure 20 summarizes the main processes documented](#)
21 [in this paper to explain the seasonality of the OMZ.](#)

23 **Acknowledgments**

24 O. Vergara was supported by a doctoral scholarship from the National Chilean Research and
25 Technology Council (CONICYT) through the program Becas Chile (scholarship 72130138). The
26 authors are thankful for the financial support received from the Centre National d'Etudes Spatiales
27 (CNES). During the preparation of this work O. Vergara was supported by a mobility scholarship from
28 the University of Toulouse, through the ATUPS program when visiting the CEAZA. M. Ramos
29 acknowledges support from FONDECYT (project 1140845) and Chilean Millennium Initiative
30 (NC120030). [O. Pizarro acknowledges support from the FONDECYT 1121041 project and the Chilean](#)

- 1 | [Millennium Initiative \(IC-120019\). The authors thank the two anonymous reviewers for their](#)
- 2 | [constructive comments that helped improving the manuscript.](#)

1 **References**

- 2 Ancapichún, S. and Garcés-Vargas, J.: Variability of the Southeast Pacific Subtropical Anticyclone and
3 its impact on sea surface temperature off north-central Chile, *Cienc. Mar.*, 41, 1-20, doi:
4 10.7773/cm.v41i1.2338, 2015.
- 5 Arévalo-Martínez, D., Kock, L. A., Löscher, C. R., Schmitz, R. A., and Bange, R. A.: Massive nitrous
6 oxide emissions from the tropical South Pacific Ocean, *Nat. Geosci.*, doi: 10.1038/NGEO2469, 2015.
- 7 Bettencourt, J.H., López, C., Hernández-García, E., Montes, I., Sudre, J., Dewitte, B., Paulmier A., and
8 Garçon, V. : Boundaries of the Peruvian Oxygen Minimum Zone shaped by coherent mesoscale
9 dynamics, *Nat. Geosci.*, doi: 10.1038/ngeo2570, 2015.
- 10 Bianchi, D., Dunne, J. P., Sarmiento, J. L., and Galbraith, E. D.: Data-based estimates of suboxia,
11 denitrification, and N₂O production in the ocean and their sensitivities to dissolved O₂, *Global*
12 *Biogeochem. Cy.*, 26, GB2009, doi:10.1029/2011GB004209, 2012.
- 13 [Bianucci, L., Fennel, K., and Denman, K. L.: Role of sediment denitrification in water column oxygen](#)
14 [dynamics: comparison of the North American East and West Coasts, *Biogeosciences*, 9, 2673–2682,](#)
15 [doi:10.5194/bg-9-2673-2012, 2012.](#)
- 16 Brandt, P., Bange, H. W., Banyte, D., Dengler, M., Didwischus, S.-H., Fischer, T., Greatbatch, R. J.,
17 Hahn, J., Kanzow, T., Karstensen, J., Körtzinger, A., Krahmann, G., Schmidtke, S., Stramma, L.,
18 Tanhua, T., and Visbeck, M.: On the role of circulation and mixing in the ventilation of oxygen
19 minimum zones with a focus on the eastern tropical North Atlantic, *Biogeosciences*, 12, 489-512,
20 doi:10.5194/bg-12-489-2015, 2015.
- 21 Cabré, A., Marinov, I., Bernardello, R., and Bianchi, D.: Oxygen minimum zones in the tropical Pacific
22 across CMIP5 models: mean state differences and climate change trends, *Biogeosciences*, 12, 6525-
23 6587, doi:10.5194/bgd-12-6525-2015, 2015.
- 24 Cambon G., Goubanova, K., Marchesiello, P., Dewitte, B., Illig, S., and Echevin, V.: Assessing the
25 impact of downscaled winds on a regional ocean model simulation of the Humboldt system, *Ocean*
26 *Model.*, 65, 11-24, 2013.
- 27 Chavez, F. P., Bertrand, A., Guevara-Carrasco, R., Soler, P., and Csirke, J.: The northern Humboldt
28 Current System: Brief history, present status and a view towards the future, *Prog. Oceanogr.*, 79, pp.

1 95–105, 2008.

2 Chaigneau, A., and Pizarro, O.: Eddy characteristics in the eastern South Pacific, *J. Geophys. Res.*, 110,
3 C06005, doi:10.1029/2004JC002815, 2005.

4 Chaigneau, A., Eldin G., and Dewitte, B.: Eddy activity in the four major upwelling systems from
5 satellite altimetry (1992–2007), *Prog. Oceanogr.*, 83 (1–4), 117–123, doi:10.1016/j.pocean.2009.07.012,
6 2009.

7 Cocco, V., Joos, F., Steinacher, M., Frölicher, T. L., Bopp, L., Dunne, J., Gehlen, M., Heinze, C., Orr,
8 J., Oschlies, A., Schneider, B., Segschneider, J., and Tjiputra, J.: Oxygen and indicators of stress for
9 marine life in multi-model global warming projections, *Biogeosciences*, 10, 1849–1868,
10 doi:10.5194/bg-10-1849-2013, 2013.

11 [Colas, F., McWillimas, J. C., Capet, X., and Kurian, J.: Heat balance and eddies in the Peru-Chile](#)
12 [current system. *Clim. Dyn.*, 39:509–529, doi:10.1007/s00382-011-1170-6, 2012.](#)

13 Combes, V., Hormazabal, S., and Di Lorenzo, E.: Interannual variability of the subsurface eddy field in
14 the Southeast Pacific. *J. Geophys. Res.*, 120, 4907–4924, doi:10.1002/2014JC010265, 2015.

15 Cornejo, M., Farías, L., and Paulmier, A.: Temporal variability in N₂O water content and its air-sea
16 exchange in an upwelling area off central Chile (36° S), *Mar. Chem.*, 101, 85–94,
17 doi:10.1016/j.marchem.2006.01.004, 2006.

18 Cornejo, M. and Farías, L.: Following the N₂O consumption at the Oxygen Minimum Zone in the
19 eastern South Pacific, *Biogeosciences*, 9, 2691–2707, doi:10.5194/bgd-9-2691-2012, 2012.

20 Czeschel, R., Stramma, L., Schwarzkopf, F. U., Giese, B. S., Funk, A., and Karstensen, J.: Middepth
21 circulation of the eastern tropical South Pacific and its link to the oxygen minimum zone, *J. Geophys.*
22 *Res.*, 116, C01015, doi:10.1029/2010JC006565, 2011.

23 Czeschel, R., Stramma, L., Weller, R. A., and Fischer, T.: Circulation, eddies, oxygen and nutrient
24 changes in the eastern tropical South Pacific Ocean, *Ocean Sci.*, 11, 455–4703. doi:10.5194/os-11-455-
25 2015, 2015.

26 daSilva A., Young, A.C., and Levitus, S.: Atlas of surface marine data 1994. Algorithms and
27 procedures. vol. 1 Technical Report 6, US Department of Commerce, NOAA, NESDIS, 1994.

1 Dewitte B., Ramos, M., Echevin, V., Pizarro, O., and duPenhoat, Y.: Vertical structure variability in a
2 seasonal simulation of a medium-resolution regional model simulation of the South Eastern Pacific.
3 Prog. Oceanogr., 79, 120-137, 2008.

4 Dewitte, B., Illig, S., Renault, L., Goubanova, K., Takahashi, K., Gushchina, D., Mosquera, K., and
5 Purca, S.: Modes of covariability between sea surface temperature and wind stress intraseasonal
6 anomalies along the coast of Peru from satellite observations (2000–2008), J. Geophys. Res., 116,
7 C04028, doi:10.1029/2010JC006495, 2011.

8 Dewitte, B., Vazquez-Cuervo, J., Goubanova, K., Illig, S., Takahashi, K., Cambon, G., Purca, S.,
9 Correa, D., Gutiérrez, D., Sifeddine, A., and Ortlieb, L.: Change in El Niño flavours over 1958–2008:
10 Implications for the long-term trend of the upwelling off Peru, Deep Sea Res., Part II, 77–80, 143–156,
11 doi:10.1016/j.dsr2.2012.04.011, 2012.

12 [Dufois, F., Penven, P., Whittle, C., and Veitch, J.: On the warm nearshore bias in Pathfinder monthly](#)
13 [SST products over Eastern Boundary Upwelling Systems. Ocean Modelling, doi:](#)
14 [10.1016/j.ocemod.2012.01.007, 2012.](#)

15 Dunn J. R., and Ridgway, K. R.: Mapping ocean properties in regions of complex topography, Deep-
16 Sea Res. Pt., 49, 591-604, 2002.

17 Dunne, J. P., Armstrong, R. A., Gnanadesikan, A., and Sarmiento, J. L.: Empirical and mechanistic
18 models for the particle export ratio, Global Biogeochem. Cy., 19, GB4026, doi:10.1029/2004gb002390,
19 2005.

20 Duteil, O. and Oschlies, A.: Sensitivity of simulated extent and future evolution of marine suboxia to
21 mixing intensity, Geophys. Res. Lett., 38, L06607, doi:10.1029/2011GL046877, 2011.

22 Duteil, O., Schwarzkopf, F.U., Böning, C. W., and Oschlies, A.: Major role of the equatorial current
23 system in setting oxygen levels in the eastern tropical Atlantic Ocean: A high-resolution model study,
24 Geophys. Res. Lett., 41, 2033–2040, doi:10.1002/2013GL058888, 2014.

25 Echevin, V., Aumont, O., Ledesma, J., and Flores, G.: The seasonal cycle of surface chlorophyll in the
26 Peruvian upwelling system: A modelling study. Progr. Oceanogr., 79, 2-4, 167-176, 2008.

27 Echevin, V., Colas, F., Chaigneau, A., and Penven, P.: Sensitivity of the Northern Humboldt Current
28 System nearshore modeled circulation to initial and boundary conditions. J. Geophys. Res., 116,

1 C07002, doi:10.1029/2010JC006684, 2011.

2 Eliassen, A., and Palm, E.: On the transfer of energy in stationary mountain waves. *Geofys. Publ.*, 22
3 (3), 1–23, 1960.

4 Farías, L., Paulmier, A., and Gallegos, M.: Nitrous oxide and N-nutrient cycling in the oxygen
5 minimum zone off northern Chile. *Deep Sea Research I* 54, 164-180. doi: 10.1016/j.dsr.2006.11.003,
6 2007.

7 Fuenzalida, R., Schneider, W., Garces-Vargas, J., Bravo, L., and Lange, C.: Vertical and horizontal
8 extension of the oxygen minimum zone in the eastern South Pacific Ocean, *Deep Sea Res., Part II*, 56,
9 992–1003, doi:10.1016/j.dsr2.2008.11.001, 2009.

10 García, H. E. and Gordon, L. I.: Oxygen solubility in seawater – better fitting equations, *Limnol.*
11 *Oceanogr.*, 37, 1307–1312, 1992.

12 Goubanova, K., Echevin, V., Dewitte, B., Codron, F., Takahashi, K., Terray, P., and Vrac, M.: Statistical
13 downscaling of sea-surface wind over the Peru–Chile upwelling region: diagnosing the impact of
14 climate change from the IPSL-CM4 model. *Clim. Dyn.* DOI 10.1007/s00382-010-0824-0, 2011.

15 Gruber, N.: The marine nitrogen cycle: Overview of distributions and processes, in: *Nitrogen in the*
16 *marine environment*, second edition, Capone, D. G., Bronk, D. A., Mulholland, M. R. and Carpenter, E.
17 J., Eds., Elsevier, Amsterdam, 1-50, 2008.

18 Gruber, N., Lachkar, Z., Frenzel, H., Marchesiello, P., Münnich, M., McWilliams, J. C., Nagai, T., and
19 Plattner, G. K.: Eddy-induced reduction of biological production in eastern boundary upwelling
20 systems, *Nat. Geosci.*, 4, 787–792, doi:10.1038/NGEO01273, 2011.

21 Gutiérrez, D., Enriquez, E., Purca, S., Quipuzcoa, L., Marquina, R., Flores, G., Graco, M.: Oxygenation
22 episodes on the continental shelf of central Peru: remote forcing and benthic ecosystem response. *Prog.*
23 *Oceanogr.* 79, 177–189, 2008.

24 Gutiérrez D., Bouloubassi, I., Sifeddine, A., Purca, S., Goubanova, K., Graco, M., Field, D., Mejanelle,
25 L., Velazco, F., Lorre, A., Salvattecí, R., Quispe, D., Vargas, G., Dewitte, B., and Ortlieb, L.: Coastal
26 cooling and increased productivity in the main upwelling zone off Peru since the mid-twentieth century.
27 *Geophys. Res. Lett.*, 38, L07603, doi:10.1029/2010GL046324, 2011.

1 Gutknecht, E., Dadou, I., Le Vu, B., Cambon, G., Sudre, J., Garçon, V., Machu, E., Rixen, T., Kock, A.,
2 Flohr, A., Paulmier, A., and Lavik, G.: Coupled physical/biogeochemical modeling including O₂-
3 dependent processes in Eastern Boundary Upwelling Systems: Application in the Benguela,
4 Biogeosciences, 10, 3559–3591, doi:10.5194/bg-10-1-2013, 2013a.

5 Gutknecht, E., Dadou, I., Marchesiello, P., Cambon, G., Le Vu, B., Sudre, J., Garçon, V., Machu, E.,
6 Rixen, T., Kock, A., Flohr, A., Paulmier, A., and Lavik, G.: Nitrogen transfers off Walvis Bay: A 3-D
7 coupled physical/biogeochemical modeling approach in the Namibian Upwelling System,
8 Biogeosciences, 10, 4117–4135, doi:10.5194/bg-10-4117-2013, 2013b.

9 Henley, B. J., Gergis, J., Karoly, D. J., Power, S. B., Kennedy, J., and Folland, C. K.: A Tripole Index
10 for the Interdecadal Pacific Oscillation. *Clim. Dyn.*, 45, 3077-3090, doi:10.1007/s00382-015-2525-1,
11 2015.

12 Henson, S. A., Sanders, R., and Madsen, E.: Global patterns in efficiency of particulate organic carbon
13 export and transfer to the deep ocean, *Global Biogeochem. Cy.*, 26, GB1028,
14 doi:10.1029/2011gb004099, 2012.

15 Illig, S., Dewitte, B., Goubanova, K., Cambon, G., Boucharel, J., Monetti, F., Romero, C., Purca S.,
16 and Flores, R.: Forcing mechanisms of intraseasonal SST variability off central Peru in 2000– 2008, *J.*
17 *Geophys. Res.*, 119, 3548–3573, doi:10.1002/ 2013JC009779, 2014.

18 Karstensen, J., Stramma, L., and Visbeck, M.: Oxygen minimum zones in the eastern tropical Atlantic
19 and Pacific oceans. *Progr. Oceanogr.* 77.4: 331-350, 2008.

20 Karstensen, J., Fiedler, B., Schütte, F., Brandt, P., Körtzinger, A., Fischer, G., Zantopp, R., Hahn, J.,
21 Visbeck, M., and Wallace, D.: Open ocean dead zones in the tropical North Atlantic Ocean,
22 Biogeosciences, 12, 2597-2605, doi:10.5194/bg-12-2597-2015, 2015.

23 Kelly, K., Beardsley, R., Limeburner, R., and Brink, K.: Variability of the near-surface eddy kinetic
24 energy in the California Current based on altimetric, drifter and moored data. *Journal Geophysical*
25 *Research* 103, 13,067–13,083, 1998.

26 [Kock, A., Arévalo-Martínez, D. L., Löscher, C. R., and Bange, H. W.: Extreme N₂O accumulation in](#)
27 [the coastal oxygen minimum zone off Peru, Biogeosciences, 13, 827-840, doi:10.5194/bg-13-827-](#)
28 [2016, 2016.](#)

1 [Large, W. G., McWilliams, J. C., and Doney, S. C.: Oceanic vertical mixing: A review and a model](#)
2 [with a nonlocal boundary layer parameterization, Rev. Geophys., 32, 363–403, doi:](#)
3 [199410.1029/94RG01872, 1994.](#)

4

5 Law, C. S., Brévière, E., de Leeuw, G., Garçon, V., Guieu, C., Kieber, D. J., Konradowitz, S.,
6 Paulmier, A., Quinn, P. K., Saltzman, E. S., Stefels, J., and von Glasow, R.: Evolving research
7 directions in Surface Ocean - Lower Atmosphere (SOLAS) science, Environ. Chem., 10, 1-16, doi:
8 10.1071/EN12159, 2013.

9 Libes, S.M.: An Introduction to Marine Biogeochemistry, John Wiley and Sons, New York, 734pp,
10 1992.

11 Llanillo, P. J., Karstensen, J., Pelegrí, J. L., and Stramma, L.: Physical and biogeochemical forcing of
12 oxygen and nitrate changes during El Niño/El Viejo and La Niña/La Vieja upper-ocean phases in the
13 tropical eastern South Pacific along 86° W, Biogeosciences, 10, 6339-6355, doi: 10.5194/bg-10-6339-
14 2013, 2013.

15 Luyten, J.R., Pedlosky, J., and Stommel, H.: The ventilated thermocline. Journal of Physical
16 Oceanography 13, 292–309, 1983.

17 McClain, C. R., Cleave, M. L., Feldman, G. C., Gregg, W. W., Hooker, S. B., and Kuring, N.: Science
18 quality SeaWiFS data for global biosphere research, Sea Technol., 39, 9, 10–16, 1998.

19 Montes, I., Colas, F., Capet, X., and Schneider, W.: On the pathways of the equatorial subsurface
20 currents in the Eastern Equatorial Pacific and their contributions to the Peru-Chile Undercurrent, J.
21 Geophys. Res., 115, C09003, doi:10.1029/2009JC005710, 2010.

22 Montes, I., Dewitte, B., Gutknecht, E., Paulmier, A., Dadou, I., Oschlies, A., and Garçon, V.: High-
23 resolution modeling of the Eastern Tropical Pacific oxygen minimum zone: Sensitivity to the tropical
24 oceanic circulation, J. Geophys. Res. Oceans, 119, doi:10.1002/2014JC009858, 2014.

25 Morales, C. E., Hormazabal, S. E., and Blanco, J.: Interannual variability in the mesoscale distribution
26 of the depth of the upper boundary of the oxygen minimum layer off northern Chile (18–24S):
27 Implications for the pelagic system and biogeochemical cycling, J. Mar. Res., 57, 909–932,
28 doi:10.1357/002224099321514097, 1999.

1 Morel, A., and Berthon, J. F.: Surface pigments, algal biomass profiles, and potential production of
 2 euphotic layer: Relationship reinvestigated in view of remote-sensing applications, *Limnol. Oceanogr.*,
 3 34, 1545–1562, 1989.

4 Nagai, T., Gruber, N., Frenzel, H., Lachkar, Z., McWilliams, J. C., and Plattner, G.-K.: Dominant role
 5 of eddies and filaments in the offshore transport of carbon and nutrients in the California Current
 6 System, *J. Geophys. Res. Oceans*, 120, 5318–5341, doi:10.1002/2015JC010889, 2015.

7 [Nerem, R.S., Chambers, D.P., Choe, C., and Mitchum, G.T.: Estimating mean sea level change from](#)
 8 [the TOPEX and Jason altimeter missions. *Marine Geodesy* 33, Supplement 1: 435-446, 2010.](#)

9 O'Reilly, J. E., Maritorena, S., Siegel, D., O'Brien, M. O., Toole, D., Mitchell, B. G., Kahru, M.,
 10 Chavez, F., Strutton, P. G., Cota, G. F., Hooker, S. B., McClain, C., Carder, K., Muller-Karger, F.,
 11 Harding, L., Magnuson, A., Phinney, D., Moore, G., Aiken, J., Arrigo, K. R., Letelier, R. M., and
 12 Culver, M.: Ocean chlorophyll a algorithms for SeaWiFS, OC2, and OC4: Version 4, in: *SeaWiFS*
 13 *Postlaunch Calibration and Validation Analyses, Part 3*, NASA Tech. Memo 2000–206892, vol. 11,
 14 Hooker, B., and Firestone, E. R., Eds., pp. 9–19, NASA, Goddard Space Flight Center, Greenbelt,
 15 Maryland, 2000.

16 Paulmier, A., and Ruiz-Pino, D.: Oxygen minimum zones (OMZs) in the modern ocean, *Prog.*
 17 *Oceanogr.*, 80, 3–4, 113–128, doi:10.1029/j.pocean.2008.08.001, 2009.

18 Paulmier, A., Ruiz-Pino, D., Garçon, V., and Farías, L.: Maintaining of the East South Pacific Oxygen
 19 Minimum Zone (OMZ) off Chile, *Geophys. Res. Lett.*, 33, L20601, doi:10.1029/2006GL026801, 2006.

20 Paulmier, A., Ruiz-Pino, D., and Garçon, V.: The Oxygen Minimum Zone (OMZ) off Chile as intense
 21 source of CO₂ and N₂O, *Contin. Shelf Res.*, 28, 2746–2756, 2008.

22 Paulmier, A., Ruiz-Pino, D., and Garçon, V.: CO₂ maximum in the oxygen minimum zone (OMZ),
 23 *Biogeosciences*, 8, 239–252, doi:10.5194/bg-8-239-2011, 2011.

24 Penven, P., Echevin, V., Pasapera, J., Colas, F., and Tam, J.: Average circulation, seasonal cycle, and
 25 mesoscale dynamics of the Peru Current System: a modeling approach. *J. Geophys. Res.*, 110, C10021,
 26 2005.

27 Pizarro, O., Shaffer, G., Dewitte, B., and Ramos, M.: Dynamics of seasonal and interannual variability
 28 of the Peru-Chile Undercurrent, *Geophys. Res. Lett.*, 29(12), 1581, doi: 10.1029/2002GL014790, 2002.

1 [Prince, E. D., and Goodyear, C. P.: Hypoxia-based habitat compression of tropical pelagic fishes. Fish.](#)
2 [Oceanogr. 15:6, 451-464, doi:10.1111/j.1365-2419.2005.00393.x, 2006.](#)

3 [Qiu, B., Chen, S., and Sasaki, H.: Generation of the North Equatorial Undercurrent jets by triad](#)
4 [baroclinic Rossby wave interactions. J. Phys. Oceanogr., 43, 2682–2698, doi: 10.1175/JPO-D-13-](#)
5 [099.1, 2013](#)

6 Rahn, D., Rosenblüth, B., and Rutllant, J.: Detecting Subtle Seasonal Transitions of Upwelling in
7 North-Central Chile. J. Phys. Oceanogr., 45, 854–867, 2015

8 Ramos, M., Dewitte, B., Pizarro, O., and Garric, G.: Vertical propagation of extratropical Rossby
9 waves during the 1997 – 1998 El Niño off the west coast of South America in a medium-resolution
10 OGCM simulation, J. Geophys. Res., 113, C08041, doi:10.1029/2007JC004681, 2008.

11 Resplandy, L., Lévy, M., Bopp, L., Echevin, V., Pous S., Sarma, V. V. S. S., [and](#) Kumar, D.: Controlling
12 factors of the oxygen balance in the Arabian Sea's OMZ, Biogeosciences, 9, 5095-5109,
13 doi:10.5194/bg-9-5095-2012, 2012.

14 [Reynolds, R. W., Smith, T. M., Liu, C., Chelton, D. B., Casey, K. S., and Schlax, M. G.: Daily high-](#)
15 [resolution blended analyses for sea surface temperature. J. Climate, 20, 5473-5496, 2007.](#)

16 Richter I.: Climate model biases in the eastern tropical oceans: causes, impacts and ways forward.
17 WIREs Clim Change doi: 10.1002/wcc.338., 2015.

18 Ridgway K. R., Dunn, J.R., and Wilkin, J. L.: Ocean interpolation by four-dimensional least squares
19 -Application to the waters around Australia, J. Atmos. Ocean. Tech., Vol 19, No 9, 1357-1375, 2002.

20 Shchepetkin, A. F. and McWilliams, J. C.: The regional oceanic modeling system: a split-explicit, free-
21 surface, topography-following-coordinate ocean model. Ocean Model. 9, 347–404, 2005.

22 Shchepetkin, A. F. and McWilliams, J. C.: Correction and commentary for “Ocean forecasting in
23 terrain-following coordinates: Formulation and skill assessment of the regional ocean modeling
24 system” by Haidvogel et al., J. Comp. Phys., 227, 3595–3624, 2009.

25 Stramma, L., Johnson, G. C., Sprintall, J., and Mohrholz, V.: Expanding oxygen-minimum zones in the
26 tropical oceans, Science, 320, 655–658, 2008.

27 Stramma, L., Johnson, G. C., Firing, E., and Schmidtko, S.: Eastern Pacific oxygen minimum zones:

1 Supply paths and multidecadal changes, *J. Geophys. Res.*, 115, C09011, doi:10.1029/2009JC005976,
2 2010.

3 Stramma, L., Oschlies, A., and Schmidtko, S.: Mismatch between observed and modeled trends in
4 dissolved upper-ocean oxygen over the last 50 yr, *Biogeosciences*, 9, 4045-4057, doi:10.5194/bg-9-
5 4045-2012, 2012.

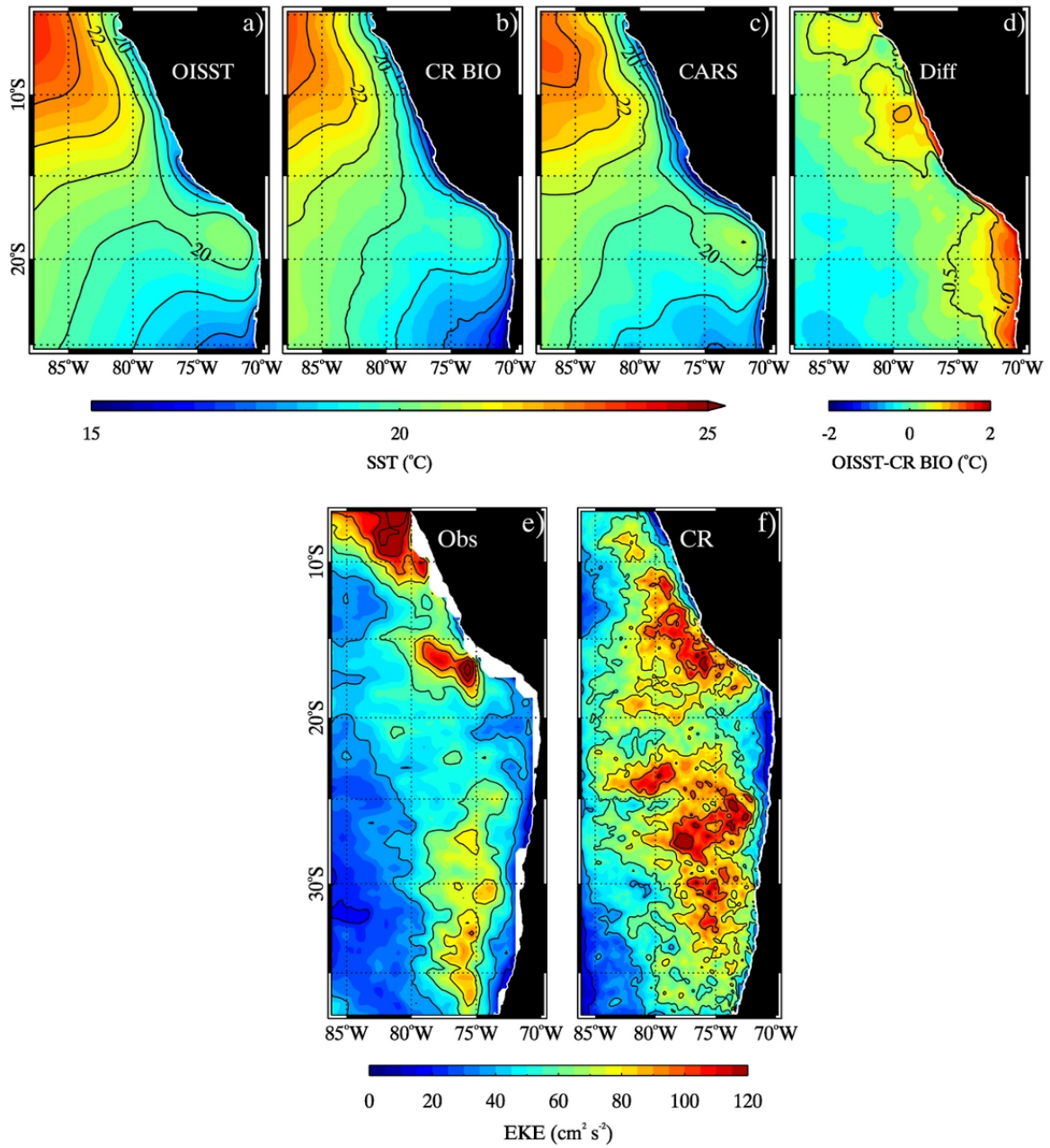
6 Stramma, L., Bange, H. W., Czeschel, R., Lorenzo, A., and Frank, M.: On the role of mesoscale eddies
7 for the biological productivity and biogeochemistry in the eastern tropical Pacific off Peru,
8 *Biogeosciences*, 10, 7293–7306, doi:10.5194/bg-10-7293-2013, 2013.

9 Stramma, L., Weller, R. A., Czeschel, R., and Bigorre, S.: Eddies and an extreme water mass anomaly
10 observed in the eastern south Pacific at the Stratus mooring, *J. Geophys. Res. Oceans*, 119, 1068–1083,
11 2014.

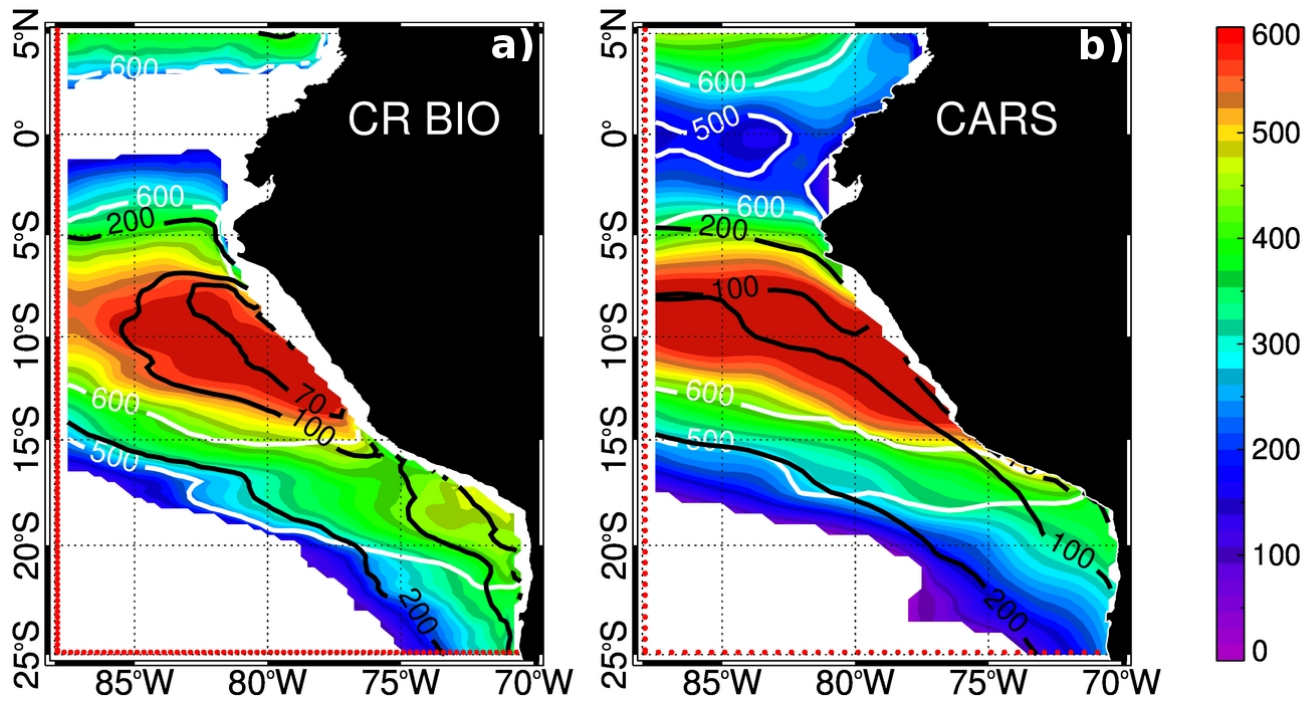
12 Thomsen, S., Kanzow, T., Krahmann, G., Greatbatch, R. J., Dengler, M., and Lavik, G.: The formation
13 of a subsurface anticyclonic eddy in the Peru-Chile Undercurrent and its impact on the near-coastal
14 salinity, oxygen, and nutrients distributions. *J. Geophys. Res. Oceans*, 120, doi:10.002/2015JC010878,
15 2016.

1 **Table 1.** Austral summer (DJF mean) and winter (JJA mean) seasonal anomalies of the DO budget,
2 averaged over the core of the Peru Under Current at 12°S (as depicted by the red contour in Figure 12).
3 The values for the seasonal cycle and the reconstructed first EOF mode (Figures 12 and 13) are
4 presented along with the difference Climatology-EOF. All values are in $10^{-6}\mu\text{M s}^{-1}$. Mixing here
5 consists in the summep-up contribution of horizontal diffusion and ($K_h \nabla^2 O_2$) and vertical diffusivity ($\frac{\partial}{\partial z} \left(K_z \frac{\partial O_2}{\partial z} \right)$).
6
7

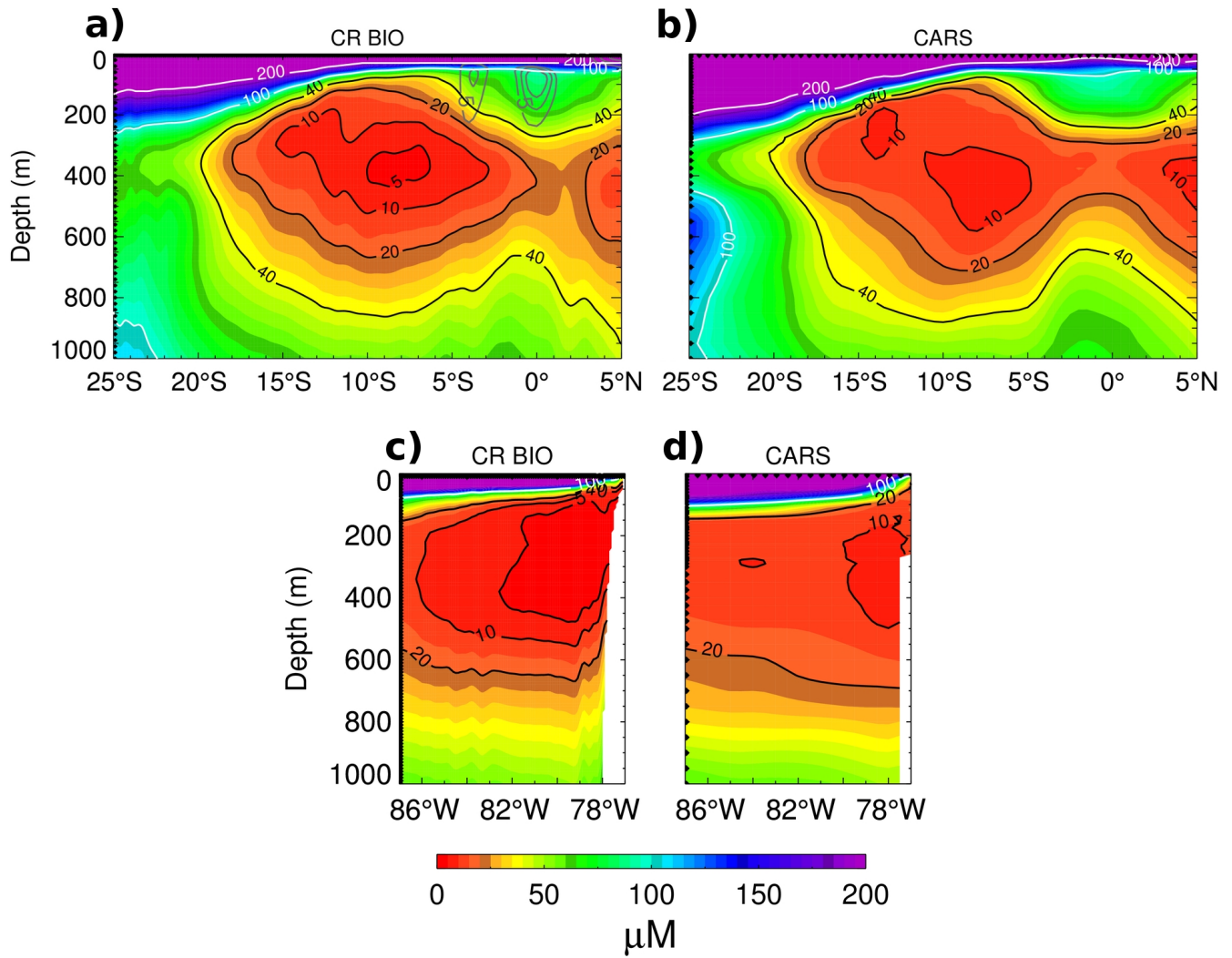
	<u>Climatology</u>		<u>EOF</u>		<u>Difference</u>	
	<u>Summer</u>	<u>Winter</u>	<u>Summer</u>	<u>Winter</u>	<u>Summer</u>	<u>Winter</u>
<u>dO₂/dt</u>	<u>1.10</u>	<u>-2.74</u>	<u>1.30</u>	<u>-2.67</u>	<u>-0.2</u>	<u>-0.07</u>
<u>Adv</u>	<u>0.61</u>	<u>-9.38</u>	<u>0.85</u>	<u>-9.30</u>	<u>-0.24</u>	<u>-0.08</u>
<u>Mixing</u>	<u>-0.42</u>	<u>7.99</u>	<u>-0.35</u>	<u>7.99</u>	<u>-0.07</u>	<u>0.0</u>
<u>Biogeochemical Flux</u>	<u>0.91</u>	<u>-1.35</u>	<u>1.00</u>	<u>-1.35</u>	<u>-0.09</u>	<u>0.0</u>



2 **Figure 1.** Mean sea surface temperature (SST) between 2000 and 2008 for (a) OISST product
3 (0.25°x0.25°), (b) the simulation (1°/12) and (c) CARS dataset (0.5°x0.5°). (d) Difference between the
4 OISST product and the simulation. Mean Eddy Kinetic Energy (EKE) between 1993 and 2008, for (e)
5 TOPEX/Poseidon Jason 1-2 merged product (0.25°x0.25°), and (f) Simulation (1°/12). EKE was
6 derived from the interannual anomalies of the geostrophic velocity field.



2 | **Figure 42.** Mean Oxygen Minimum Zone core thickness (color scale in meters) for (a) the simulation
3 | and (b) CARS. Depth of the lower (white) and upper (black) limits of the OMZ core are also depicted.
4 | The OMZ core is defined as $[DO] < 20 \mu M$. [The red dots denote the horizontal resolution of the DO](#)
5 | [field.](#)



2 **Figure 23.** Mean oxygen concentration for a meridional section at 85°W (a and b) and a cross shore
3 section at 12°S (c and d), for both the simulation and CARS. Gray contours in (a) show mean zonal
4 speed of 5,10 and 15 cm s⁻¹ respectively. The black dots denote the horizontal and vertical resolution of
5 the DO field.

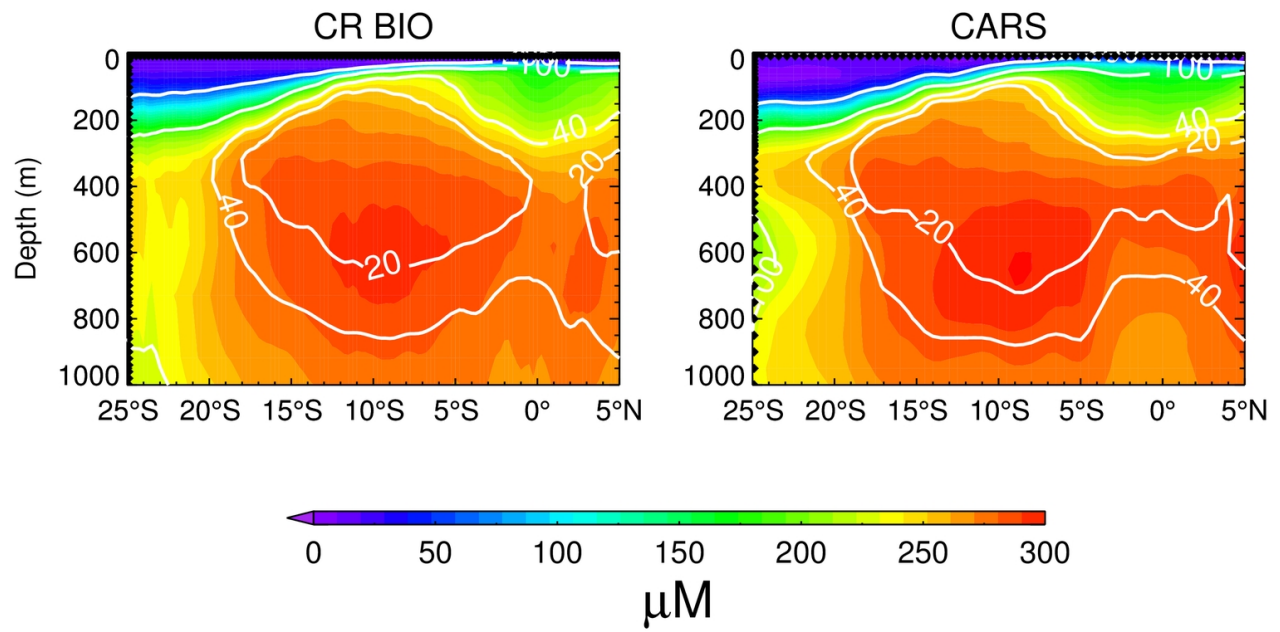
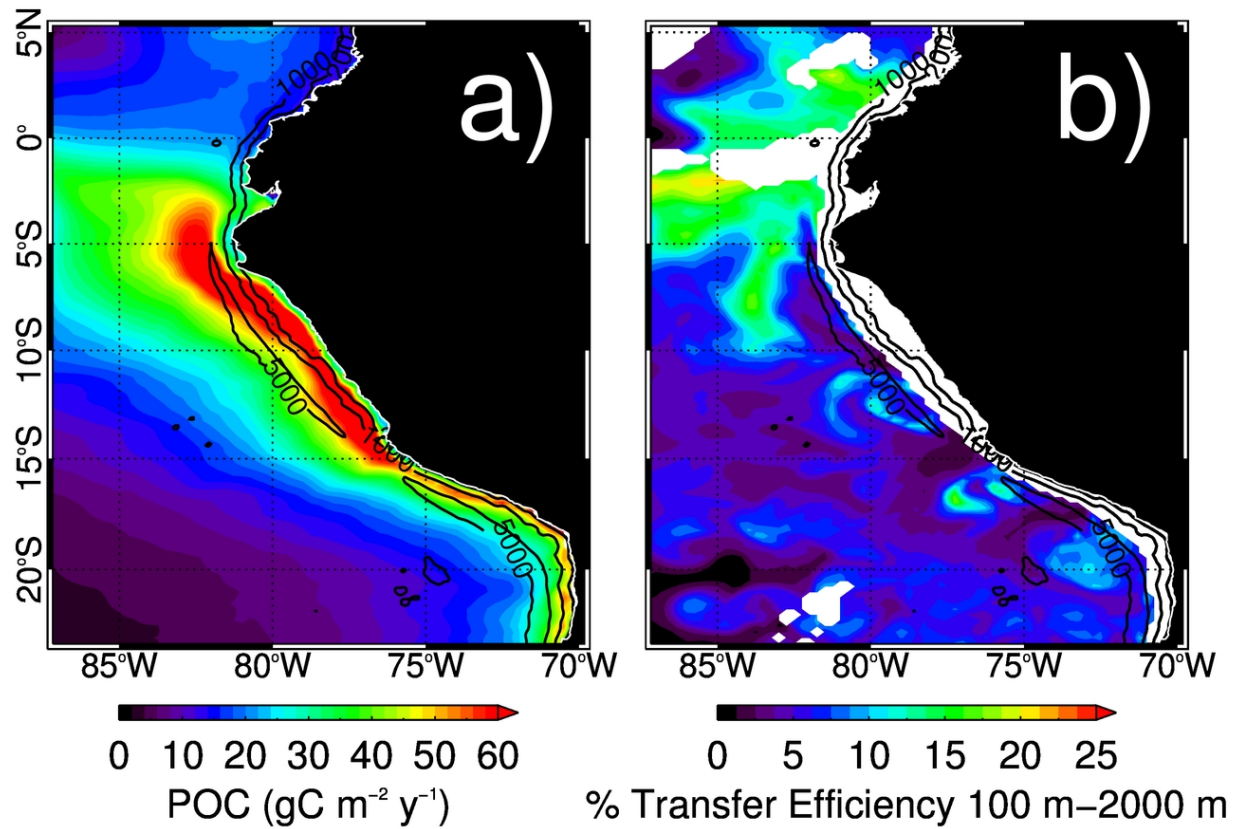
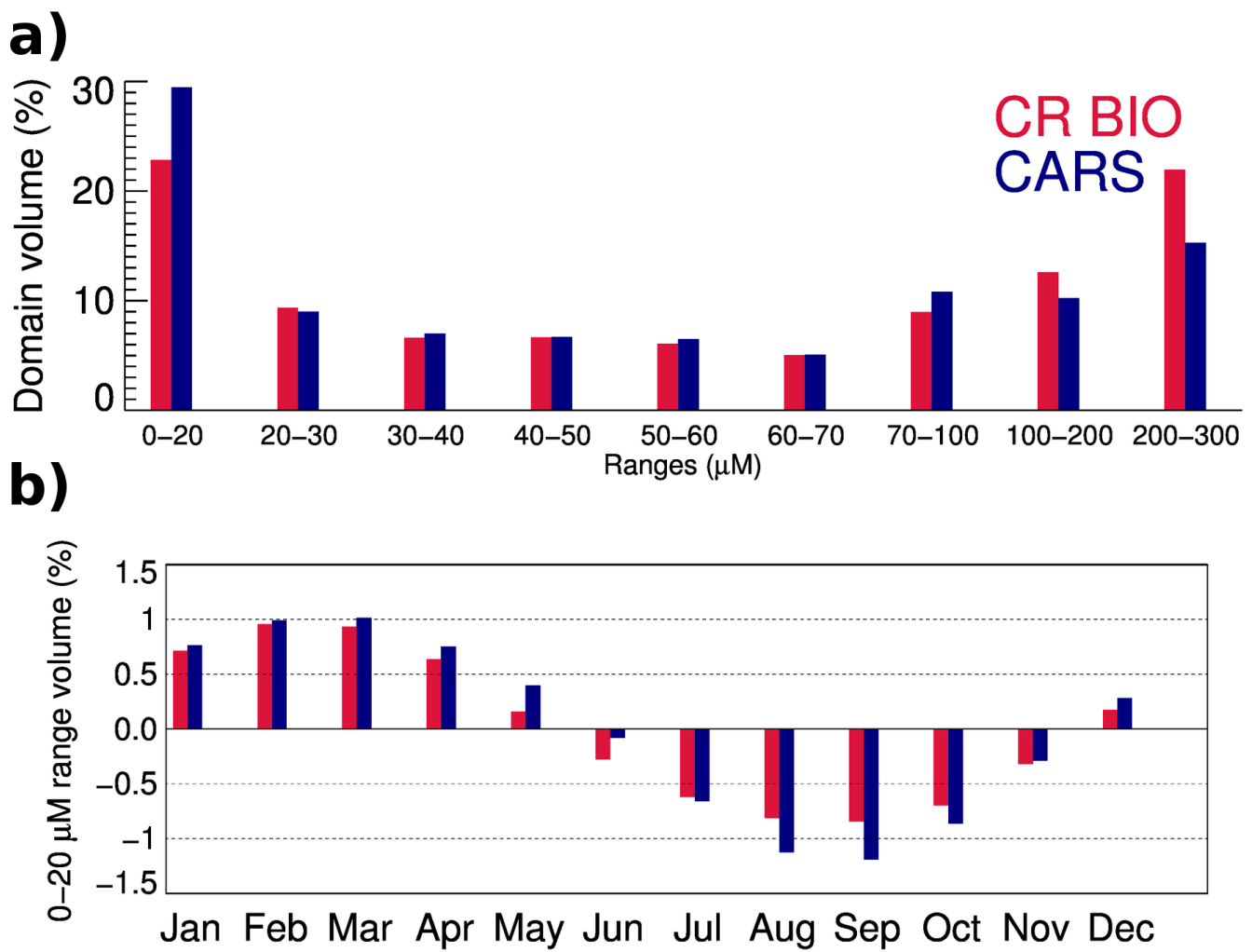


Figure 34. Mean Apparent Oxygen Utilization (AOU) at 85°W for both CR BIO and CARS. White contours denote the mean oxygen concentration isopleths (in μM). [The black dots denote the horizontal and vertical resolution of the DO field.](#)



2 **Figure 45.** (a) Particulate Organic Carbon (POC) flux at 100 m and (b) POC transfer efficiency
 3 between 100 m and 2000 m (POC flux at 2000 m divided by POC flux at 100 m), computed from the
 4 simulation. Total flux at 100 m depth: $0.8 \text{ Pg C year}^{-1}$. Integrated carbon flux at the depth of 100 m: 0.8
 5 Pg C year^{-1} . Black contours correspond to the 200, 1000 and 5000 meters isobaths.

6



1
2
3
4
5
6

Figure 56. (a) Domain volume distribution (25°S - 5°N , 88°W - 70°W) as a function of the oxygen concentration, and (b) annual cycle, relative to the mean, of the volume distribution inside the OMZ core (DO value range [correspondingcorrespondig](#) to 0 - $20 \mu\text{mol L}^{-1}$), for both CARS and the simulation.

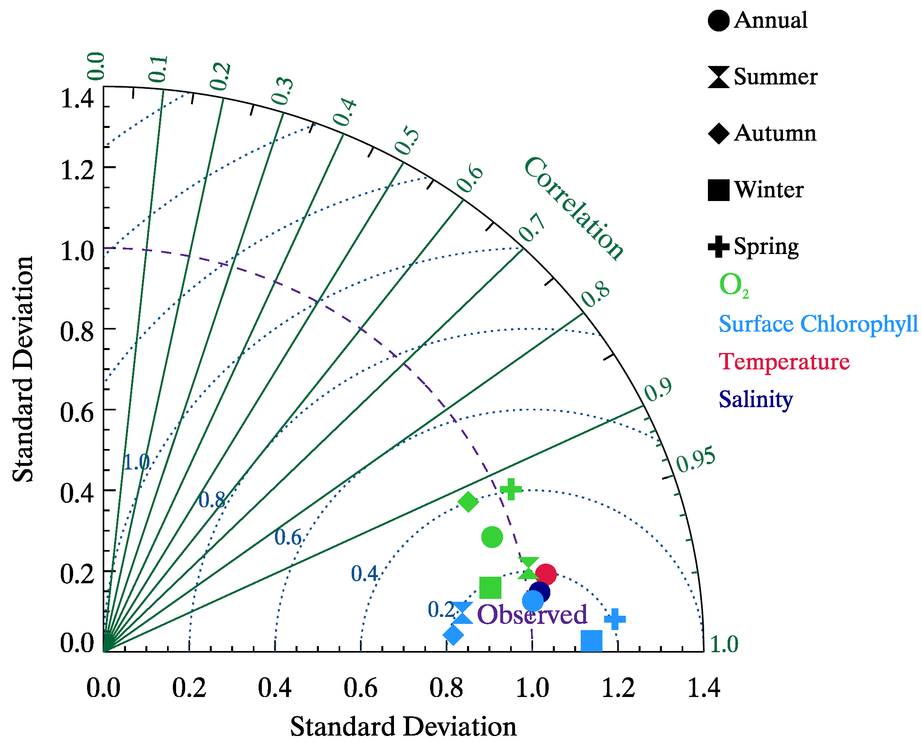


Figure 7. Taylor diagram of the seasonal mean (hourglass, diamond, square and cross) and annual mean (circle) pattern of DO and Surface Chlorophyll (25°S-5°N, 88°W-70°W). Only annual mean pattern comparisons are shown for temperature and salinity (same spatial domain). DO, temperature and salinity were vertically averaged between 100 and 600m depth (focus on the OMZ core). Only the surface chlorophyll values within 250 km next to the coast were considered. The comparisons are made between the simulation and CARS (for DO, temperature and salinity) and SeaWiFS (for surface chlorophyll). Ordinate and abscissa axes represent the standard deviation normalized by the observations standard deviation. Blue dotted radial lines indicate the RMS difference between the observations and the simulation.

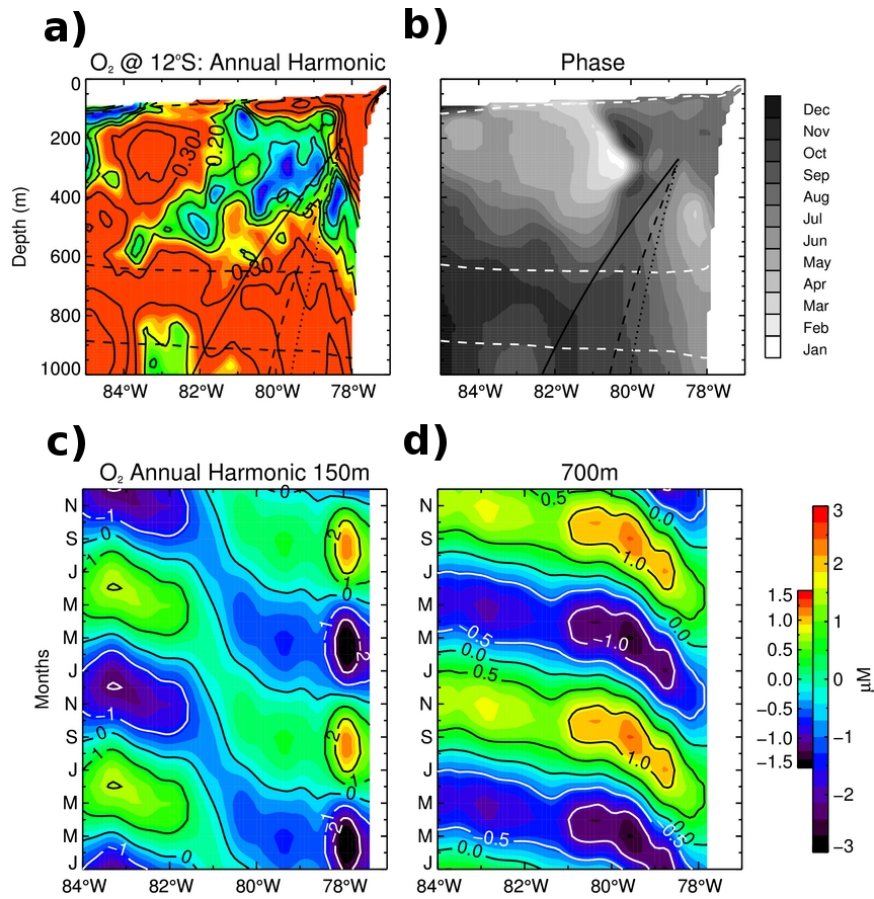
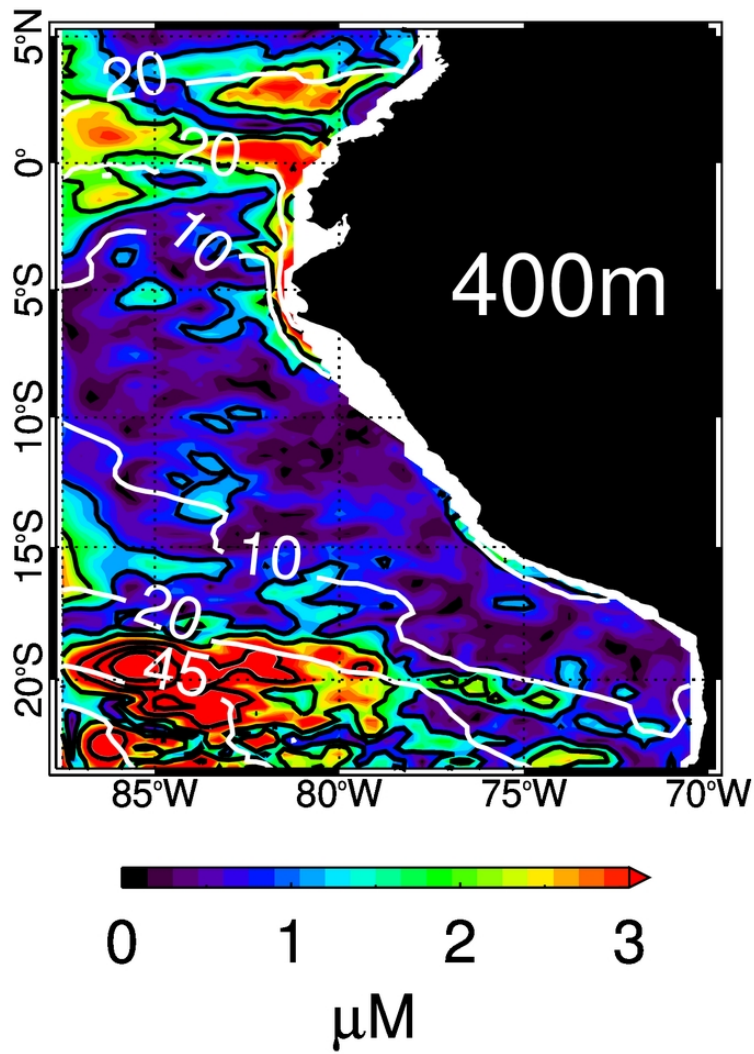
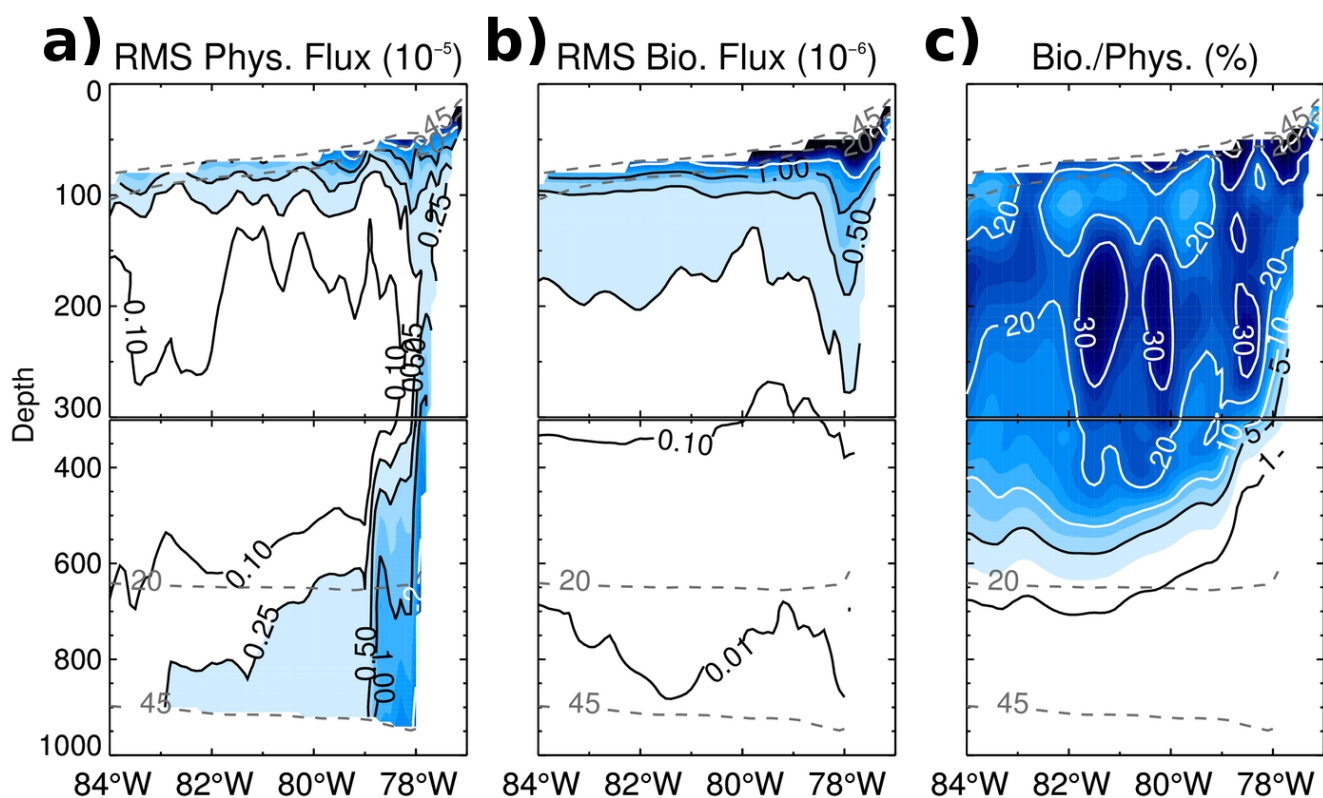


Figure 68. Amplitude (a) and phase (b) of the annual harmonic of the normalized oxygen concentration at 12°S. The slanted vertical lines show the theoretical WKB raypaths for the first (full), second (dashed) and third (dotted) baroclinic modes (1 year period) of a long Rossby wave. Dashed contours in (a) and (b) depict the 45 and 20 μM mean oxygen values. (c) Annual harmonic of the Oxygen concentration at 12°S, at 150 m and (d) 700 m depth. Small color scale corresponds to 700 m and the large color scale denotes the levels used in (c). (a) Amplitude and (b) phase of the annual maximum (in months) of the annual harmonic of the normalized DO concentration at 12°S. The slanted vertical lines indicate the theoretical WKB ray paths at a frequency of $\omega=2\pi\cdot 1\text{year}^{-1}$, for different value of phase speed. The theoretical trajectories were computed using the phase speed of the first (full), second (dashed) and third (dotted) baroclinic modes of a long Rossby wave. Dashed contours in (a) and (b) depict the 45 and 20 μM mean DO values. Land and the region outside the 45 μM mean DO isopleth are masked in white. (c) Annual harmonic of the DO concentration at 12°S, at 150 m and (d) 700 m depth. Small color scale corresponds to 700 m and the large color scale denotes the levels used in (c).



1
2
3 | **Figure 79.** Annual DO harmonic amplitude at 400 meters depth. White contours denote the 10, 20 and
4 45 μM mean oxygen isolines. Black contours denote the 1, 2, 4, 6 and 8 μM levels.
5



2 | **Figure 810.** Root mean square of the seasonal cycle of (a) Physical and (b) Biogeochemical oxygen
3 | fluxes (in $10^{-5} \mu\text{M s}^{-1}$ and $10^{-6} \mu\text{M s}^{-1}$, respectively) for CR BIO at 12°S. c) Ratio between the RMS of
4 | the biogeochemical fluxes and the physical fluxes, expressed as percentage. Dashed contours depict the
5 | 45 and 20 μM mean oxygen values. Note the vertical scale change at 300m depth. [Land and the region](#)
6 | [outside the 45 \$\mu\text{M}\$ mean DO isopleth are masked in white.](#)

7

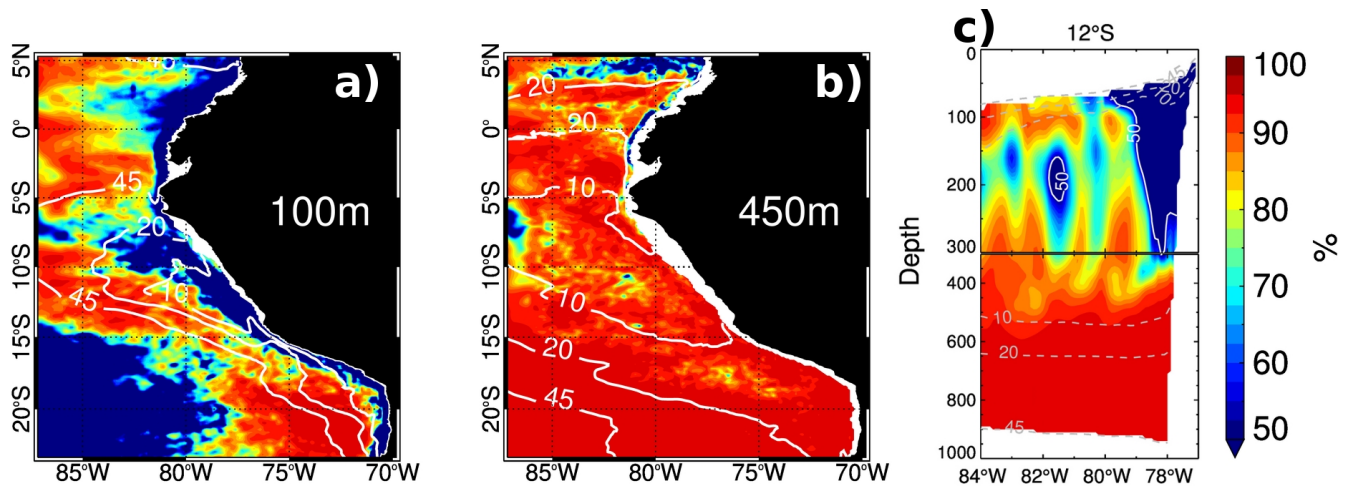


Figure 911. Percentage of the seasonal DO rate variance explained by the physical fluxes, at (a) 100 and (b) 450 meters depth, and along a cross shore section at 12°S. White Solid white lines (a,b) and dashed gray lines (c) contours denote the 10, 20 and 45 μM mean oxygen DO isopleths. Land and the region outside the 45 μM mean DO isopleth are masked in white in (c).

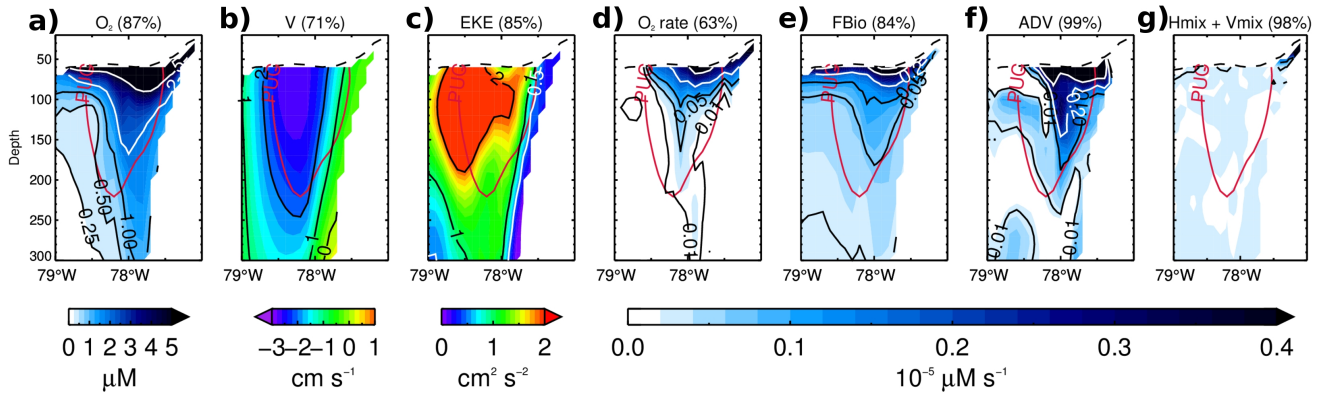
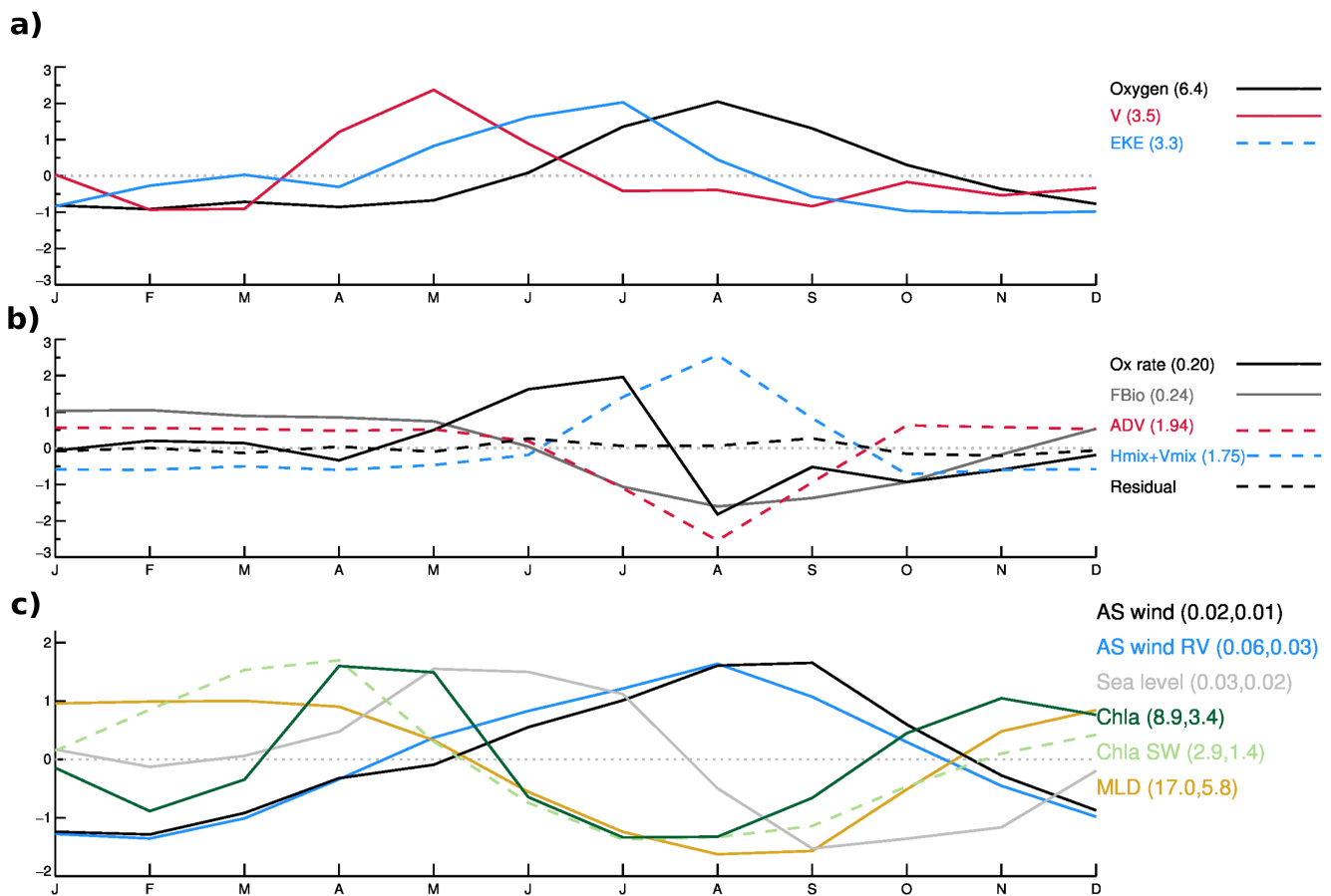


Figure 1012. Dominant climatological EOF modes (and percentage of explained variance): (a) oxygen concentration (in μM), (b) meridional currents (in cm s^{-1}), (c) eddy kinetic energy (in $\text{cm}^2 \text{s}^{-2}$), (d) oxygen rate (in $10^{-5} \mu\text{M s}^{-1}$), (e) biogeochemical flux (in $10^{-5} \mu\text{M s}^{-1}$), (f) advective terms (including u, v and w , in $10^{-5} \mu\text{M s}^{-1}$) and (g) mixing term (in $10^{-5} \mu\text{M s}^{-1}$) for CR BIO at 12°S . Red contour denotes the Peru Under Current (4 cm s^{-1} southwards). Dashed contour depicts the $45 \mu\text{M}$ isopleth. First EOF mode pattern of (a) DO, (b) alongshore currents component, (c) Eddy Kinetic Energy, (d) oxygen rate, (e) biogeochemical flux, (f) advective terms (sum of horizontal and vertical components) and (g) mixing terms (sum of horizontal and vertical components). Percentage of explained variance by each EOF mode pattern is indicated in parentheses on top of each panel. The red contour denotes the mean position of the Peru Under Current core, defined here as alongshore southward current exceeding 4 cm s^{-1} . The black dashed contour denotes the mean DO $45 \mu\text{M}$ isopleth. Land and the region outside the $45 \mu\text{M}$ mean DO isopleth are masked in white. The EOF mode patterns were multiplied by the RMS of the PC timeseries. Multiplying the EOF pattern by the PC timeseries plotted in Figure 13 yields the contribution of the first EOF mode to the original field, in dimensionalized units (i.e. $\mu\text{M s}^{-1}$ for the tendency terms).



2 **Figure 1413.** Principal components associated to the EOF modes in Figure 10 (a and b). Residual
3 corresponds to the difference between Ox rate and the sum of the other oxygen budget terms.
4 Multiplying the principal components with the RMS (indicated in parenthesis) yields the seasonal cycle
5 with the same units as in Figure 10. (c) Normalized seasonal cycle of: coastal alongshore wind,
6 alongshore wind Running Variance (variance over a 30 day running window), coastal sea level, surface
7 chlorophyll-a from CR-BIO, surface chlorophyll-a from SeaWiFS and Mixed Layer Depth. Mean and
8 RMS used to normalize each time series, are indicated in parenthesis. Original seasonal cycle is found
9 by multiplying the normalized series by its RMS and then adding the mean. Original units are N m^{-2} , m ,
10 mg m^{-3} , and m respectively (a, b) Non dimensional principal components (PC) associated with the EOF
11 patterns in Figure 12. Multiplying the principal component by the associated EOF pattern (from Fig.
12 12) yields a first EOF-mode reconstruction of the original field. RMS values of the principal
13 components are indicated in parenthesis (corresponding units as in Fig. 12). The residual corresponds
14 to the difference between the rate of DO change and the sum of all the terms of the rhs of Eq. 1 in terms
15 of the normalized PC timeseries. The weak residual indicates that the seasonal DO budget can be

1 interpreted from the EOF decomposition. The EOF decomposition was performed over the
2 climatological (mean seasonal cycle) fields. (c) Normalized seasonal cycle of: coastal alongshore wind
3 (AS wind) and coastal alongshore wind Running Variance (variance over a 30 day running window) at
4 12°S, sea level at the coast at 12°S, surface chlorophyll-a from CR BIO (Chla) and from SeaWiFS
5 (Chla SW) averaged over a coastal band of 2° width at 12°S, and Mixed Layer Depth at the coast
6 (MLD) at 12°S. Mean and RMS used to normalize each time series, are indicated in parenthesis.
7 Original seasonal cycle is found by multiplying the normalized series by its RMS and then adding the
8 mean. Original units are N m^{-2} , m, mg m^{-3} , and m respectively.

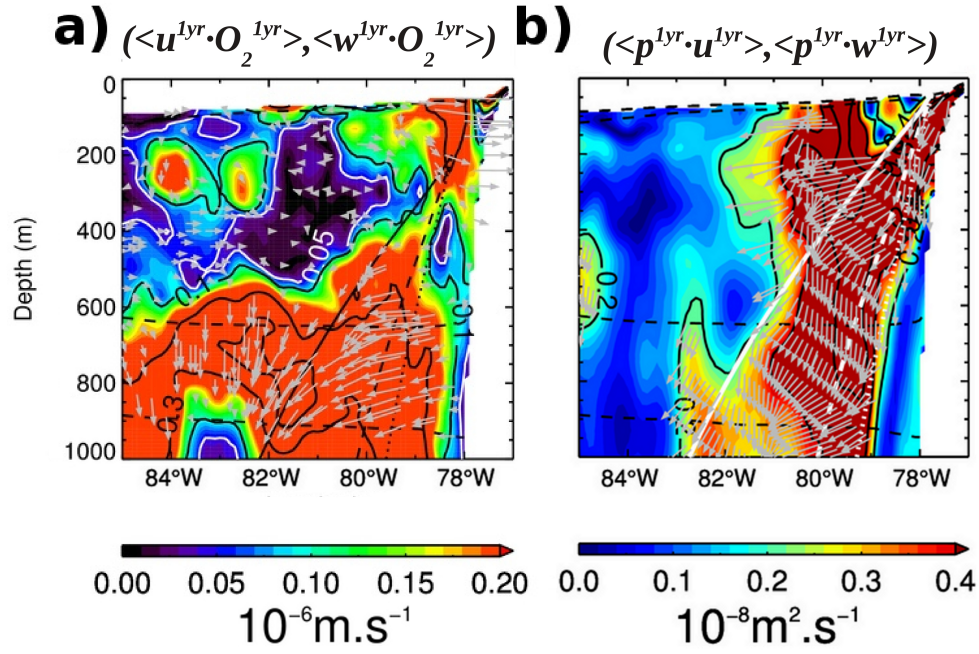


Figure 14. (a) Norm of the annual DO flux vector (i.e. $\sqrt{\langle u^{1yr} \cdot O_2^{1yr} \rangle^2 + \langle w^{1yr} \cdot O_2^{1yr} \rangle^2}$) for a cross shore section at 12°S. Arrows indicate the vector direction (i.e. $[\langle u^{1yr} \cdot O_2^{1yr} \rangle, \langle w^{1yr} \cdot O_2^{1yr} \rangle]$). The DO signal was normalized by its Root Mean Square value before computing the annual harmonic, in order to emphasize the flux patterns where DO concentration is very low. (b) Norm of the annual energy flux vector (i.e. $\sqrt{\langle p^{1yr} \cdot u^{1yr} \rangle^2 + \langle p^{1yr} \cdot w^{1yr} \rangle^2}$). Arrows inside the 0.2 contour indicate the vector direction (i.e. $[\langle p^{1yr} \cdot u^{1yr} \rangle, \langle p^{1yr} \cdot w^{1yr} \rangle]$). A range of theoretical WKB trajectories (1 year period) originating from near the coast at the surface are drawn for phase speed values of a first (full), second (dashed) and third (dotted) baroclinic modes. The range of phase speed values (modes 1-3) are obtained from a vertical mode decomposition of the mean model stratification. Dashed black contours indicate the 45 and 20 μM mean DO isopleths. Land and the region outside the 45 μM mean DO isopleth are masked in white.

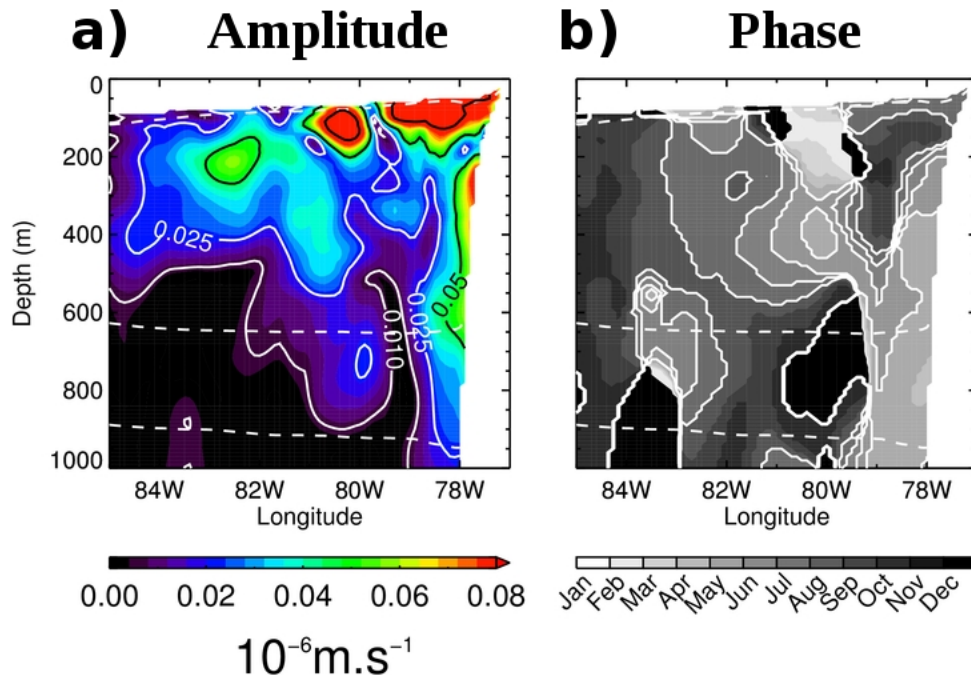
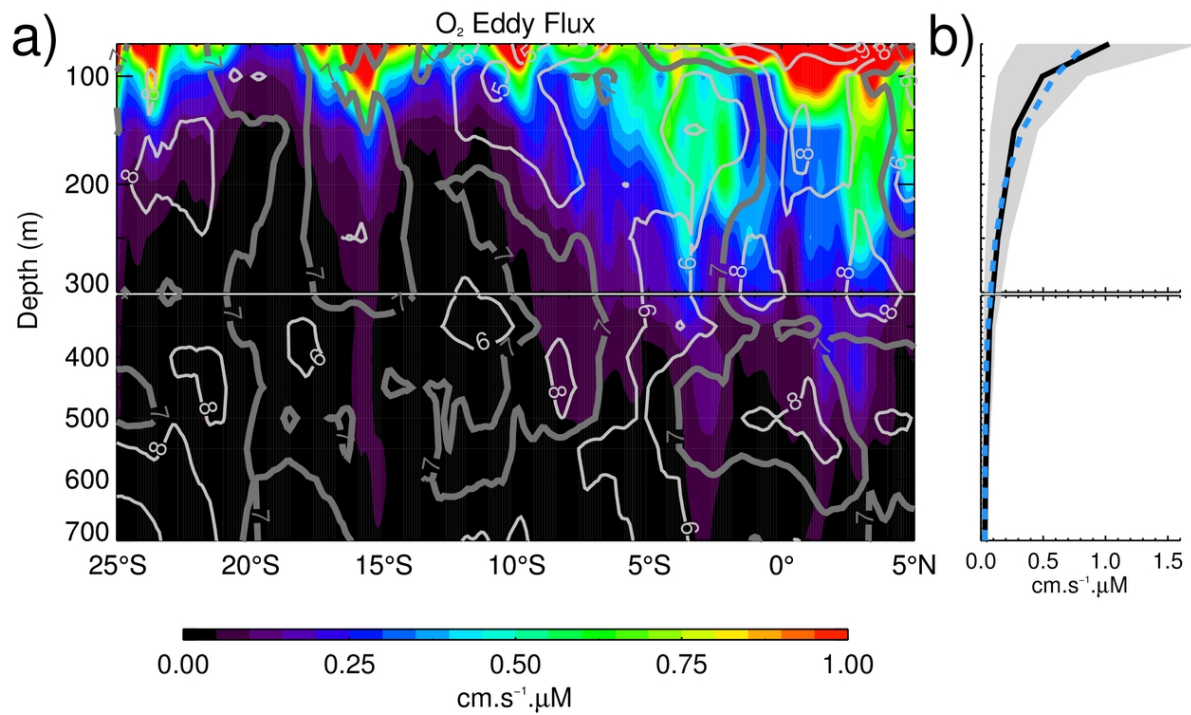
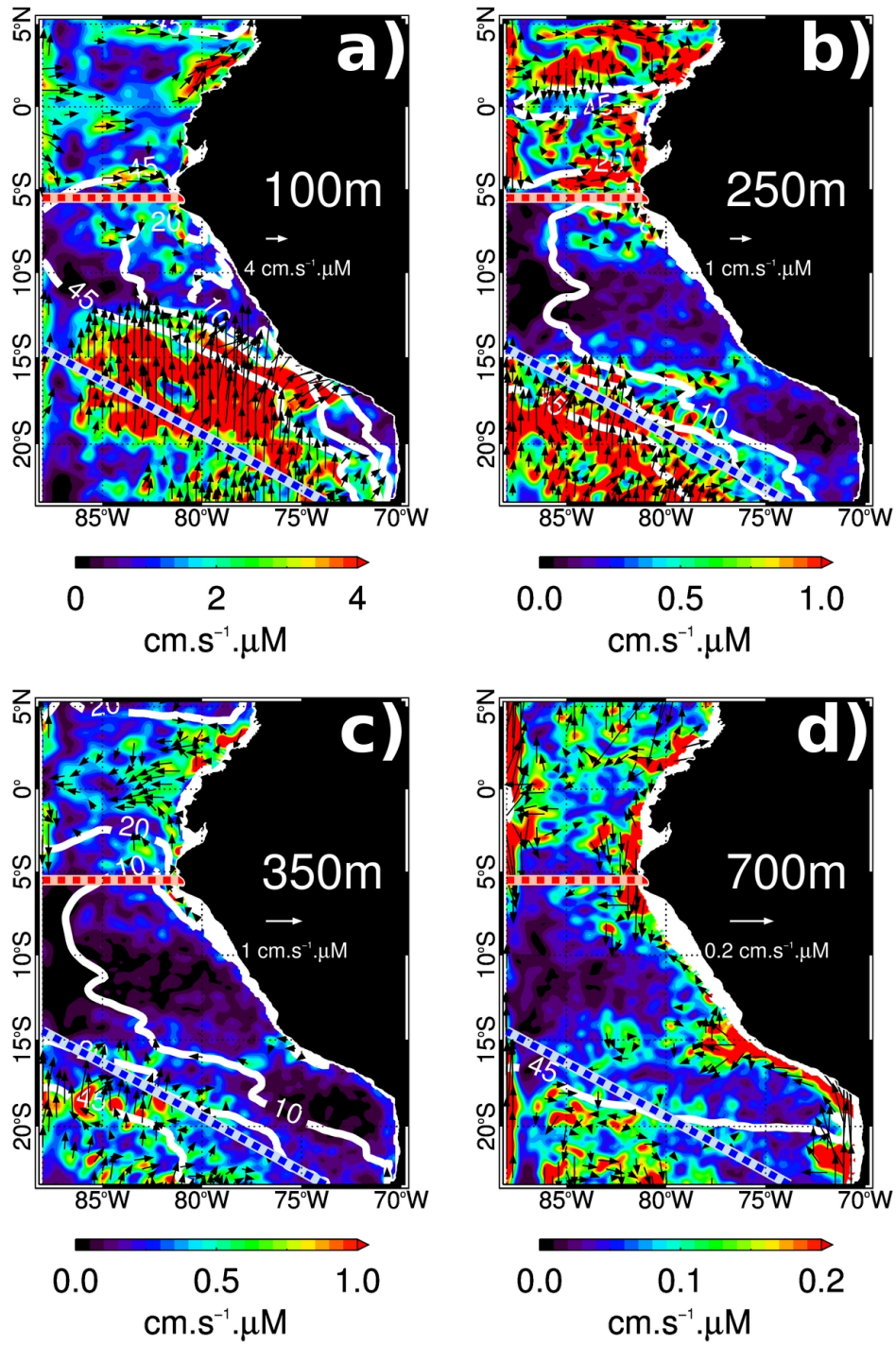


Figure 15. Zonal section of the annual harmonic of the module of the seasonal DO eddy flux vector $(\langle u' \cdot O_2' \rangle, \langle w' \cdot O_2' \rangle)$ at 12°S. (a) Amplitude of the harmonic and (b) phase of the annual maximum (in months). Dashed white contours indicate the 45 and 20 μM mean DO isopleths. DO was normalized by its RMS prior to carrying out analysis. Land and the region outside the 45 μM mean DO isopleth are masked in white.

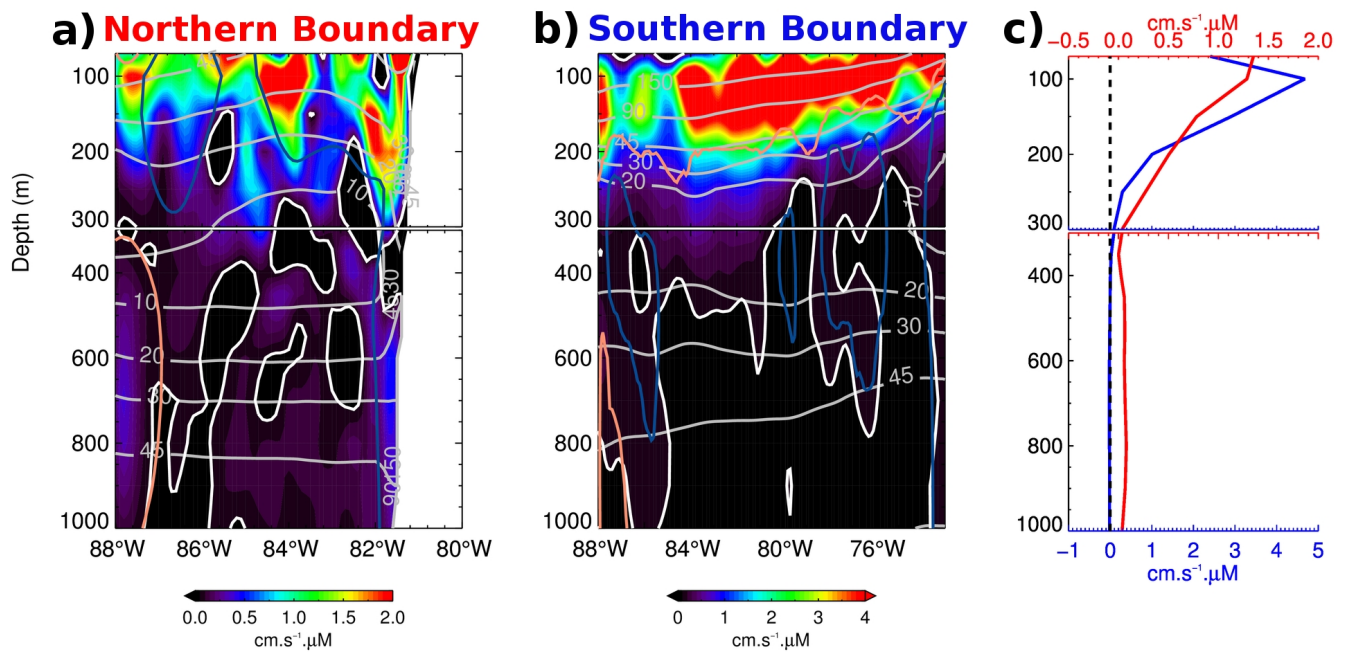


2 **Figure 1316.** (a) Amplitude (color shading) and phase (months, gray contours) of the annual harmonic
 3 of the climatological DO eddy-oxygen flux along the coast. The climatology of DO eddy flux was
 4 averaged over a coastal fringe of 2° width starting from 1° from the coast. (b) Meridional average
 5 vertical profile (black line), average profile +/- RMS (gray shading). An exponential model fitted to the
 6 average vertical profile (dashed blue line) yields a vertical decay scale of ~90 m.



1
2

3 **Figure 1417.** Module of the mean-oxygen DO eddy flux vector $(\langle u' \cdot O_2' \rangle, \langle v' \cdot O_2' \rangle)$ at (a) 100 m, (b)
4 250 m, (c) 350 m and (d) 700 m depth. Arrows -displayed only for values above the central value in
5 each colorbar- denote the vector direction and strength. White contours correspond to the 45, 20 and 10
6 μM mean DO values. Red and blue lines denote the position of vertical sections.



1 **Figure 1518.** (a) Mean ~~oxygen DO~~ eddy flux normal to the section denoted by the red line in Fig.
2 ~~1417~~. (b) Mean ~~oxygen DO~~ eddy flux normal to the section denoted by the blue line in Figure ~~1417~~. (c)
3 Horizontal mean of (a) and (b) (red and blue lines, respectively). Gray contours denote ~~oxygen mean~~
4 ~~DO~~ concentrations, and light red/blue contours correspond to positive/negative values of mean currents
5 normal to the section ($1.0/-1.0 \text{ cm s}^{-1}$ in (a) and $0.4/-0.2 \text{ cm s}^{-1}$ in (b)). White contour denotes the 0
6 value. The sign convention was chosen so that a positive horizontal flux indicates transport towards the
7 interior of the OMZ.

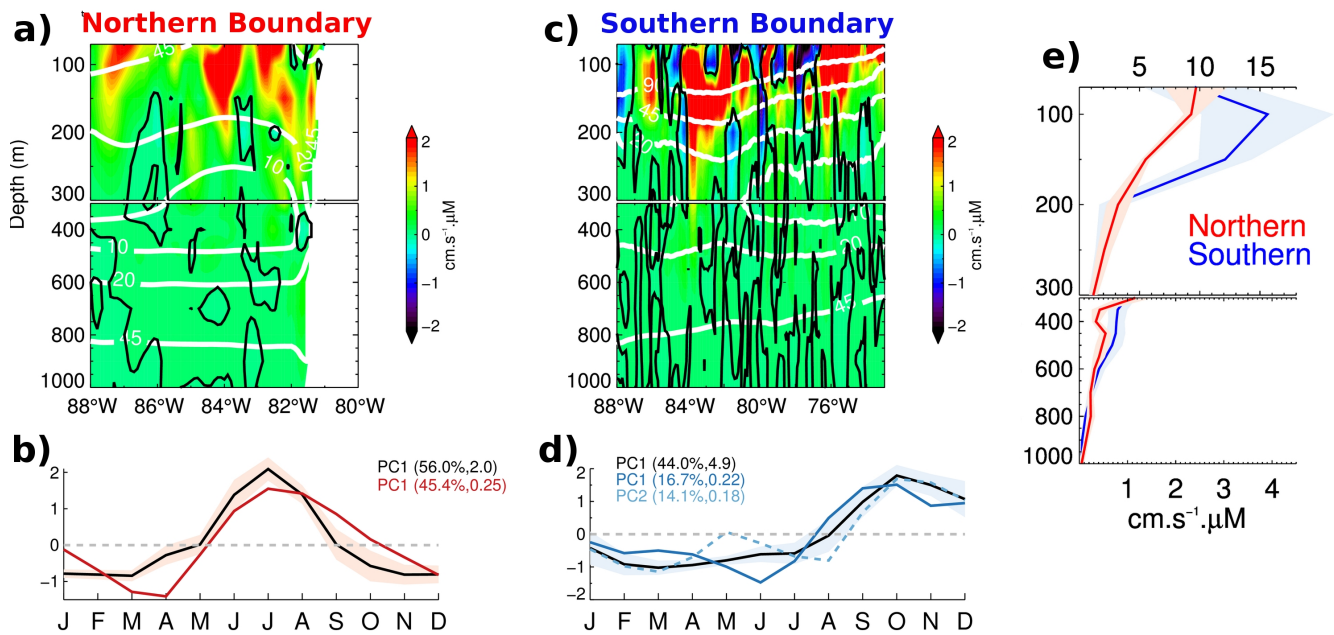


Figure 1619. (a) Dominant EOF mode of the seasonal cycle of the oxygen eddy flux normal to the red section depicted in Figure 14. (b) Principal component associated to the EOF mode (black line). Red line corresponds to the seasonal cycle of the 30 days running variance of the (intraseasonal anomaly) currents (dominant EOF mode) normal to the section. (c) First EOF mode of the seasonal cycle of the oxygen eddy flux normal to the oblique section depicted in Fig. 14. (d) Principal component associated to the EOF pattern (black line) and seasonal cycle of the currents normal to the section (blue lines; computed as in (b)). Percentage of explained variance and RMS value are indicated in parenthesis (in $\text{cm.s}^{-1}.\mu\text{M}$ and cm.s^{-1} , for oxygen eddy flux and currents respectively). White contours in (a) and (c) denote mean oxygen concentration values, in μM . (e) RMS of the spatial patterns (a) and (c), computed along the horizontal direction. Note the scale leap at 300 m. Red/blue shading in (b), (d) and (e) represents a dispersion of ± 1 standard deviation, computed over a band 2° width around the sections depicted in Fig. 14. (a) First EOF mode of the seasonal cycle of the DO eddy flux normal to the section depicted in Fig. 17 by the dashed red line (Northern boundary). (b) Principal component (PC) timeseries associated with the first EOF mode (black line). The red line in (b) corresponds to the PC timeseries associated with the first EOF mode of the seasonal cycle of the 30-day running variance of intraseasonal currents normal to the section. (c) First EOF mode of the seasonal cycle of the DO eddy flux normal to the oblique section depicted in Fig. 17 by the dashed blue line (Southern boundary). (d) PC timeseries associated with the first EOF mode (black line). The blue curves (full and dashed lines) in (d) corresponds to the PC timeseries associated with the first and second EOF modes of the seasonal

1 cycle of the 30-day running variance of the intraseasonal currents normal to the section (computed as in
2 (b)). Percentage of explained variance and RMS value are indicated in parentheses in the panels (b) and
3 (d) (in $\text{cm s}^{-1} \mu\text{M}$ and cm s^{-1} , for DO eddy flux and currents respectively). White contours in (a) and (c)
4 denote mean DO concentration values, in μM . (e) RMS of the spatial patterns (a) and (c), computed
5 along the horizontal direction. Note the scale leap at 300 m. Red/blue shading in (b), (d) and (e)
6 represents an estimate of the error associated with slight changes in the location of the boundaries, that
7 is when the EOF is performed over a section that is located at a distance from the original section (cf.
8 Figure 17) compromised between $\pm 120\text{km}$ (see text). The error corresponds to the standard deviation
9 among 12 PC timeseries (for (b) and (d)) and EOF patterns (for (e)).

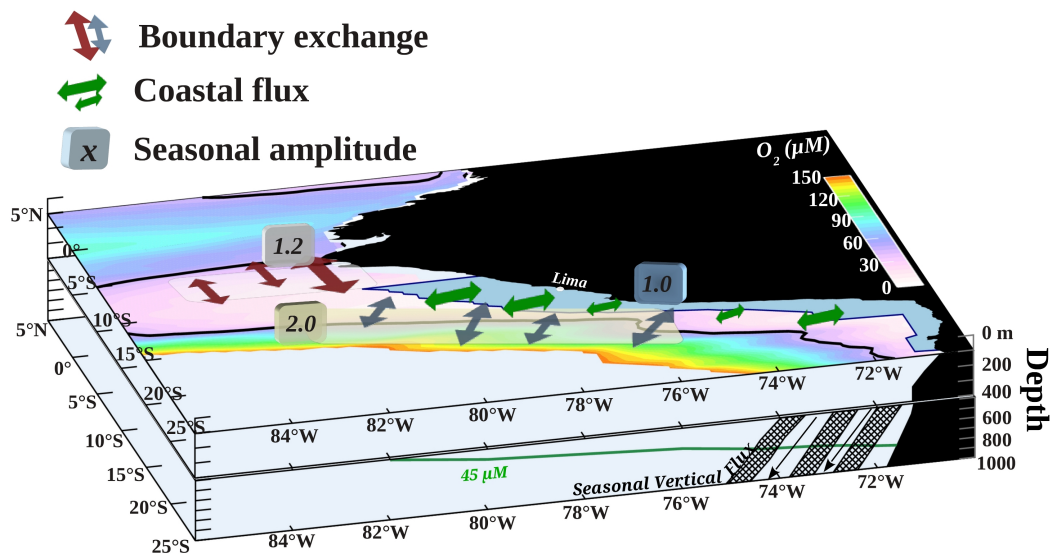


Figure 1720. Schematic of the main processes driving the seasonal variability in the SEP OMZ: The oxygen eddy flux through the northern-southern boundaries and the oxygen flux that extends from the coastal boundary into the OMZ. The coastal band limits are defined by the light blue shading adjacent to the coast. A scale of the seasonal amplitude of the eddy driven DO flux at each OMZ boundary is indicated (units in $\text{cm s}^{-1} \mu\text{M}$). The position of the 45 μM is also represented (thick black contours). The vertical/offshore oxygen flux induced by the propagation of the annual ETRW across the lower oxycline is represented in the bottom panel. Schematic of the main processes driving the seasonal variability in the SEP OMZ: The DO eddy flux through the northern-southern boundaries and the DO flux that takes place at the coastal boundary of the OMZ. The coastal band limits are defined by the light blue shading adjacent to the coast. A scale of the seasonal amplitude of the eddy driven DO flux at each OMZ boundary is indicated (units in $\text{cm s}^{-1} \mu\text{M}$). The mean DO concentration (color shading) and the position of the 45 μM isopleth (thick black contour) at 100 m depth are also represented. The vertical/offshore DO flux induced by the propagation of the annual ETRW across the 45 μM isopleth at 25°S is represented in the bottom panel.